INVESTIGATION OF THE INTERACTION OF CO_2 AND CH_4 HYDRATE FOR THE DETERMINATION OF FEASIBILITY OF CO_2 STORAGE IN THE BLACK SEA SEDIMENTS

A THESIS SUBMITTED TO
THE GRADUATE SCHOOL OF NATURAL AND APPLIED SCIENCES
OF
MIDDLE EAST TECHNICAL UNIVERSITY

BY

OYTUN ÖRS

IN PARTIAL FULFILLMENT OF THE REQUIREMENTS
FOR
THE DEGREE OF MASTER OF SCIENCE
IN
PETROLEUM AND NATURAL GAS ENGINEERING

SEPTEMBER 2012

Approval of the thesis

INVESTIGATION OF THE INTERACTION OF CO_2 AND CH_4 HYDRATE FOR THE DETERMINATION OF FEASIBILITY OF CO_2 STORAGE IN THE BLACK SEA SEDIMENTS

submitted by **OYTUN ÖRS** in partial fulfillment of the requirements for the degree of **Master of Science in Petroleum and Natural Gas Engineering Department, Middle East Technical University** by,

Prof. Dr. Canan Özgen
Dean, Graduate School of **Natural and Applied Sciences** _____

Prof. Dr. Mahmut Parlaktuna
Head of Department, **Petroleum and Natural Gas Engineering** _____

Asst. Prof. Dr. Çağlar Sınayuç
Supervisor, **Petroleum and Natural Gas Eng. Dept., METU** _____

Examining Committee Members

Prof. Dr. Ender Okandan
Petroleum and Natural Gas Engineering Dept.,METU _____

Asst. Prof. Dr. Çağlar Sınayuç
Petroleum and Natural Gas Engineering Dept.,METU _____

Prof. Dr. Tanju Mehmetoğlu
Petroleum and Natural Gas Engineering Dept.,METU _____

Prof. Dr. Mahmut Parlaktuna
Petroleum and Natural Gas Engineering Dept.,METU _____

Dr. Sevtaç Bülbül
METU Petroleum Research Center _____

Date: 14.09.2012

I hereby declare that all information in this document has been obtained and presented in accordance with academic rules and ethical conduct. I also declare that, as required by these rules and conduct, I have fully cited and referenced all material and results that are not original to this work.

Name, Last name: Oytun ÖRS

Signature:

ABSTRACT

INVESTIGATION OF THE INTERACTION OF CO_2 AND CH_4 HYDRATE FOR THE DETERMINATION OF FEASIBILITY OF CO_2 STORAGE IN THE BLACK SEA SEDIMENTS

Örs, Oytun
M.Sc., Department of Petroleum and Natural Gas Engineering
Supervisor: Asst. Prof. Dr. Çağlar Sınayuç

September 2012, 156 pages

Recently, carbon dioxide injection into deep sea sediments has become one of the carbon dioxide mitigation methods since carbon dioxide hydrates are stable at the prevailing pressure and temperature conditions.

The Black Sea, which is one of the major identified natural methane hydrate regions of the world, can be a good candidate for carbon dioxide storage in hydrate form. Injected carbon dioxide under the methane hydrate stability region will be in contact with methane hydrate which should be analyzed thoroughly in order to increase our understanding on the gaseous carbon dioxide and methane hydrate interaction.

For the storage of huge amounts of CO_2, geological structure must contain an impermeable barrier. In general such a barrier may consist of clay or salt. In this

study, sealing efficiency of methane hydrate and long term fate of the CO_2 disposal under the methane hydrate zone is investigated.

In order to determine the interaction of CO_2 and CH_4 hydrate and the sealing efficiency of CH_4 hydrate, experimental setup is prepared and various tests are performed including the CH_4 hydrate formation in both bulk conditions and within sand particles, measurement of the permeability of unconsolidated sand particles that includes 30% and 50% methane hydrate saturations and injection of CO_2 into the CH_4 hydrate.

Results of the experiments indicate that, presence of hydrate sharply decreases the permeability of the unconsolidated sand system and systems with hydrate saturations greater than 50% may act as an impermeable layer. Also, CO_2-CH_4 swap within the hydrate cages is observed at different experimental conditions. As a result of this study, it can be concluded that methane hydrate stability region in deep sea sediments would be a good alternative for the safe storage of CO_2. Therefore, methane hydrate stability region in the Black Sea sediments can be considered for the disposal of CO_2.

Keywords: CO_2 Storage, Natural Gas Hydrates, CO_2-CH_4 hydrate interaction, Permeability of hydrates, CO_2-CH_4 swap, The Black Sea.

ÖZ

KARADENİZ SEDİMANLARINDA CO_2 DEPOLANMASININ FİZİBİLİTESİNİN BELİRLENMESİ İÇİN CO_2 VE CH_4 HİDRATI ETKİLEŞİMİNİN İNCELENMESİ

Örs, Oytun
Yüksek Lisans, Petrol ve Doğal Gaz Mühendisliği Bölümü
Tez Yöneticisi: Yard. Doç. Dr. Çağlar Sınayuç

Eylül 2012, 156 sayfa

Son günlerde, derin deniz sedimanlarına karbondioksit enjeksiyonu, atmosferdeki karbondioksit oranını azaltma tekniklerinden biri haline gelmiştir, çünkü karbondioksit hidratları mevcut sıcaklık ve basınç değerlerinde kararlı halde bulunmaktadır.

Dünyanın en önemli metan hidrat rezervlerinden birine sahip olan Karadeniz, karbondioksitin de hidrat formunda depolanması için iyi bir aday olabilir. Metan hidrat kararlılık zonunun altına enjekte edilen karbondioksit metan hidratı ile etkileşim içerisinde olacaktır ve bu etkileşim hakkında daha fazla fikir sahibi olmak için sistem detaylı bir şekilde analiz edilmelidir.

CO_2'nin büyük oranlarda depolanabilmesi için, jeolojik yapının geçirimsiz katman içermesi gerekmektedir. Genellikle böyle bir katman kil veya tuzdan oluşmaktadır. Bu çalışmada, metan hidratının geçirimsizlik açısından yeterliliği

ve CO_2'nin metan hidrat katmanı altında uzun vadedeki davranışı incelenecektir.

CO_2 ve CH_4 hidratı etkileşimi ve CH_4 hidratının geçirimsizlik açısından yeterliliğinin belirlenmesi amacıyla deney düzeneği oluşturulmuş ve çeşitli deneyler yapılmıştır. Bu deneyler, CH_4 hidratının su içerisinde ve sedimanlarda oluşturulması, %30 ve %50 metan hidratı içeren gevşek sedimanların geçirgenliğinin ölçülmesi ve CH_4 hidratına CO_2 enjeksiyonu yapılmasını içermektedir.

Deney sonuçları, gevşek sedimanlardaki hidrat varlığının sistemin geçirgenliğini büyük oranda etkilediğini ve hidrat saturasyonu %50'den fazla olan sistemlerin geçirimsiz bariyer olarak görev yapabileceğini göstermiştir. Ayrıca farklı deney koşullarında, hidrat kristallerinde CO_2-CH_4 takası gözlemlenmiştir. Bu çalışmanın sonunda, derin deniz sedimanlarında bulunan metan hidratı kararlılık zonunun CO_2'nin güvenli şekilde depolanması için iyi bir seçenek olabileceği sonucuna varılmıştır. Bu sebeple, Karadeniz sedimanları CO_2'nin depolanması için değerlendirilebilir.

Anahtar Kelimeler: CO_2 depolama, Doğalgaz Hidratları, CO_2-CH_4 hidratı etkileşimi, Hidratların geçirgenliği, CO_2-CH_4 takası, Karadeniz.

ACKNOWLEDGEMENTS

I would like to acknowledge and express my sincere gratitude to my thesis advisor Asst. Prof. Dr. Çağlar Sınayuç for his support, encouragement, advice, interesting conversations and supervision throughout the study. Without his invaluable insights, this study would not have been accomplished. I also appreciate the freedom and opportunity provided to me during the laboratory work.

I would like to thank Prof. Dr. Mahmut Parlaktuna, the chairperson of Department of Petroleum and Natural Gas Engineering, for introducing me about natural gas hydrates in his lectures. I would also like to thank my thesis committee members for their valuable suggestions, comments and contributions.

I also wish to thank Şükrü Merey for his help in the experimental studies and I appreciate the time we have spent in the laboratory. I would like to thank Dr. Sevtaç Bülbül, whose professional experience contributed a lot to me. I also want to thank my officemates and dear friends for their friendship.

I would like to thank technical staff of the department, namely; Murat Çalışkan and Naci Doğru for their help during the experiments.

This study was supported by the Scientific and Technological Research Council of Turkey under National Scholarship Programme for MSc Students.

TABLE OF CONTENTS

LIST OF TABLES

TABLES

LIST OF FIGURES

FIGURES

CHAPTER 1

INTRODUCTION

1.1 General Background

Recently, climate change has become one of the most important global challenges of the world; therefore, reducing and avoiding the emission of enormous amounts of greenhouse gases is one of the serious problems of this century that should be addressed immediately. Among all the greenhouse gases, CO_2 deserves particular attention as the atmospheric CO_2 concentration has been increasing since the industrial revolution. The fundamental source of CO_2 emissions is fossil fuel combustion for power generation and transportation. When the global dependence of fossil fuel is considered, it can be concluded that it is almost impossible to cut the anthropogenic CO_2 emissions. One possible way to diminish the anthropogenic CO_2 emissions to the atmosphere is storing the significant amount of CO_2 in another domain of the planet for example, the geosphere. Carbon capture and sequestration techniques enable the disposal of large amount of CO_2 and there is considerable interest in use of these techniques as a climate change mitigation option. As a result, many studies and researches have been carried out in order to mitigate CO_2 emissions and many capture and sequestration techniques have been proposed. Some possible options for geologic storage of CO_2 are; CO_2 injection into depleted oil and gas reservoirs, deep saline aquifers, and unmineable coalbeds.

1.2 Scope of the study

Aim of this study is determination of the feasibility of CO_2 disposal below the methane hydrate stability zone in the Black Sea. Seismic studies conducted by Korsakov *et al.* (1989) suggest that the Black Sea has the convenient conditions for natural gas hydrate formation. Results of seismic studies, which were conducted by Russian scientists, indicated that there are five regions in the Black Sea that are highly prosperous for hydrate formation. Furthermore, evidences of methane hydrate accumulation (Fig. 1.1) and volume of methane at STP (Standard temperature and pressure) (Fig. 1.2) makes the Black Sea technically and economically feasible site for the CO_2 sequestration, especially when the amount of CH_4 that might be produced from the hydrates is considered.

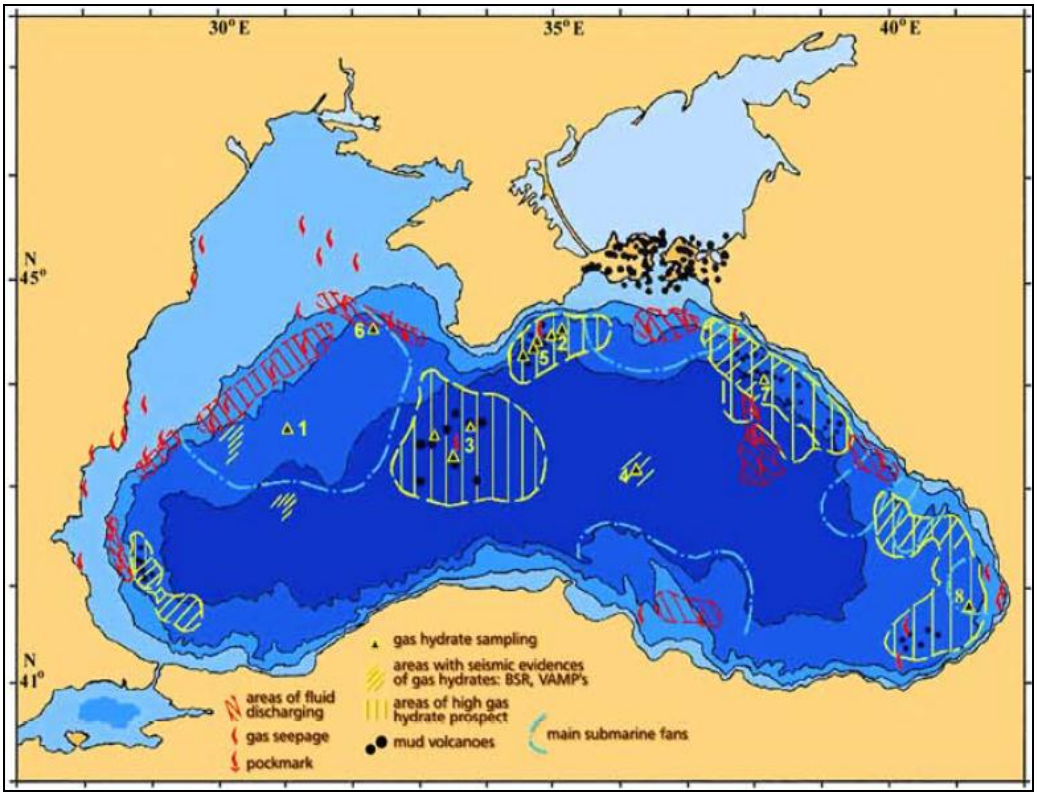

Figure 1. 1 Evidences of methane hydrate from the Black Sea (Vassilev & Dimitrov, 2003)

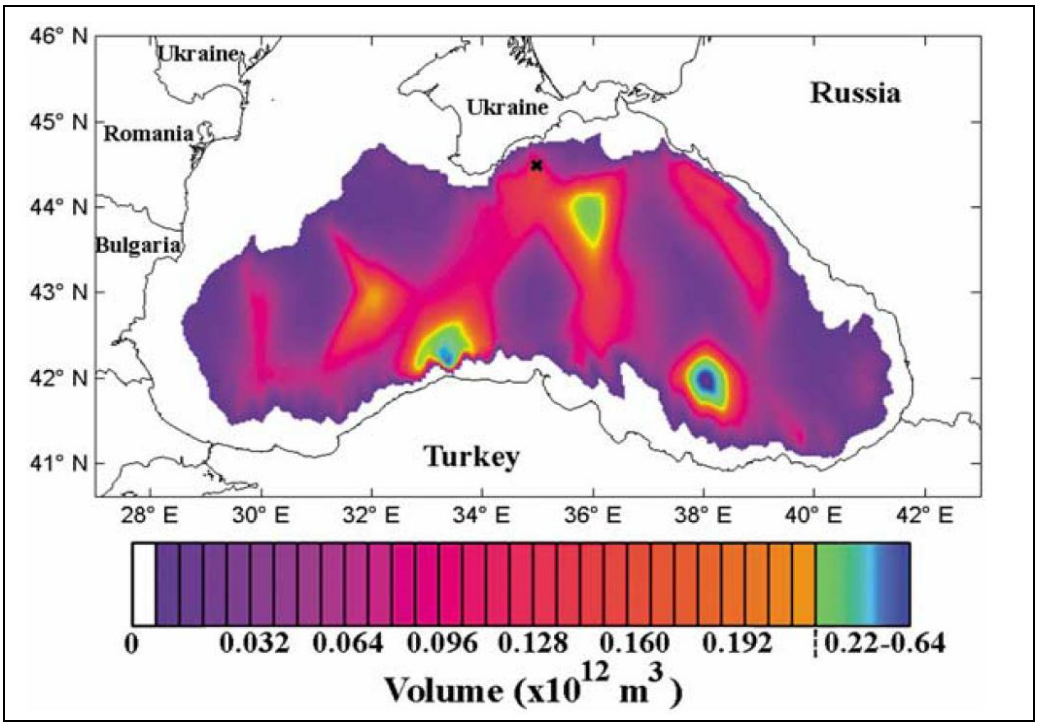

Figure 1. 2 Volume of CH_4 (STP) in hydrate at the Black Sea (Klauda & Sandler, 2003)

This study, considers the injection of CO_2 into the sediments of the Black Sea, especially in the regions where significant methane hydrate accumulation exists. The idea behind the CO_2 injection below the methane hydrate stability zone is similar to the CO_2 injection below the permafrost region. However, permafrost regions are generally take place on remote locations and transportation of CO_2 to these areas is not feasible. On the other hand, when CO_2 is injected below the methane hydrate stability zone, methane hydrate will act as a seal for the injected CO_2. Any injected CO_2, which is able to find flow pathways through the impermeable methane hydrate layer, will form CO_2 hydrate as long as it encountered water-rich sediment. Furthermore, CO_2 hydrate may be more stable than the methane hydrate under the prevailing conditions. Moreover, as the presence of CO_2 increases the stability zone of the methane hydrate, injected CO_2 may increase the sealing capacity of the methane hydrate.

As a result this study focuses on the following topics:

i. Interaction between the injected CO_2 and the methane hydrate.
ii. CO_2 hydrate formation within the sediments.
iii. Sealing efficiency of methane hydrate.
iv. Possible methane production by means of CO_2 injection.

The research results are organized in the following chapters:

Chapter 2 is a review of the literature on the natural gas hydrates, hydrate structures, guest molecules, some properties of CH_4 and CO_2 hydrates, formation characteristics of hydrates in porous rock, effects of hydrate on the permeability and hydrate formation conditions.

Chapter 3 presents a detailed description of the hydrate stability region calculations and gives information about thermodynamic model for the hydrate phase equilibrium.

Chapter 4 gives information about carbon sequestration and presents a detailed description of the possible CO_2 sequestration techniques.

Chapter 5 presents the idea of CO_2 sequestration by means of hydrates into deep sea sediments and mentions about storage and stability conditions of hydrates within deep sea sediments, properties of carbon dioxide and methane mixtures, equilibrium conditions in porous media and modeling studies, effect of pore size and porous material on the hydrate formation and stability conditions, flow characteristics of hydrate containing porous media, replacement of CH_4 in the hydrate by use of CO_2 and some properties of the Black Sea.

Chapter 6 presents an explicit statement of the problem.

Chapter 7 presents experimental setup and procedure.

Chapter 8 presents results of the experiments and their interpretative discussions.

CHAPTER 2

NATURAL GAS HYDRATES

2.1 Gas Hydrates

Gas hydrates, also called gas clathrates, are solid, crystalline, ice like materials, which may form under suitable pressure and temperature values. In general, formation of gas hydrates requires low temperature and high pressure. Gas hydrates consist of water cavities (host) that are composed of hydrogen-bonded water molecules and hydrophobic gas molecules (guests) that are encapsulated in water cavities. Methane, ethane, propane and carbon dioxide are the some common gas molecules which are trapped in water cavities to form clathrates.

Hydrates are first discovered and documented in 1810 by Sir Humphrey Davy. After identifying the chlorine hydrate in a laboratory study, he included brief comments on chlorine (then called oxymuriatic gas) in the Bakerian lecture to the Royal Society in 1810. Actually, it was suggested that Priestley might have discovered hydrates more than 30 years before Davy's discovery. In his laboratory studies, Priestley observed that vitriolic air (SO_2) would impregnate water and enables it to freeze and refreeze, whereas marine acid air (HCl) and fluor acid air (SiF_4) would not result in same phenomena. However, Priestley conducted his experiments at a temperature value of -8.3 ^{o}C (17 ^{o}F) which is below the ice point. Therefore, there is no clear evidence that the frozen system was hydrate. As a result, Davy's discovery of chlorine hydrate is generally credited as the first remark (Sloan, 1990).

In 1888, Villard discovered the methane, ethane, and propane hydrates. In 1934, Hammerschmidt found out that hydrates are plugging the gas transmission lines. After his remark, hydrates are considered by the oil industry. However, it took some 35 years until gas hydrates recognized as an energy source (Sloan, 1990).

Gas hydrates are considered as a potential energy source because of their extensive geographical distribution all over the world. Researchers located many hydrate occurrences at different locations of the world; strictly, permafrost and oceanic regions, as a result of temperature and pressure requirements for hydrate formation. Besides the appropriate temperature and pressure values, sufficient amount of hydrate former and water are also required for hydrate formation (Sloan, 1990). Kvenvolden (2003) stated that, gas hydrates may occur up to 150 m below the surface level in permafrost regions. However, in deep sea sediments, gas hydrates may occur at water depths greater than 300 m.

In addition to their worldwide distribution, gas hydrates are considered to be a potential energy source due to their huge gas storage capacities. The methane storage capacity of hydrates is found out to be 170 volumes of methane at standard conditions for one volume of methane hydrate. Considering the potential and distribution of the gas hydrates, studies have focused on the amount of energy stored in gas hydrates and Sloan (1991) stated that, energy stored in hydrates is estimated to be twice of all the fossil fuels in the world.

2.2 Hydrate Structures

Hydrates are formed by means of water molecules that constitute the cavities. Generally, these cavities are composed of pentagonal and hexagonal faces. These geometric structures are crucial to understand the nature of gas hydrates, as the combination of different faces result in formation of different hydrate structures. Two types of hydrates, which are very common in petroleum

industry, are Structure I and II. Another type of hydrate, which is less common in petroleum industry, is Structure H. The common property of all three gas hydrate structure is a tetrahedral arrangement of water molecules held together by hydrogen bonds. The tetrahedral bonded waters in hydrates resemble the tetrahedral arrangement of water molecules in hexagonal ice, (ice Ih) which is the most common solid form of water. In fact, the difference between the bond lengths is only about 1% and the angles between oxygen atoms differ by less than 4^{o} (Sloan, 1998-a). The essential dissimilarity derives from the arrangement of water tetrahedral. The gas hydrate structure includes a series of polyhedral cages while ice contains a collection of non-planar "puckered" hexagonal rings. Consequently, due to this difference gas hydrates are able to trap guest molecules inside its crystal lattice. For this reason, thermodynamic conditions necessary for hydrate formation is different than the conditions required for ice formation and gas hydrates have the capability to form at temperatures above the freezing point of water as long as the adequate gas molecules and water is available.

2.2.1 Structure I

Structure I, a body-centered cubic structure, consists of 6 large and 2 small cavities per unit cell, which also includes 46 hydrogen bonded water molecules. Unit cell can be defined as a cube of predetermined dimensions comprising known number of crystal units and molecules. The hydration number (N_H), which is the water gas ratio in hydrate, ranges from 5.75 to 7.67. The average hydration number in the Structure I hydrates is 6 and the lowest hydration value is obtained when all crystal units are occupied whereas highest value is obtained for large guest molecules that cannot fill small cages. Structure I hydrates are formed by gas molecules smaller than propane; therefore these hydrates can be found in situ in deep oceans with biogenic gases containing mostly methane, ethane, carbon dioxide and hydrogen sulfide.

2.2.2 Structure II

Structure II, a diamond lattice within a cubic framework, consists of 8 large and 16 small cavities per unit cell, which also includes 136 hydrogen bonded water molecules. The hydration number is 5.67 when all crystal units are occupied, whereas 17 when large guest molecules are not able to fill the small cages. Structure II hydrates are formed by gas molecules larger than ethane but smaller than pentane; consequently, this structure represents hydrates from thermogenic gases. Structure II may form when heavier gases like propane or iso-butane exists. If all the cages of either structure (sI or sII) are occupied, there will be 15 gas molecules per 85 water molecules in other words, the guest to water ratio becomes 1: 5 ⅔.

2.2.3 Structure H

Ripmeester *et al.* (1987) discovered the Structure H by using the NMR spectroscopy and x-ray powder diffraction. Actually, it is possible that Structure H was first prepared (but not identified) by de Forcrand in 1883 during his laboratory investigations. Binary (double) hydrates with iso-butyl chloride or bromide as the large guest were prepared by de Forcrand, where these guest molecules are similar in size to iso-pentane, now known to be a sH hydrate former. However, Structure H is not considered significant until Sassen and MacDonald proved existence of this structure in the Gulf of Mexico continental slope in 1994 (Sloan, 1998-b). Formation of this structure necessitates small guest molecules like methane, nitrogen or carbon dioxide for the 5^{12} and $4^3 5^6 6^3$ cages, but the molecules in the $5^{12}6^8$ cage should be larger than 0.7 nm but smaller than 0.9 nm like methyl cyclohexane. These hydrate structures consist of three 5^{12}, two $4^3 5^6 6^3$ and one $5^{12}6^8$ crystal units in a unit cube. When the cages of structure H are occupied, there will be 6 gas molecules per 34 water molecules in other words, the guest to water ratio becomes 1: 5 ⅔.

2.3 Guest Molecules

For the stabilization of cavities, a guest molecule that does not impede the presence of hydrogen bonding is necessary (Jeffrey, 1984). The ideal ratio of molecular to cavity diameter for the cages to become stable is at least 0.76. However, this rule does not present at all times and size of the cavity and structure is reliant on the size of the guest molecule.

Small guest molecules like methane (CH_4) and hydrogen sulfide (H_2S) are able to stabilize both the small and large cavities of Structure I. Other gas molecules, which may stabilize Structure I are ethane (C_2H_6) and carbon dioxide (CO_2). Nitrogen (N_2), propane (C_3H_8) and iso-butane (C_4H_{10}) are the formers of Structure II. However, some of these gas molecules may only fill the larger cages and for this reason Structure II is generally present as mixtures of different gases. Absence of smaller gas molecules decreases the probability of formation of Structure II hydrates. For example, in order to form these structures benzene (C_6H_6) and cyclohexane (C_6H_{12}) relies on help gases, such as methane (CH_4) or xenon (Xe) (Sloan & Koh, 2008).

2.4 Methane Hydrates

Methane hydrates are perhaps the most important hydrate types since great deal of recovered natural gas hydrate samples have been Structure I hydrates with methane comprising more than 90% of the guest molecules. The methane in these samples is primarily derived from biogenic origin. Methane that is produced at elevated temperatures and pressures, acts on carbon-rich sediments. When methane migrates to shallow depths, where temperatures are relatively low, methane hydrate will be formed. Figure 2.1 shows the pressure and temperature stability region for methane gas hydrate as determined from experiments.

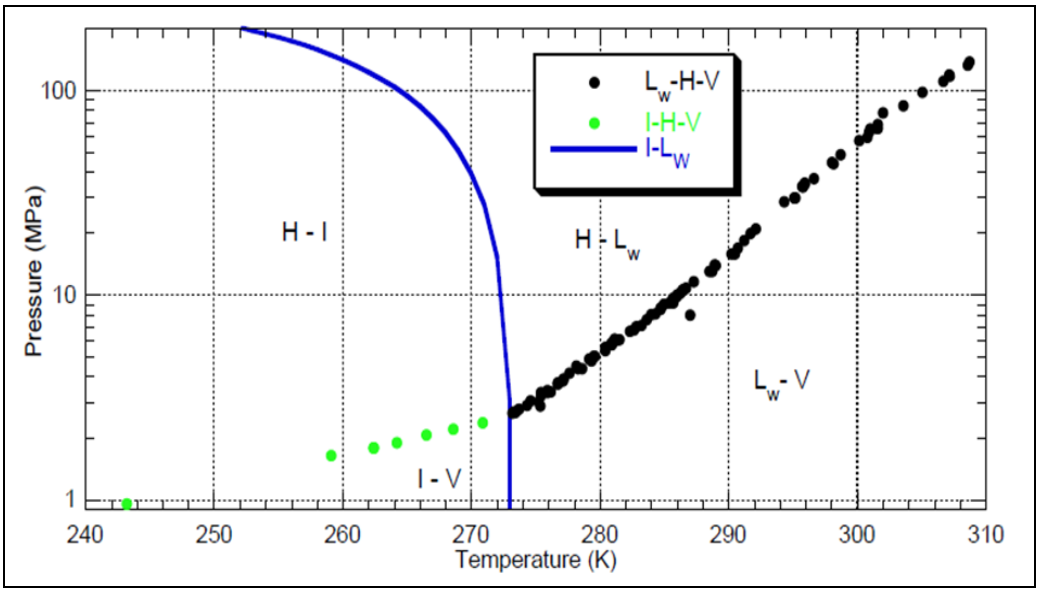

Figure 2. 1 Methane hydrate pressure and temperature stability field. Each point represents an equilibrium temperature and pressure measurement for the given phase combination (H = Gas Hydrate, I=Ice, L_w= Liquid Water, V = Methane Gas) (Helgerud, 2001).

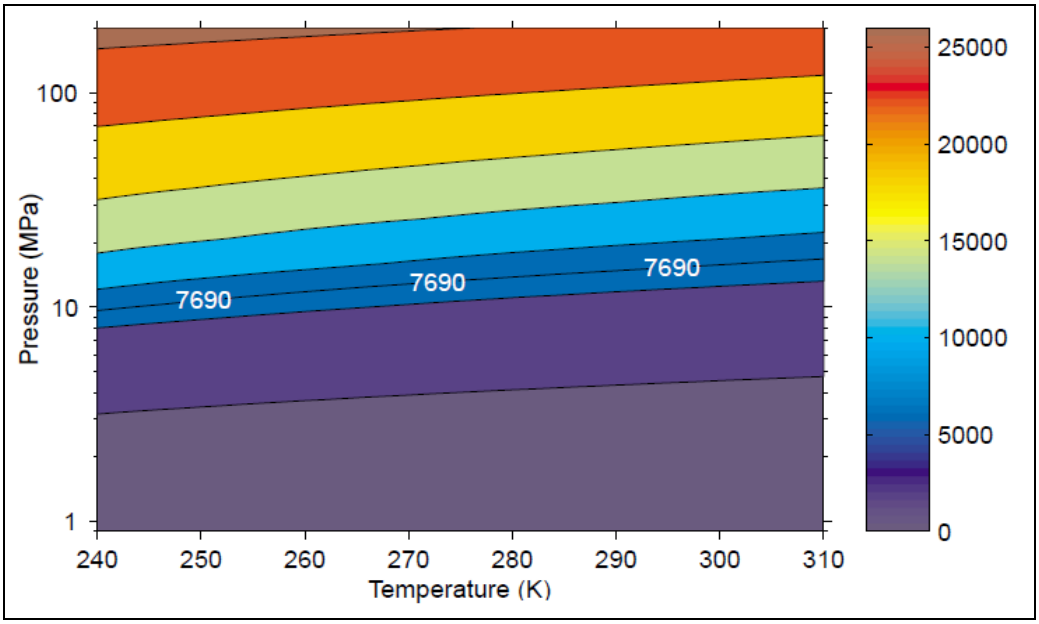

Figure 2. 2 Moles of methane gas in a cubic meter volume as a function of pressure and temperature, calculated after Sychev et al. (1987). The labeled contour (7690) is the theoretical maximum molar density of methane in methane hydrate. Comparing to Figure 2. 1, it can be deduced that at many pressures and temperatures, methane in the gas phase is more compressed than methane in the hydrate phase.

In addition, Figure 2.2 shows the number of moles of methane gas in one cubic meter as a function of pressure and temperature based on the modified equation of state for methane prepared by Sychev *et al.* (1987). The labeled contour is the theoretical maximum number of moles of methane stored in one cubic meter of methane hydrate. This plot suggests that, for pressure values less than about 10-15 MPa, gas hydrate formation represents a compression of the methane relative to the free gas phase. Because, at these pressure values, a cubic meter of methane hydrate structure was able to keep more methane, when compared with the free gas at the same volume. However, as can be seen from this figure, the free gas phase stores more gas molecules at higher pressure and temperature values. In this figure, 10-15 MPa is equivalent to a water depth of 1.0 to 1.5 km with the assumption of water density as 1000 kg/m^3.

2.5 CO_2 Hydrates

When CO_2 is introduced into sufficient amount of water at low temperatures and high pressures CO_2 hydrates may be formed. Figure 2.3 shows the pressure and temperature stability region for CO_2 gas hydrate, which is produced by experiments and model. CO_2 hydrate molecule holds approximately six water molecules and one surrounding CO_2 molecule.

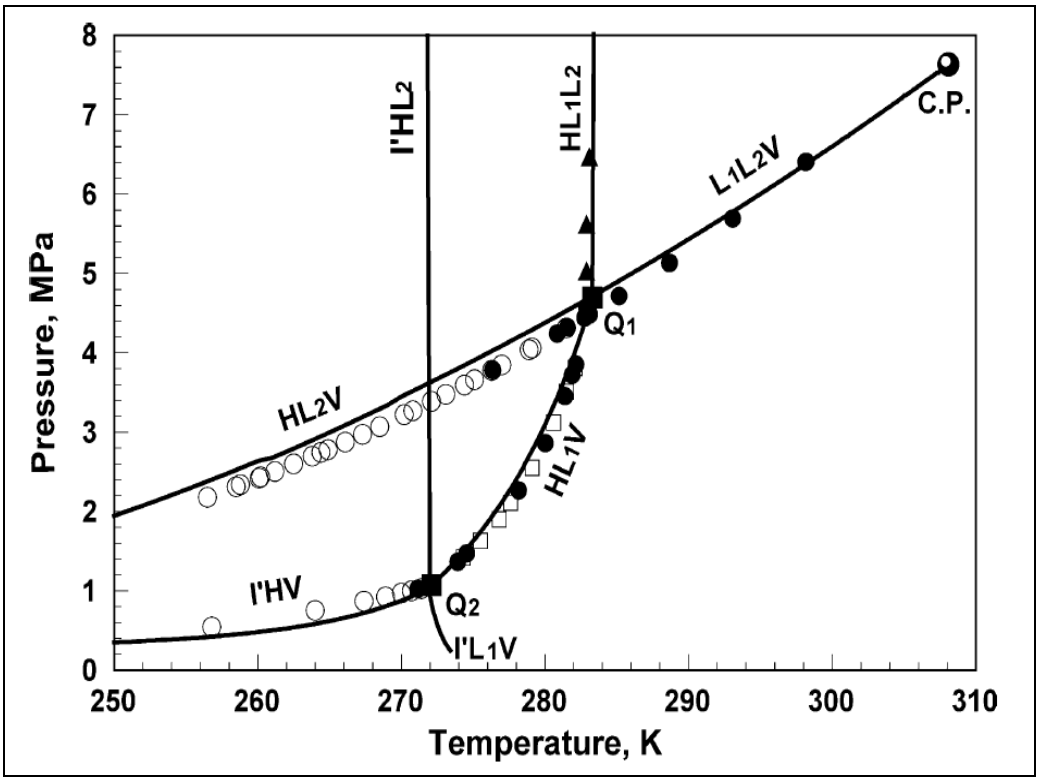

Figure 2. 3 Phase diagram of triple-point (three-phase) equilibria of water–carbon dioxide binary mixtures in the temperature–pressure projection. Solid lines were calculated by the model and symbols represent the experimental data. (H: solid (clathrate hydrate); L_1: carbon dioxide-rich liquid; L_2: water-rich liquid; V: vapor; I: pure ice coexisting with hydrates; Q_1 and Q_2: upper and lower quadruple points; CP: vapor–liquid critical point (Yokozeki, 2004).

Many researches have focused on formation of CO_2 hydrate. For example, Holder *et al*. (2001) established the CO_2 hydrates from a CO_2 rich water solution. As a result, common properties of CO_2 hydrates and some factors which influence the formation of CO_2 hydrates (such as, salinity of sea water) are postulated in the literature. Also, natural occurrences of CO_2 hydrates were reported in the literature and possible presence of CO_2 hydrates at different locations were evaluated (Sakai *et al.*, 1990) (Prieto-Ballesteros *et al.*, 2005). Furthermore, CO_2 hydrates have been the topic of interest for their potential to store large volumes of CO_2 to reduce atmospheric emissions of greenhouse gases as a climate change mitigation strategy (Koide *et al.*, 1997) (House *et al.*, 2006).

2.6 Formation of gas hydrates in porous rock

Formation of hydrate cages is an interfacial reaction. Composition and amount of gas and water, pressure, temperature, degree of supercooling, intensity of creating free gas-water interface, diffusive properties of medium, sorption activity of the forming hydrates, and rate of heat removal are the some basic properties that influence the hydrate formation process. Depending on the structural state of water, the metastable state of the system in static conditions may last many hours even at large supercooling (Makogon *et al.*, 2006).

During hydrate formation, small gas-water clusters (hydrate nuclei) grow and disperse until the nuclei reach a critical size for continued growth (Natarajan, 1994). In general, hydrate nucleation occurs at the vapor/liquid interface as the interface lowers the Gibbs free energy of nucleation and it is the location, where very high concentration of water and gas molecules exists. In the literature, there are two theories for hydrate nucleation. One is labile cluster, i.e. liquid water molecules are arranged around a dissolved solute molecule in a "prehydrate" structure. The other is local structuring, i.e. the "prehydrate" structure consists of a locally ordered water-guest structure rather than individual hydrate cavities, and nucleation arises on the vapor side of the interface (Sloan & Koh, 2008). Although experimental observation is the best way to have an insight on nucleation theories, that kind of experiments are restricted by various factors at present. For this reason, which nucleation theory best describes the hydrate nucleation is still unknown.

Hydrate nucleation is the process which requires a driving force and this driving force is the supersaturation. Supersaturation is defined as the difference in chemical potential between the aqueous solution and the hydrate crystal (Kaschiev & Firoozabadi, 2002). Chemical potential is the term which defines the stability of compound. Negative chemical potential values indicate that the compound is stable. For instance, the chemical potential of gas hydrate is less

than the chemical potential of a hydrate forming gas and water solution when the solution is supersaturated with respect to gas hydrate. As expected, a system always has a tendency to diminish the chemical potential; therefore, a hydrate forming gas and water solution will react to form gas hydrate, when the conditions are suitable for hydrate formation. In porous media, sediments have a crucial role on hydrate formation, since it may alter the thermodynamic conditions for stability (Handa & Stupin, 1992) (Clennell *et al.*, 1999) or it may provide nucleation sites for hydrate to grow (Cha *et al.*, 1988). Also, it is stated that, although most of the ocean floor lies within the hydrate stability region, hydrate formation in ocean is generally confined to the sediments along continental margins (Hyndman & Davis, 1992) (Kvenvolden *et al.*, 1993).

Many researches have been carried out to determine the formation and growth pattern of hydrates in porous media (Kleinberg *et al*., 2003-b). Most of these researches have focused on questions like whether hydrate formation favorably occurs on grain surface or in the center of the pore space and how pore size and surface properties of the host material effect the hydrate growth and distribution. In order to illustrate hydrate distribution relative to pore size and sediment type a capillary-thermodynamic model was proposed by both Clennell *et al*. (1999) and Henry *et al*. (1999).

Experiments indicated that stability of hydrates is dependent on pore size and surface properties of the host sediment grain (Sloan, 1990) (Yousif *et al*., 1991) (Handa & Stupin, 1992). Hydrates are more stable in bulk aqueous conditions when compared with the hydrates in porous medium. Especially, Handa & Stupin (1992) suggested that hydrate in a porous media behaves in much the same way as ice i.e. it requires relatively low temperature and high pressure values.

Within the porous media the thermodynamic potential of chemical components may vary when compared with the bulk conditions. Differences mainly derive from (1) molecular interactions at the pore walls, usually attraction of the fluid molecules by hydrophilic mineral surfaces and (2) the energy required to maintain capillary equilibrium. Bonding of water molecules with hydrophilic mineral surfaces diminishes water activity. As a result, reactions are inhibited in fine grained sediments. It is also stated by Clennell *et al*. (1999) that water adsorption plays an important role in inhibiting hydrate formation especially when gas saturation is high. In addition, capillary forces also inhibit the hydrate formation; therefore, extra thermodynamic drive is required to promote the reaction.

A model established by Winters *et al*. (2004-a) indicated that, hydrate may occur in porous media as pore filling, frame building or cementing agent between grains. Tohidi *et al*. (2001-a), who used synthetic porous media in their experiments, concluded that gas hydrates formed within the center of the pore spaces, rather than the grain surfaces. They suggested that, cementation of grains occurred in regions where the grain size is small (0.070 mm) or where a significant fraction of pore space was filled with hydrate. During cementation stage, saturation, hydrate growth pattern and sediment mineralogy is very important, because presence of hydrate may also inhibit further cementation. Cementation term is often used, when describing the reduction in the permeability of the unconsolidated sediments as a result of hydrate formation. However, cementation means, cementing or attaching the mineral surfaces whereas, it should be kept in mind that hydrate is unable to attach to the mineral surfaces due to incompatibility between the surface hydrogen bonded water molecules and geometrical structures of partial charges on atoms in surfaces of minerals. Therefore, even at high clathrate saturation, a thin film of free water (4 - 6 layers of water molecules with varying degrees of structure) would be enough to separate the hydrate from the mineral surfaces. These nano-scale

channels between the hydrates and the mineral surfaces are insignificant in terms of cementing properties, but important for the thermodynamic stability of the hydrate as long as hydrate is composed of gas under saturated with water or water under saturated with hydrate formers (Birkedal *et al*., 2010). As a result, if majority of the pore space is not filled with hydrate and if growth of hydrate favorably occurs in the center of pores, this means that clathrates restrict the cementing effect on grains**.**

2.7 Change in the permeability in presence of hydrates

One of the most important drawbacks of the modeling hydrate formation and dissociation in porous rock is the change in the permeability in presence of hydrates. Variation of permeability directly affects the hydrate dissociation process; therefore, various numerical and experimental studies have been carried out to clarify this impact. Dissociation of hydrate occurs at the interface of gas and the hydrate. Therefore, if the hydrate zone has certain permeability, then mobile phase will enter into flow paths and increase the contact area between the gas and the hydrate. As a result, increase in the permeability of hydrate phase will also increase the hydrate dissociation rate.

In addition, permeability variation in porous media as a result of hydrate formation should also be understood for the modeling studies. Hydrate formation in porous media decreases the porosity as the hydrate fills the pores. Furthermore, permeability may also decrease since hydrates may plug the migration pathways. At this stage, hydrate growth pattern and its interaction with the rock grains is very important. As it was stated before, hydrate may occur in porous media as pore filling, frame building or cementing agent between grains. If hydrate acts as a cementing agent between grains, decrease in the permeability is expected to be high. However, if hydrate occurs in porous media as pore filling or frame building then the permeability reduction is expected to be small.

Hydrate growth pattern in pores is poorly understood as several factors influence the hydrate formation reaction including saturation of gas in the pores. Acoustic and seismic data are often used in order to determine the growth pattern of hydrate in porous media (Berge *et al*., 1999) (Helgerud, 2001). CCl_3F hydrate was formed by Berge *et al*. (1999) inside unconsolidated sand pack system. By observing the behavior of acoustic wave velocities they noticed two different growth patterns depending on the saturation of the hydrate. They suggested that, hydrate cements the sand grains when the hydrate saturation is higher than 35%. Examination of acoustic data from Blake Ridge, Alaska, and the Mackenzie Delta, where gas saturation in marine sediments is relatively low, showed the pore-filling behavior (Helgerud, 2001). Tohidi *et al*. (2001-a) formed THF, CH_4, and CO_2 hydrate in glass micro models that simulates the porous media. They concluded that, a thin film of water layer formed on grain surfaces and hydrate favorably formed at the center of pores.

Kumar (2005) conducted several experiments to determine the permeability of the porous medium in presence of hydrate by flowing CO_2 through the system. He determined the gas permeability at hydrate saturations of 20%, 25%, 30%, 35%, 42% and 49%. Hydrate saturations less than 35% showed good correlation with theoretical estimates for the grain coating model whereas, hydrate saturation greater than 35% indicated the pore filling tendency of hydrate.

Hydrate formation and dissociation in porous media depends on hydraulic permeability which is the function of hydrate saturation, pore space microgeometry and hydrate growth pattern. Winters *et al*. (2004-a) defined and schematically illustrated (Figure 2.4) the interaction between the hydrate and unconsolidated mineral grains. In this figure, (a) indicates the host sediment before hydrate formation; (b) shows the hydrate growth in the interior of pores partially supporting the frame, (c) illustrates the hydrate formation preferentially at grain contacts, acting as a cement even in small quantities; (d)

demonstrates the cementing behavior of hydrate as the hydrate saturation increases. Also, hydrate growth may occur without noteworthy interaction with the frame.

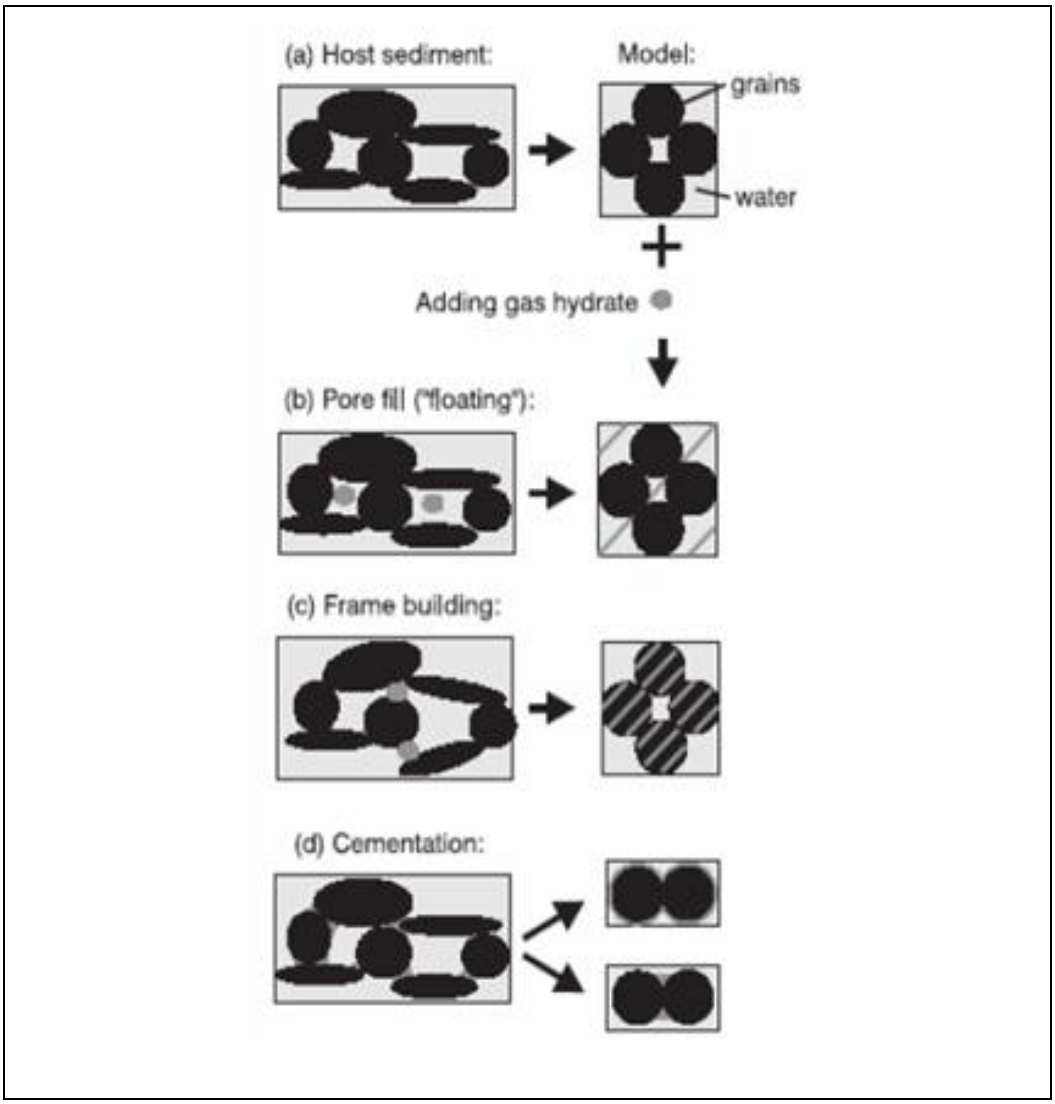

Figure 2. 4 Probable distribution of hydrates in pore structure (Winters *et al*., 2004-a)

2.8 Permeability Models

The permeability of a porous media that includes certain amount of hydrate is related to the hydrate growth pattern within the pore space. Several models have been developed to represent the permeability reduction in the porous media.

2.8.1 Parallel Capillary Models

Scheidegger (1960) proposed the simplest model of a porous medium that consists of a bunch of straight, parallel cylindrical capillaries having inner radius a and length L. Therefore, fluid flow through a unit cross-sectional area containing n number of such capillaries can be estimated with the following formula;

$$q = \frac{n\pi a^4}{8\mu}\frac{\Delta P}{L} \tag{2.1}$$

where μ is the dynamic viscosity and $\Delta P / L$ is the pressure gradient. The hydraulic permeability, k is defined by the following formula;

$$q = \frac{k}{\mu}\frac{\Delta P}{L} \tag{2.2}$$

Number of capillaries per unit cross-sectional area, n, is related to the porosity;

$$\phi = n\pi a^2 \tag{2.3}$$

Therefore by using the above equations in the absence of hydrates, permeability can be estimated with the following equation;

$$k_0 = \frac{\phi a^2}{8} \tag{2.4}$$

2.8.1.1 Hydrate Coats Capillary Walls

When hydrate coats the walls of the capillaries, radius of the water-filled pore space will be reduced to a_r . Therefore equation takes the following form;

$$q = \frac{n\pi a_r^4}{8\mu}\frac{\Delta P}{L} \tag{2.5}$$

By using the Equation (2.3), the permeability to water can be defined with the below equation;

$$k(S_h) = \frac{\phi a_r^4}{8a^2} \tag{2.6}$$

where S_h denotes the volume fraction of pore space occupied by hydrate, and

$$a_r^2 = a^2(1-S_h) \tag{2.7}$$

therefore,

$$k(S_h) = \frac{\phi a^2(1-S_h)^2}{8} \tag{2.8}$$

The relative permeability to water is given as,

$$k_{rw} = \frac{k(S_h)}{k_0} \tag{2.9}$$

For the pore filling hydrate,

$$k_{rw} = (1-S_h)^2 = S_w^2 \tag{2.10}$$

2.8.1.2 Hydrate Occupies Capillary Centers

Lamb (1945) proposed the simplest permeability model where hydrate avoids coating the grain surfaces and forms in the centers of pores. In this model, pore radius is denoted by a, and the radius of the formed hydrate is b. Therefore, this model assumes that there is a flow path for water between the hydrate and the grain surface. In this case, volumetric fluid flow rate takes the following form,

$$Q = \frac{\pi}{8\mu}\frac{\Delta P}{L}\left[a^4 - b^4 - \frac{(a^2 - b^2)^2}{\log\left(\frac{a}{b}\right)}\right] \tag{2.11}$$

The hydrate saturation is,

$$S_h = \left(\frac{b}{a}\right)^2 \tag{2.12}$$

By combining the above equations, permeability of a material composed of a bunch of capillaries is,

$$k(S_h) = \frac{\phi a^2}{8}\left[1 - S_h^2 - \frac{(1 - S_h)^2}{\log\left(\frac{1}{S_h^{0.5}}\right)}\right] \tag{2.13}$$

The relative permeability to water is given as,

$$k_{rw} = 1 - S_h^2 + \frac{2(1 - S_h)^2}{\log(S_h)^2} = 1 - (1 - S_w)^2 + \frac{2S_w^2}{\log(1 - S_w)} \tag{2.14}$$

2.8.2 Kozeny Grain Models

Permeability prediction for granular media is different than that for channels. Channels are assumed to be regular whereas, the pore spaces are irregular and it is hard to define straight-line distance L of the flow paths. To represent the permeability of the pore spaces the Kozeny family of hydraulic permeability equations is a good point to start (Scheidegger, 1960). There are a number of equivalent forms (Hearst *et al.*, 2000), where A denotes the internal surface area of the pore space: (1) expressed in terms of the ratio of the pore surface area to the pore volume;

$$k = \frac{\phi}{v\tau(A/V)^2_{pore}} \tag{2.15}$$

(2) expressed in terms of the ratio of the pore surface are to the overall rock volume;

$$k = \frac{\phi^8}{v\tau(A/V)^2_{rock}} \tag{2.16}$$

(3) expressed in terms of the ratio of the pore-surface area to grain volume;

$$k = \frac{\phi^8}{vr(1-\phi)^2(A/V)^2_{grain}} \tag{2.17}$$

where v is a shape factor, which is on the order of unity and tortuosity is,

$$\tau = \left(\frac{L_a}{L}\right)^2 \tag{2.18}$$

where L_a represents the length of the flow path, which is longer than the straight-line distance L associated with the pressure drop ΔP. Hearst *et al.*,

(2000) introduced the following relation between the tortuosity τ, the electrical formation factor F, and the porosity ϕ is;

$$\tau = F\phi \tag{2.19}$$

Combination of the above equations with the assumption of the shape factor v does not change with hydrate saturation gives;

$$k_{rw} = \frac{F_o}{F(S_h)}\left(\frac{A_o}{A(S_h)}\right)^2\left(\frac{V(S_h)}{V_o}\right)^2 \tag{2.20}$$

In order to estimate the Kozeny grain-pack relative permeability from the above equation, change in the electrical formation factor and the surface-to-volume ratio in the presence of hydrate should be well understood. For this reason, Spangenberg (2001) studied the electrical formation factor for various hydrate growth pattern and introduced the below equation to illustrate the relationship between the formation factor in a hydrate saturated medium, $F(S_h)$, and in a fully water-saturated rock, F_0;

$$\frac{F(S_h)}{F_0} = (1 - S_h)^{-n} \tag{2.21}$$

where n is the Archie saturation exponent. Furthermore, replacement of the pore water volume ratio, $V(S_h)/V_0 = 1 - S_h$ in the above equation gives;

$$k_{rw} = (1 - S_h)^{n+2}\left(\frac{A_0}{A(S_h)}\right)^2 \tag{2.22}$$

2.8.2.1 Hydrate Coats Grains

As the hydrate coats the grain surfaces, the surface area of the water-filled section diminishes. In this case, the cylindrical pore model is the simplest approach. If the pore radius for $S_h = 0$ is a and the pore radius in the presence of hydrate is a_r, then the surface area ratio can be defined as;

$$\frac{A_0}{A(S_h)} = \frac{a}{a_r} \tag{2.23}$$

and since $S_h = 1 - (a_r / a)^2$

$$\frac{A_0}{A(S_h)} = (1 - S_h)^{-0.5} \tag{2.24}$$

Therefore, Equation (2.22) takes the following form;

$$k_{rw} = (1 - S_h)^{n+1} = S_w^{n+1} \tag{2.25}$$

For this model, Spangenberg (2001) gives the saturation exponent n as 1.5 for $0 < S_h < 0.8$ $(1 > S_w > 0.2)$. He stated that, for S_h values greater than 0.8, the saturation exponent diverges. However, for these values, the relative permeability to water is very small, and the effect of increase in the saturation exponent is negligible. For this reason, Equation (2.10) and Equation (2.25) are very similar though their models have distinct origins.

2.8.2.2 Hydrate Occupies Pore Centers

As the hydrate grows in the pore centers, the pore surface area increases. In the cylindrical model;

$$A(S_h) = A_0(1 + S_h^{0.5}) \tag{2.26}$$

So,

$$k_{rw} = \frac{(1 - S_h)^{n+2}}{(1 + S_h^{0.5})^2} = \frac{S_w^{n+2}}{(1 + (1 - S_w)^{0.5})^2} \tag{2.27}$$

Spangenberg (2001) indicated that, neglecting the capillary effects, the saturation exponent increases from $n = 0.4$ at $S_h = 0.1$ to unity at $S_h = 1$.

2.8.3 Other Models

Numerical reservoir simulators have been developed to mimic the response of hydrate bearing formations to change in the temperature and pressure. These simulators take into account the formation and dissociation of gas hydrate, and large-scale flows of heat, water and gas. More detailed information about the reservoir simulators can be found in the paper writtten by Sawyer *et al*. (2000).

2.8.3.1 University of Tokyo Model

Model developed by Masuda *et al.* (1997) takes the capillary tube as a starting point. In this model, it is assumed that the hydrate line the walls of the capillary and below equation is derived;

$$k_{rw} = (1 - S_h)^N = S_w^N \tag{2.28}$$

where $N = 2$ is the result of the geometrical computation. Masuda *et al.* (1997) indicated that N can be increased to consider the preferential accumulation of

hydrate in pore throats. Masuda *et al.* (1997) selected $N = 10$ and $N = 15$, but there is not any explanation about these choices.

2.8.3.2 Lawrence Berkeley National Laboratory Model

The EOSHYDR/THOUGH2 software which is developed by Moridis *et al.* (1998) uses a relative permeability model published by Van Genuchten (1980).

$$k_{rw} = \bar{S}_w^{1/2}\left[1-(1-\bar{S}_w^{1/m})^m\right]^2 \tag{2.29}$$

with

$$\bar{S}_w = \frac{S_w - S_r}{1 - S_r} \tag{2.30}$$

where S_r is the irreducible water saturation. Parker *et al*. (1987) stated that $m = 0.46$ for sands, silts and sandstones.

2.9 Stability of Gas Hydrates

Hydrate formation is affected by various parameters; such as, temperature, pressure, ionic strength of the water and composition and amount of hydrate formers (Sloan, 1998-c). Figure 2.5 shows the required pressure and temperature values for the stability of pure methane hydrate. As can be seen from this figure, at relatively high temperatures such as 15 °C, methane hydrate requires very high pressure values (>10 MPa). In addition, figure shows the influence of CO_2, H_2S, ethane and propane on the methane hydrate stability curve. Presence of these parameters shifts the stability curve to a higher temperature at a given pressure, increasing the stability zone of methane hydrate. On the other hand, presence of dissolved ions in the pore fluids shifts the stability curve to a lower temperature at a given pressure, decreasing the stability zone of methane hydrate. It was also indicated that, temperature values

for the stability of methane hydrate are 1.1 °C lower in water with 33% NaCl concentration when compared with the hydrate formation in pure water (Dickens & Quinby-Hunt, 1994).

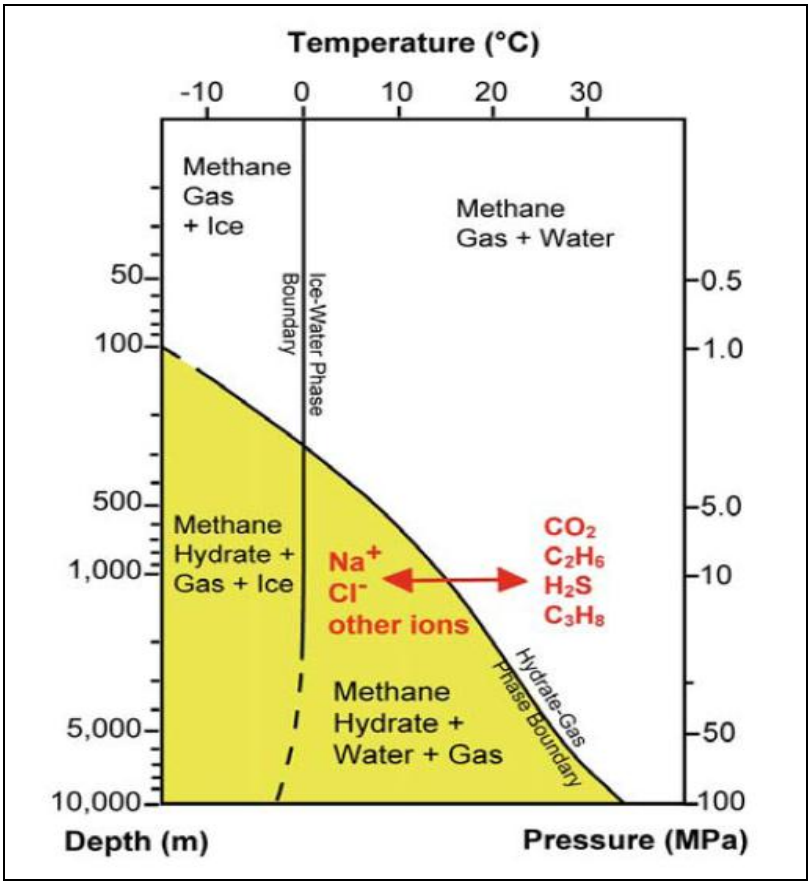

Figure 2. 5 Phase diagram showing the boundary between methane hydrate (in yellow) and free methane gas (white) for a pure methane/H_2O system (Kvenvolden, 1998)

Henry *et al.* (1999) estimated the influence of pore size on the stability of the empty hydrate structure. Also, they used this information to find the temperature depression values for different pore size at a given pressure of the methane clathrate equilibrium. During their studies, surface tension between hydrate and water was assumed to be similar with the surface tension between ice and water (approximately 26-30 mJ/m^2) whereas, Zatsepina & Buffett

(2001) concluded that surface tension between hydrate and water is 18 times smaller than the surface tension between ice and water. Another assumption was that, enthalpy of formation of ice is close to enthalpy of formation of bulk hydrate; however, Handa & Stupin (1992) experimentally observed that the enthalpy values required for ice can be considerably less than enthalpy values required for bulk hydrate. Clennell *et al*. (1999) stated that, capillary pressure of free gas bubbles which is at the equilibrium with water in the microporous media may be on the order of several MPa. For this reason, fugacity (escaping tendency) of methane gas increases for any particular values of the pore water pressure, which also leads the rise of the methane concentration in the water. This mechanism, called capillary supersaturation, helps the stability of hydrate. Henry *et al.* (1999) investigated that, when gas bubbles and clathrates exist in a given pore size, then the net effect is increase in the stability of hydrate when compared with the bulk conditions.

Handa *et al*. (1992) stated that, synthetic porous materials that are used in experiments have single pore size due to narrow pore size distribution. However, Clennell *et al*. (1999) stated that, real sediments have a broader pore size distribution and a nonwetting phases (gas, ice, hydrate) favorably fill the largest pores available to minimize the surface energy. This means that, magnitude of surface effects in sediment depends on the fraction of pore space filled by nonwetting phases. Therefore, gas-hydrate-pore water equilibrium is also related with the fraction of each nonwetting phase on the pores.

The United States Geological Survey (USGS), a scientific agency of the United States government, has established a program to combine field, laboratory, and modeling results by measuring physical properties of sediments containing natural and laboratory formed gas hydrate. This study was also helpful since it enables comparison of observations obtained from both field and laboratory. For example, direct observations and modeling shows that laboratory-formed

methane gas hydrate cements Ottawa sand, whereas natural hydrate may not. This is important since cementation has a profound effect on acoustic velocity and other sediment behavior, including shear strength. Winters *et al*. (2004-b) suggested that, different results that are obtained from field and laboratory may result from the different formation mechanisms at in situ and the lab. For example, in field, hydrate is generally formed by means of gas dissolved in the aqueous phase; however, in the lab, hydrate is formed from bubble-phase methane. Cementation in the lab may also be caused by hydrate forming at locations coated with water molecules, that is, on grain surfaces and at grain contacts.

In terms of the solid-solution model, hydrate stability is directly dependent on the activity of water (van der Waals & Platteew, 1959). When the water activity diminishes, higher pressures for the corresponding temperature or lower temperatures for the corresponding pressure are required for the hydrate formation. This phenomenon is observed in systems that also include inhibitors as the inhibitors depress the freezing point of water resulting decrease in water activity. Handa *et al*. (1992) stated that this phenomenon can also be observed when water confined in small pores as the freezing point of pure water is also depressed considerably when confined in small pores. As a result, influences of the presence of geometrical constraints on the activity of water are almost same with the effects of inhibitors. In the nature, presence of inhibitors, geometrical constraints, amount of dissolved salts and capillary forces in the compacted sediments are the main parameters that alter the activity of water. In the light of this information, it can easily be said that the phase-equilibria and thermodynamic properties of hydrates formed inside the porous media and bulk conditions are different. Consequently, the experimental results on hydrates formed in bulk conditions may not valid for hydrates in porous media. Furthermore, a significant amount of water in confined space is often found to be present as bound water and does not undergo the freezing transition. In

general, this water will not enter into hydrate formation reaction under the same pressure-temperature (P-T) conditions as the pore water, and the naturally occurring hydrates will also be associated with bound or unfrozen water (Handa & Stupin, 1992).

2.10 Hydrate Formation Conditions

It is assumed that either abundant water or excess free gas exists within the stability region. For this reason, only two phases will be present at the stability region. For instance, in Polar Regions, where the temperatures are below the freezing point, methane hydrate with methane gas is likely to be present. In oceanic regions, where the temperatures are higher than the freezing point of water, methane hydrate with water is likely to be present. In the natural environment, water is generally abundant; therefore, the availability of gas is the limiting factor for the hydrate occurrence. In the nature, where hydrate formation is expected, hydrostatic pressure is generally greater than the three-phase hydrate-liquid-gas or hydrate-ice-gas equilibrium gas pressure. As a result, hydrostatic pressure will be transmitted to any free gas present and this free gas which is exposed hydrostatic pressure greater than the hydrate formation pressure will react with the ice or water to form hydrate until consuming all the gas in free phase. Enns *et al.* (1965) showed that when hydrostatic pressure is applied on a solution of gas in water it will squeeze the gas out of solution and reduce its solubility below the saturation solubility with respect to the free gas phase. In analogous with this case, it can be expected that at the disappearance of the gas phase, hydrate formation should still continue until the concentration of dissolved gas falls below its saturation value to a value corresponding to the hydrostatic pressure.

There have been some debates about the necessary conditions for the hydrate formation. It has frequently been said that methane undergoes an abrupt fall in solubility in liquid water when hydrates begin to form. According to this

approach, hydrate former should be present in the gaseous state and liquid water should be supersaturated with gas before hydrates can form. Handa (1990) stated that, both observations are actually thermodynamically incorrect. In addition, Miller (1974) proved that the presence of free gas is not compulsory for the hydrate formation by calculating the effect of hydrostatic pressure on the solubility of methane in liquid water in equilibrium with hydrate, without letting for a change of hydrate composition with pressure. Understanding of the equilibrium of methane solubility is important as the minimum amount of methane required for formation of hydrates is a function of solubility. Zatsepina & Buffet (1997) stated that, when the hydrate is present, gas solubility decreases sharply with decrease in temperatures. It can be deduced from this phenomenon that hydrate directly forming from aqueous solution, without need for free gas. Moreover, experiments conducted by Handa & Stupin (1992) proved that the hydrate can form in porous media under realistic conditions when free gas is absent.

In the literature, there exist several experiments in which hydrates are formed from an aqueous solution in a porous medium. During these experiments, free gas was not present in the porous medium prior to hydrate formation. Results of these experiments indicated that, the hydrate can form in an aqueous solution, even when the dissolved gas concentration is 40% lower than the peak concentration that occurs when the hydrate forms in the presence of free gas (Buffet & Zatsepina, 2000).

Gas solubility in water is directly related with the presence of hydrate. When hydrate is absent at high temperatures, experiments showed that solubility increases with decreasing temperature. On the other hand, when hydrate is present gas solubility decreases sharply with decreasing temperature (Zatsepina & Buffet, 1997). When the gas concentrations are low, thermodynamic arguments are questioned due to the common belief that hydrate crystals may be

difficult to nucleate at low gas concentrations. On the contrary to the liquid phase, hydrate structure requires high concentration of gas to become stable. Therefore, especially at the critical gas concentrations, size of the nuclei that can initiate hydrate growth, may become critical issue. In addition to the experiments, gas solubility in presence of hydrate can be estimated by means of equilibrium thermodynamics. These estimates suggest that, gas solubility in liquid phase decreases as the temperature is reduced, whereas this trend cannot continue indefinitely. After a certain point, the likelihood of bringing together a sufficient number of widely spaced gas molecules into a small nucleation volume become too low to permit hydrate nucleation (Hwang *et al.*, 1990). Therefore, it can be concluded that for a given pressure value there is a minimum temperature value to initiate hydrate formation from the aqueous solution. Below this temperature value, concentration of widely dispersed gas molecules in liquid phase becomes too low to initiate hydrate nucleation. For this reason, it can also be said that temperature is more significant when compared with pressure for the equilibrium conditions in marine sediments (Zatsepina & Buffet, 1997).

CHAPTER 3

HYDRATE STABILITY REGION CALCULATIONS

3.1 Hand Calculation Methods

3.1.1 The gas gravity method

According to Carroll & Duan (2009), for paraffin hydrocarbons there exists a good correlation between hydrate formation pressure and the molar mass of the hydrate former. For this purpose, hydrate formation conditions at 0 °C was experimentally investigated in order to see whether there is a correlation for other hydrate formers. As a result, it was found that hydrogen sulfide, carbon dioxide, and nitrogen shows great deviations from the correlation trend line that was constructed for paraffin hydrocarbons.

3.1.1.1 Molar mass

Figure 3.1 illustrates the hydrate formation pressure at 0 °C as a function of the molar mass. As can be seen from the below graph, there is a strong correlation between these two quantities for the hydrocarbon components. A basic equation that represents the correlation between the molar mass and the hydrate pressure is stated below;

$$\log P = 3.03470 - 2.23793 * \log M \tag{3.1}$$

where P is in MPa and M is in kg/kmol (or equivalently g/mol).

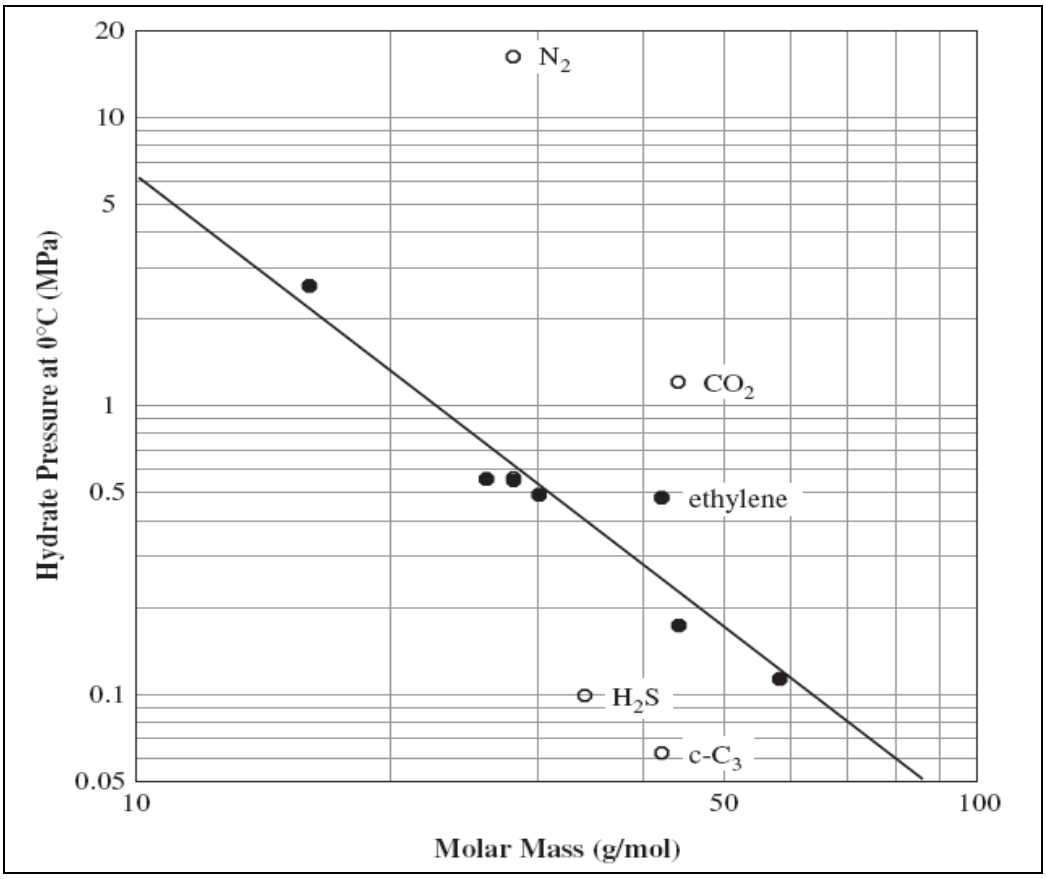

Figure 3. 1 Hydrate pressure at 0 ^{o}C as a function of the molar mass (Carroll & Duan, 2009)

Propylene is the only hydrocarbon component that greatly deviates from the trend line, also ethylene shows some deviation as well, but it is considerably low when compared with the propylene. On the other hand, three non-hydrocarbon components exhibit significant deviation from the trend line. Equation above over predicts the hydrate pressure of hydrogen sulfide while under predicts the hydrate pressure for both nitrogen and carbon dioxide. For this reason, when using simply gas gravity method for predicting hydrate forming pressure, components such as nitrogen, carbon dioxide, and hydrogen sulfide should be treated as special components and requires corrections.

3.1.1.2 Boiling point

Relationship between the boiling point and the hydrate formation conditions was also considered as the boiling point related with the volatility of the hydrate former. Figure 3.2 shows the change in the hydrate formation conditions as a function of the boiling points.

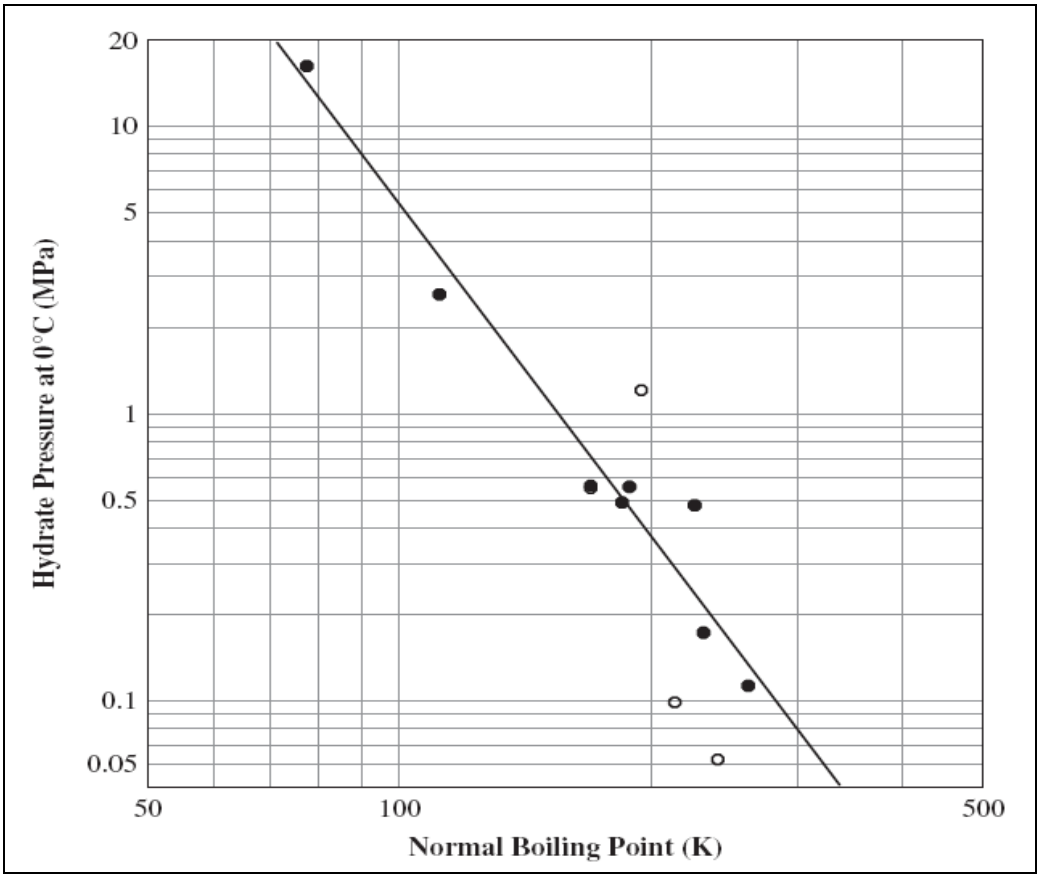

Figure 3. 2 Hydrate pressure at 0 °C as a function of the normal boiling point (Carroll & Duan, 2009)

3.1.1.3 Density

Another approach was the observation of the correlation between hydrate formation conditions and the density of hydrate former. Figure 3.3 shows the change in the hydrate formation pressure at 0 °C as a function of the density.

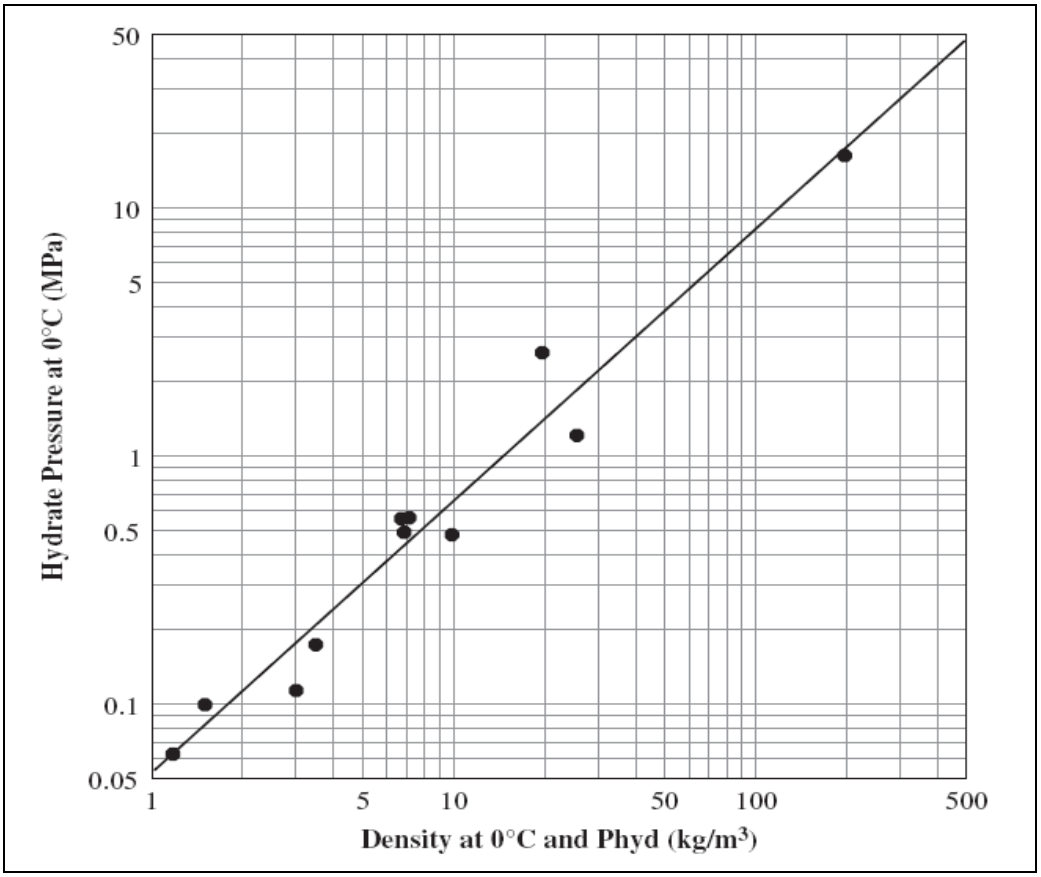

Figure 3. 3 Hydrate pressure at 0 °C as a function of the density (Carroll & Duan, 2009)

3.1.2 The K-factor method

The second and perhaps the most popular hand calculation method is the K-factor method that was developed by Carson & Katz (1942). The K-factor can be defined as follows;

$$K_i = y_i / s_i \tag{3.2}$$

where y_i and s_i are the mole fractions of component i in the vapor and hydrate phases, respectively. Therefore, the K-factor can also be defined as the ratio of the component in the vapor phase to the hydrate phase. These mole fractions are on a water-free basis; therefore, water saturation is ignored in the calculations and it is assumed that sufficient amount of water is present in the system.

The basic idea behind this technique is that determination of hydrate formation pressure when the temperature and gas composition is given. Similarly, hydrate formation temperature can also be calculated when the composition and the temperature are given.

The functions that should be solved are;

$$f_1(T) = 1 - \sum y_i / K_i \tag{3.3}$$

$$f_2(P) = 1 - \sum y_i / K_i \tag{3.4}$$

Depending on the objective, suitable equations should be selected. Then, iterations should be conducted until the summation is equal to unity.

Until 1975, the K-factor method was widely used in order to estimate the hydrate formation conditions. However, after the emergence of computer based rigorous programs, this method has lost its popularity. Nevertheless, it is very

accurate for predicting hydrate locus of pure methane, ethane, carbon dioxide, and hydrogen sulfide (Carroll & Duan, 2009).

Furthermore, researchers argued about the possibility of including the hydrate type in the K-factor method. For example, Mann *et al*. (1989) presented two sets of K-factors for the hydrate formers, Structure I and Structure II. However, this method has not gained acceptance in the gas processing industry.

3.1.3 Baillie-Wichert Method

Another hand calculation technique for predicting hydrate formation conditions is proposed by Baillie & Wichert (1987). This method is based on charts that are more complex than the Katz gravity method. This method utilizes the gas gravity for the prediction of hydrate formation conditions.

Furthermore, this method also considers the presence of hydrogen sulfide (up to 50 mol%) and propane (up to 10%). The influence of propane comes in the form of a temperature correction, which is a function of the pressure and the H_2S concentration. In addition, this method is developed for use with sour gas, which is a significant advantage over other methods. However, this method is only applicable for gases with gravity between 0.6 and 1.0.

3.1.4 Other Correlations

3.1.4.1 Makogon (1981)

Makogon (1981) introduced a basic correlation to estimate the hydrate formation pressure when the temperature and the gas gravity are given for paraffin hydrocarbons. His correlation is as shown below;

$$\log P = \beta + 0.0497(t + kt^2) - 1 \tag{3.5}$$

where P is in MPa, t is in Celsius.

Makogon (1981) also introduced complicated graphical correlations for β and k, but Elgibaly & Elkamel (1998) provided the simple correlations;

$$\beta = 2.681 - 3.811\gamma + 1.679\gamma^2 \tag{3.6}$$

$$k = -0.006 + 0.011\gamma + 0.011\gamma^2 \tag{3.7}$$

where γ is the gas gravity.

3.1.4.2 Kobayashi et al. (1987)

Kobayashi *et al*. (1987) presented the following complicated equation for estimating hydrate formation conditions as a function of the gas gravity;

$$\begin{aligned} 1/T = {} & 2.7707715*10^{-3} - 2.782238*10^{-3}*\ln(P) - 5.649288*10^{-4}\ln\gamma \\ & - 1.298593*10^{-3}*\ln(P)^2 + 1.407119*10^{-3}\ln(P)\ln(\gamma) \\ & + 1.785744*10^{-4}\ln(\gamma)^2 + 1.130284*10^{-3}\ln(P)^3 \\ & + 5.9728235*10^{-4}\ln(P)^2\ln(\gamma) - 2.3279181*10^{-4}\ln(P)\ln(\gamma)^2 \\ & - 2.6840758*10^{-5}\ln(\gamma)^3 + 4.6610555*10^{-3}\ln(P)^4 \\ & + 5.5542412*10^{-4}\ln(P)^3\ln(\gamma) - 1.472765*10^{-5}\ln(P)^2\ln(\gamma)^2 \\ & + 1.393808*10^{-5}\ln(P)\ln(\gamma)^3 + 1.4885010*10^{-5}\ln(\gamma)^4 \end{aligned} \tag{3.8}$$

3.1.4.3 Motiee (1991)

Motiee (1991) introduced simple correlation for hydrate formation pressure and temperature calculation when the gas gravity is given.

$$\begin{aligned} T = {} & -283.24469 + 78.99667\log(P) - 5.352544\log(P)^2 \\ & + 349.473877\gamma - 150.854675\gamma^2 - 27.604065\log(P)\gamma \end{aligned} \tag{3.9}$$

where the temperature, T, is in Rankine, the pressure, P, is in psia, and γ is the gas gravity, dimensionless.

3.1.4.4 Towler & Mokhatab (2005)

Towler & Mokhatab (2005) developed a simple equation for estimating hydrate temperatures as a function of the pressure and the gas gravity;

$$T = 13.47\ln(P) + 34.27\ln(\gamma) - 1.675\ln(P)\ln(\gamma) - 20.35 \quad (3.10)$$

To sum up, each hand calculation method has its own benefits and drawbacks. However, methods involving charts may give less accurate results due to difficulties in chart reading process.

3.2 Computer methods

3.2.1 Phase equilibrium

The phase equilibrium concept, which was established by Gibbs a century ago, is still used as a basis in hydrate equilibrium calculations. This concept involves three fundamental criteria. Firstly, the temperature and pressure of the phases are equal. Secondly, the chemical potentials of each of the components in each of the phases are equal. Finally, the global Gibbs free energy is a minimum. These three main criteria can be applied to the phase equilibrium involving hydrates and constitutes the basis for the models that involve hydrate equilibrium calculations.

Most of the equilibrium calculations shifted from chemical potentials to fugacities; however, hydrate calculations are generally carried out based on chemical potentials. For the hydrate calculations, the free energy minimization is also important, whereas stable hydrate phase (Type I, II, or even H) results in a minimum in the Gibbs free energy. For this reason, there is no point to check the third criteria when the first and the second criteria have been already met.

From a thermodynamic point of view, hydrate formation can be modeled as a process that requires two steps. During the first step, pure water forms the empty hydrate cage. Although this step is hypothetical, it is still beneficial for the calculations. During the second step hydrate former fills the empty hydrate lattice. The process can be summarized in following way;

pure water (α) => empty hydrate lattice (β) => filled hydrate lattice (H)

The change in chemical potential for this process can be stated as;

$$\mu^H - \mu^\alpha = (\mu^H - \mu^\beta) + (\mu^\beta - \mu^\alpha) \tag{3.11}$$

where μ denotes the chemical potential and the superscripts represents the phases. The first term at the right hand sight of the equation represents the stabilization of the hydrate lattice. Estimation of this term is the main difference between the various models. The second term at the right hand sight of the equation represents a phase change for the water and can be calculated by regular thermodynamic techniques. This term can be determined as;

$$\frac{\mu^\beta - \mu^\alpha}{RT} = \frac{\Delta\mu(T,P)}{RT} = \frac{\Delta\mu(T_o,P_o)}{RT_o} - \int_{T_o}^{T} \frac{\Delta H}{RT^2}\,dT + \int_{P_o}^{P} \frac{\Delta V}{R\bar{T}}\,dP \tag{3.12}$$

where R is the universal gas constant, T is the absolute temperature, P is the pressure, H is the enthalpy, V is the molar volume, the subscript 0 represents a reference state, and the Δ terms denotes the change from a pure water phase (either liquid or ice) to a hydrate phase (either Type I or II). The bar over the temperature in the last term shows that this is an average temperature. The various properties related to hydrates and above formula have been introduced in the literature (Pedersen *et al*., 1989).

3.2.2 Van Der Waals & Platteeuw

The first and the foremost model for calculating hydrate formation conditions was developed by (van der Waals & Platteeuw, 1959). According to this statistical model, concentration of the non-water species in the hydrate was treated in a manner similar to the adsorption of a gas onto a solid. For a single guest molecule, this term can be predicted as;

$$\mu^H - \mu^\beta = RT \sum_i v_i \ln(1 - Y_i) \tag{3.13}$$

where v_i denotes the number of cavities of type I, and Y denotes the probability function. The Y is the probability that a cavity of type i is occupied by a guest molecule and is given by;

$$Y_i = \frac{c_i P}{1 + c_i P} \tag{3.14}$$

The c_i in the above equation is a function of the guest molecule and the cage occupied, and P is the pressure.

3.2.3 Parrish & Prausnitz

Van der Waals & Platteeuw method is a good approach for performing hydrate calculations; however, it is not considered satisfactory for engineering calculations. One of the first models that developed for engineering calculations was that of Parrish & Prausnitz (1972).

Basically, there exist two main differences between the original form of the van der Waals & Platteeuw model and Parrish & Prausnitz model. Firstly, model proposed by Parrish & Prausnitz extended the model to mixtures of hydrate formers. This is done as follows;

$$\mu^H - \mu^\beta = RT \sum_i v_i \ln(1 - \sum_K Y_{Ki}) \tag{3.15}$$

where the second sum is over all components. Therefore, the probability function for a component takes the following form;

$$Y_{Ki} = c_i P_K \Big/ (1 + \sum_j c_{ij} P_j) \tag{3.16}$$

where the summation is over all components and the P followed by a subscript is the partial pressure for a given component.

The other components are also covered in this term as they are trying to fill the same cages. Therefore, existence of other guest molecule will decrease the probability that a given guest molecule can enter the hydrate structure.

Furthermore, Parrish & Prausnitz modified the probability function by replacing the partial pressure with the fugacity. From the thermodynamic point of view, there is no simple definition for the term fugacity. However, it can be considered as a "corrected" pressure, which takes into account for non-idealities. Therefore, putting the fugacity term into the equation in place of partial pressure results in;

$$Y_{Ki} = c_i \hat{f}_K \Big/ (1 + \sum_j c_{ij} \hat{f}_j) \tag{3.17}$$

where $\hat{f}_K$ is the fugacity of component i in the gaseous mixture.

This modification enables the model to consider the non-idealities in the gas phase; therefore, the model becomes applicable for higher pressures also.

Moreover, different set of c_i's is required for the fugacity model than for the pressure model to adjust the changes and to improve the overall fit of the model.

3.2.4 Ng & Robinson

Another advanced model was prepared by Ng & Robinson (1977) that can be used to predict the hydrate formation in equilibria with a hydrocarbon liquid.

In order to predict the hydrate formation equilibria with a hydrocarbon liquid, phase equilibrium equations should be modified by changing the enthalpy and volume. In the model proposed by Ng & Robinson, the fugacities were calculated using the equation of state of Peng & Robinson (1976). This equation of state can be used for both gases and the non-aqueous liquids. Also, some minor adjustments were made to the parameters in the model to improve the overall fit of the model.

Furthermore, equation of state proposed by Soave (1972) is also applicable for both gas and liquid state. Moreover, new versions of the Parrish & Prausnitz method are also applicable to systems containing liquid formers.

3.3 Thermodynamic Model

Method for predicting the hydrate equilibrium conditions is based on the criterion of equality of chemical potential as below;

$$\mu_w = \mu_H \tag{3.18}$$

where μ_H is chemical potential of water in hydrate phase and μ_w is chemical potential of water in the water rich or ice phase.

By using the μ_β, the chemical potential of an unoccupied hydrate lattice, as the reference state, the condition of equilibrium can be rewritten as,

$$\mu_\beta - \mu_w = \mu_\beta - \mu_H \tag{3.19}$$

$$\Delta\mu_w = \Delta\mu_H \tag{3.20}$$

Calculation of $\Delta\mu_w$: The chemical potential difference as a function of pressure and temperature can be written as,

$$d\left(\frac{\Delta\mu_w}{RT}\right) = -\left(\frac{\Delta H_w}{RT^2}\right)dT + \left(\frac{\Delta V_w}{RT}\right)dP \tag{3.21}$$

where ΔH_w and ΔV_w are enthalpy and volume difference between ice or water and empty hydrate.

Holder *et al*., (1980) provided a simple method to determine the effect of temperature, pressure, and composition on $\Delta\mu_w$ as below,

$$\frac{\Delta\mu_w}{RT} = \frac{\Delta\mu(T,P)}{RT} = \frac{\Delta\mu^0}{RT_0} - \int_{T_o}^{T} \frac{\Delta H}{RT^2}\, dT + \int_{P_0}^{P} \frac{\Delta V}{RT}\, dP - \ln \gamma_w \varphi_w \tag{3.22}$$

The first term on the right accounts for the chemical potential difference between the theoretical empty hydrate and liquid water at its reference pressure and temperature (273.15 K, 0 MPa), the second term on the right represents the change in chemical potential difference due to temperature at zero pressure. The third term represents the change in chemical potential difference due to pressure. The fourth term accounts for the solubility of gas in the pure water. The activity coefficient of water γ_w, is taken to be equal to 1.0 when only gas and water systems are considered. Many times this is the case due to low solubility of gases in water.

The temperature dependence of the enthalpy difference can be calculated by,

$$\Delta H_w = \Delta H_w^0 + \int_{T_o}^{T} \Delta C_{P_w}\, dT \tag{3.23}$$

where ΔH_w^0 represents an experimentally found reference enthalpy difference between the empty hydrate lattice and the water phase and $\Delta C_{P\,w}$ indicates the heat capacity difference between the empty hydrate lattice and the water phase. Therefore, $\Delta C_{P\,w}$ is a temperature dependent parameter and can be evaluated by the following equation,

$$\Delta C_{P_w} = \Delta C_{P_w}{}^0 + b(T - T_0) \tag{3.24}$$

where $\Delta C_{P\,w}{}^0$ is an experimentally found reference heat capacity difference, and b is a constant fitted to experimental data. On the other hand, ΔV is constant and depends on the phase present in the system.

Calculation of $\Delta\mu_H : \Delta\mu_H$ can be calculated by the following equation,

$$\Delta\mu_H = -RT\sum_i v_i \ln(1-\sum y_{ki}) \tag{3.25}$$

Here y_{ki} is the fraction of the cavity type i occupied by the hydrate former k. It follows the Langmuir's isotherms as follow,

$$y_{ki} = \frac{c_{ki} f_k}{1+\sum_j c_{ji} f_j} \tag{3.26}$$

where c_{ki} is the Langmuir constant of hydrate former k in cavity type i, which is determined by integrating the gas-water potential function over the volume of the cavity and f_k is the gas phase fugacity of hydrate guest component evaluated by a separate equation of state (EOS). Langmuir constant for spherical molecules can be evaluated by using the Kihara Potential function,

$$C = \frac{1}{kT}\int_0^{2\pi}\int_0^{\pi}\int_0^{R} \exp\left(-\frac{W}{kT}\right) r^2 \sin\theta dr d\theta d\varphi \tag{3.27}$$

where $W = W(r,\theta,\varphi)$ is the total potential energy of interaction between the enclathrated gas molecule and water molecules at positional coordinates (r,θ,φ) which describe the location of gas molecule within a three dimensional cavity.

Vanderwaal and Platteeuw model (1959) assumes that hydrate cavity as a uniform distribution of water molecules smeared over a sphere of radius R. Therefore above equation becomes independent of angular coordinates. Simplifying the equation gives,

$$C = \frac{4\pi}{kT} \int_0^{(R-a)} \exp\left(-\frac{W(r)}{kT}\right) r^2 dr \tag{3.28}$$

The cell potential is obtained as below,

$$W(r) = 2Z\varepsilon\left[\frac{\sigma^{12}}{R^{11} r}\left(\delta^{10} + \frac{a}{R}\delta^{11}\right) - \frac{\sigma^{6}}{R^{5} r}\left(\delta^{4} + \frac{a}{R}\delta^{5}\right)\right] \tag{3.29}$$

where,

$$\delta^N = \frac{1}{N}\left[\left(1 - \frac{r}{R} - \frac{a}{R}\right)^{-N} - \left(1 + \frac{r}{R} - \frac{a}{R}\right)^{-N}\right] \tag{3.30}$$

where N is equal to 4, 5, 10, and 11. R is the cell or cavity radius, Z is the coordination number of the cavity and r is the distance of the gas molecule from the center of the cavity. Also, a is the core radius of interaction for gas and water molecules, σ is the core-to-core distance between a gas molecule and a water molecule and ε is the depth of the intermolecular well. Parameters of the Kihara Potential function are illustrated in table presented by Sloan (Sloan, 1998-a).

3.3.1 Numerical Scheme

Equation (3.31) has the following form,

$$\Delta\mu_w - \Delta\mu_H = 0 \tag{3.31}$$

Substitution of Equation (3.22), (3.23), (3.24), (3.25) and (3.26) into the Equation (3.31) gives,

$$f(P) = f(T) + \frac{1}{23}\ln\left(\frac{1}{1+c_s f}\right) + \frac{3}{23}\ln\left(\frac{1}{1+c_l f}\right) + \frac{\Delta V}{RT}P - \ln\varphi_w = 0 \tag{3.32}$$

Above equation can be applied only for simple hydrates. Where $f(T)$ is defined as,

$$f(T) = \frac{\Delta\mu^0}{RT_0} - \int_{T_0}^{T}\frac{\Delta H}{RT^2}dT \tag{3.33}$$

Since Equation (3.32) is a nonlinear function with two unknown parameters pressure and temperature. Therefore this equation can be solved by using the Newton Rapson Technique as shown below,

$$P_{new} = P_{old} - \frac{f(P)}{f'(P)} \tag{3.34}$$

Where $f'(P)$ can be calculated from the below equation,

$$f'(P) = -\frac{1}{23}\left(\frac{c_s}{1+c_s f}\right)\left(\frac{df}{dP}\right) - \frac{3}{23}\ln\left(\frac{c_l}{1+c_l f}\right)\left(\frac{df}{dP}\right) + \frac{\Delta V}{RT} + \left(\frac{d(\ln(1-X_g))}{dP}\right) = 0$$

(3.35)

The solubility of gas in water can be found by means of Henry's law as shown below,

$$X_g = \frac{f}{Hc} \tag{3.36}$$

In this equation, f denotes the fugacity of gas at a given temperature and pressure, Hc is Henry's coefficient for gas dissolution in water at the prevailing conditions.

Henry's coefficient for dissolution of hydrocarbon in the water is primarily a function of temperature only. Therefore, Equation (3.35) takes the following form,

$$f'(P) = -\frac{1}{23}\left(\frac{c_s}{1+c_s f}\right)\left(\frac{df}{dP}\right) - \frac{3}{23}\ln\left(\frac{c_l}{1+c_l f}\right)\left(\frac{df}{dP}\right) + \frac{\Delta V}{RT} + \frac{1}{Hc - f}\left(\frac{df}{dP}\right) = 0$$

(3.37)

Equation (3.36) can be used for pressures up to 10 MPa whereas, for higher pressures, Henry's coefficient is not only the function of temperature and effect of pressure should also be taken into account. Reid & Prausnitz (1980) determined the Henry's coefficient on pressure is as follows,

$$\ln Hc = \ln Hc^0 + \frac{V_2^{\infty}(P - P_{VP_1})}{RT} \tag{3.38}$$

where, Hc^0 is Henry's Coefficient calculated as a function of temperature, V_2^{∞} is volume of hydrocarbon in water at infinite dilution, and P_{VP_1} is Vapor

pressure of solvent at temperature T. As a result, equation for hydrate formation from mixture of CO_2 and CH_4 is developed as follows,

$$f(P) = f(T) + \frac{1}{23}\ln\left(\frac{1}{1 + c_{s,CO_2} f_{CO_2} + C_{s,CH_4} f_{CH_4}}\right) + \frac{3}{23}\ln\left(\frac{1}{1 + c_{l,CO_2} f_{CO_2} + c_{l,CH_4} f_{CH_4}}\right) + \frac{\Delta V}{RT} P - \ln(X_w) \tag{3.39}$$

3.3.2 Hydrate Phase Equilibrium in the presence of Salt

The presence of salt causes a shift in P-T phase equilibrium curve of hydrates towards higher pressures. A method proposed by Englezos & Bishnoi (1988) considers the effect of salt on hydrate equilibrium curves. This method uses the activity of water, α_w instead of $\gamma_w \varphi_w$ in Equation (3.22). Activity of water can be determined by means of Pitzer's activity coefficient model (Pitzer & Mayorga, 1973). Equations representing this model is as follows,

$$\ln \alpha_w = -\frac{18 v m}{1000}\Phi \tag{3.40}$$

where, Φ is defined with the following equation,

$$\Phi = 1 + \left|Z_m Z_x\right| f^{\Phi} + m\left(\frac{2 v_m v_x}{v}\right) B_{mx}^{\Phi} + m^2\left(\frac{2(v_m v_x)^{1.5}}{v}\right) C_{mx}^{\Phi} \tag{3.41}$$

and, $$f^{\Phi} = -\frac{A^{\Phi} I^{0.5}}{1 + bI^{0.5}} \tag{3.42}$$

where m is molality of electrolyte in solution, v is stoichiometric number of moles of ions in one mole of salt, Z_+, Z_- are charges on each ion in the salt, I is ionic strength of solution, and A^{Φ} is Debye-Huckel coefficient. Correlations

for A^{Φ}, B^{Φ}_{mx}, C^{Φ}_{mx} are introduced in the literature (Pitzer & Moyorga, 1973) (Bradley & Pitzer, 1979).

This approach valid for low pressure values when the solubility of hydrocarbons in the water is low, whereas epsecially at high pressures hydrocarbon solubility becomes an important factor. For this reason, Narsifar & Moshfeghian (2001) proposed the following technique.

$$\ln \alpha_w = \ln \alpha_{w,el} + \ln \alpha_{w,gas} \tag{3.43}$$

where $\alpha_{w,el}$ is activity of water in the presence of salt and $\alpha_{w,gas}$ is the activity of water in the presence of gas and it can be approximated as the mole fraction of water by Lewis-Randoll rule. Thus, $\alpha_{w,gas} \approx \Psi_w$.

Another approach for the systems with salt is the predicition of the temperature difference due to salt concentration. According to this approach, in systems with salt, the hydration temperature is decreased by ΔT^{hyd}, the value of which is calculated with the method proposed by Sloan (1998-b).

$$\frac{\Delta T^{hyd}}{T_w (T_w - \Delta T^{hyd})} = 0.6652 \frac{\Delta T^{fus}}{T_f (T_f - \Delta T^{fus})} \tag{3.44}$$

where T_w is the hydration temperature under a certain P_e for salt-free system, ΔT^{fus} is the depression of water freezing temperature under low pressure (e.g. 1 atm) caused by salt, and T_f is the freezing temperature of pure water, which is 0 ^{o}C (273.2 K). The constant 0.6652 comes from the calculations by Sloan (1998-b) along with the hydrate dissociation enthalpy data for SI methane hydrate by Handa (1986). The depression of freezing temperature ΔT^{fus} can be determined as a function of salt concentration in the aqueous-phase. For sodium

chloride (NaCl), a regression formula can be obtained from the data given by CRC Handbook of Chemistry and Physics (2004/2005),

$$\Delta T^{fus} = w_A^s(164.49 w_A^s + 49.462) \tag{3.45}$$

where ΔT^{fus} is in K and w_A^s is the mass fraction of NaCl in aqueous-phase in kg salt/kg solution. Equation is valid in the range of w_A^s between 0 and 0.22. In addition to the depression of hydration temperature, another effect of introducing salt into the system is that an additional phase of salt precipitate may appear when the salt concentration in the aqueous-phase exceeds the solubility.

CHAPTER 4

CARBON SEQUESTRATION

Global atmospheric CO_2 concentration and other greenhouse gases have been increasing since the industrial revolution because of the rise in fossil fuel combustion. This ascending trend has raised the concerns about possible global climate change. Therefore CO_2, which is estimated to be responsible for over two-thirds of any climate change, constitutes the fundamental problem in terms of climate change. As the main source of CO_2 is the combustion of fossil fuels, various alternative energy sources like wind, solar and nuclear were proposed. However, it is evident that these alternative energy sources will not be able to diminish the CO_2 emission to the desired levels. Consequently, researches have primarily concentrated on various carbon capture and sequestration techniques. Some possible alternatives for geologic storage of CO_2 are; injection of CO_2 into depleted oil and gas reservoirs, deep saline aquifers, and unmineable coalbeds.

Recently, global warming has become a genuine concept for public. The concentration of carbon dioxide in the atmosphere has been increasing since industrialization in the 19^{th} century and nowadays, common belief is that mankind has a visible impact on the world's climate. It is widely acknowledged that burning of fossil fuels triggers the global warming by increasing the concentration of greenhouse gases in the atmosphere. Because these gases have tendency to absorb radiation strongly in the far infrared portion of the spectrum and that area is associated with thermal heating. Therefore greenhouse gases serve to trap heat inside the atmosphere.

Researches which have been carried out in the last three decades indicate that climate change is already taking place and global average temperatures are increasing day by day. Similarly, anthropogenic CO_2 emissions have also been increasing in the same time frame. Therefore, by analyzing the increase in the global average temperatures and CO_2 emissions one can suggest that, anthropogenic CO_2 emissions are mainly responsible for the global warming.

Some important greenhouse gases are carbon dioxide, methane, nitrous oxide and sulfur hexafluoride. Among these gases, the greatest contribution to the global warming over the past century has been come from the carbon dioxide by means of deforestation and burning of fossil fuels. Methane is the second greatest contributor and mostly evolves from coal deposits, leaking natural gas pipelines, landfills, forest fires, wetlands, rice growing, cattle rising. Nitrous oxide is third and arises from agricultural practices, fuel burning and industrial processes. Sulfur hexafluoride is the most powerful contributor (IPCC, 2007) but its concentration in the atmosphere is low when compared with other greenhouse gases; therefore, it has a limited effect on global warming. Sulfur hexafluoride mainly evolves as the result of its use in the magnesium production industry, and by electrical utilities and electronics manufacturers.

The global warming issue has become one of the most important problems in the agenda of Europe and developing countries. For this reason, through Kyoto Protocol, developed countries agreed to diminish their CO_2 emissions by 5.2% below 1990 levels. Increase in the world energy demand as a result of the increase in global population and economic growth in the developing countries, suggests that our dependence on fossil fuels will continue in near future. Therefore, CO_2 sequestration is crucial to control its concentration in the atmosphere.

4.1 Geological Sequestration

Geologic sequestration involves capturing and storing carbon dioxide into suitable underground formations for storage. The primary types of geologic reservoirs for the disposal of CO_2 includes depleted oil and gas reservoirs, unmineable coal seams, and deep formations containing salty water. In general, these reservoirs have naturally stored crude oil, natural gas, brine and CO_2 over millions of years. Therefore, industry has a lot of experience dealing with the geologic storage, monitoring and verifying the fluid in reservoirs or at least certain that these sites have the potential to store CO_2 from anthropogenic sources.

Once the CO_2 is injected underground, it will rise due to buoyant forces until it is trapped beneath an impermeable barrier. In general, this trapping mechanism has the ability to retain CO_2 for thousands to millions of years. By time, some of the injected CO_2 will begin dissolving in ground water, and some may be trapped in the form of carbonate minerals formed by chemical reactions with the surrounding rock. All of these trapping mechanisms play an important role on the effectiveness or permanence of the stored CO_2 and also they are susceptible to change over time after CO_2 injection. Therefore, researches have been focused on efficiency of these trapping mechanisms and possible alternative ways to prevent geologically sequestered CO_2 to leak back to the atmosphere.

4.1.1 Seal Trapping

Seal trapping which is also known as stratigraphic and structural trapping, is the primary trapping method for the CO_2 sequestration in geological formations. CO_2 can be trapped as a gas or supercritical fluid under low permeability rock layers as in the case of natural gas trapped in natural gas reservoirs. In a structural trap, anticline or tilted fault block prevents release of the stored CO_2 back into the atmosphere by means of sealing rock (or cap rock). If the geometry of the subsurface does not contain faults or folds, the trapping mechanism is stratigraphical. Once the CO_2 is trapped by the seal, it will remain trapped unless the height of the CO_2 layer produces a capillary pressure that would enable it to enter the seal. This height is the function of pore radius of the sealing rock, relative densities, surface tensions of CO_2 and water. When the reservoir has closed structural trap, it is very likely that much of the CO_2 (supercritical or gas phase) is trapped by seal trapping mechanism and the rest is trapped by other mechanisms.

4.1.2 Hydrodynamic Trapping

Hydrodynamic trapping is a long term process that mainly occurs in saline formations. The injected CO_2 travels upward in saline water and dissolves in saline water after being trapped by stratigraphic formation. Regions where groundwater is flowing downward and down gradient are preferable for CO_2 disposal, because the residence time of the groundwater will be much larger; therefore, it will enhance the effects of CO_2 hydrodynamic and mineral trapping. To make the hydrodynamic trapping more efficient, the CO_2 should be stored in its dense or supercritical phase, i.e. above the critical pressure of 7.4 MPa and critical temperature of 31 ^{o}C. For a hydrostatic pressure gradient of 10.5 MPa per km, these criteria can be satisfied below about 700 m. Below this depth, CO_2 will be less dense than formation water and it will rise to the top of the reservoir; therefore, a trap is again required for the safe disposal (Holloway *et al.* 1996) (Otto, 1998).

4.1.3 Mineral Trapping

Mineral trapping can be considered as the most permanent type of geological storage mechanisms. Mineral trapping takes place as a result of some geochemical reaction with rock such as anorthite, albite, diopside etc. and formation water. Various carbonates such as calcite, dolomite, and siderite can be formed in the brine aquifer by mineral trapping. The chemistry of formation water and the rock mineralogy are the two important parameters when determining the potential for CO_2 storage through geochemical reactions. When CO_2 injected into an aquifer, some of the CO_2 dissolves as bicarbonate in water but only small amounts of bicarbonate (and a proton) will be produced. Gunter *et al.* (1993) stated that brackish and dilute formation water can take up more CO_2 than brine. Also, salting-out effect limits the maximum solubility of CO_2 in brines due to the salting-out effect at higher ionic strengths. For these reasons, merely brines are not considered for CO_2 sinks.

When CO_2 dissolves in formation water pH of the water will decrease and acidic conditions will take place. During dissolution, silicate minerals (feldspars and clays) present in the aquifer are attacked and free ions of Ca, Mg and Fe are released. The free calcium ion reacts with the bicarbonate to precipitate calcite, which forms the basis for sequestering CO_2 as the mineral calcite. Reactions are similar during the formation of dolomite and siderite. As a result, mineral trapping mechanism is more efficient when the aquifer matrix contains minerals that absorb the protons such as the basic silicate and clay minerals; therefore, sandstone aquifers are more favorable than the carbonate aquifers containing brackish formation water.

4.1.4 Adsorption Trapping

Adsorption trapping mechanism is achieved by adsorption of gaseous CO_2 onto the coal. Coal has high affinity to CO_2; therefore, coal seams at great depths and considered to be uneconomical for mining may be safe storage sites for CO_2. By means of this mechanism, carbon dioxide from anthropogenic sources can be injected into these coal seams and permanently locked in without emitting it to the atmosphere unless the coal is mined. This mechanism also provides good ground for the concept of methane recovery in coal seam with the sequestration of CO_2, which is defined as Enhanced Coalbed Methane (ECBM) recovery. Methane produced by means of this process may offset the cost of capture, compression, transportation, and storage of CO_2.

4.1.5 Residual Trapping

As the injected CO_2 migrates, it will form a CO_2 plume. As the plume migrates, the concentration of the CO_2 at the tail of plume will decrease gradually and finally fall below a certain level. In the meantime, formation water moves into the CO_2 saturated zone. At the pore scale, CO_2 is continuous in porous media, whereas pore constrictions impede the continuity of the CO_2. Once a portion of the non-wetting CO_2 is separated from the continuum, it will get trapped due to capillary forces (Dullien, 1992). This trapping mechanism is referred to as residual gas or capillary trapping. This trapping mechanism takes place very quickly when the CO_2 bubble occupying within a large pore space is not able to pass through a pore neck due to interfacial tension. Also, by time, this residually trapped CO_2 can dissolve into the formation water and another trapping mechanism, solubility trapping may take place.

4.1.6 Solubility Trapping

This trapping mechanism involves the CO_2 dissolution within the brine. As CO_2 migrates through the formation, some of it dissolves in the formation water. In the CO_2 plume, dissolution of CO_2 in formation water can be considered to be in equilibrium as the water and CO_2 coexist at the pore scale (Suekane *et al.*, 2006). On the other hand, at the aquifer scale, dissolution is considerably slow, because it is limited by the diffusion of CO_2 in the water outside of the plume and natural convection due to the difference in densities between water saturated with CO_2 and unsaturated water (Ennis-King & Paterson, 2003). The solubility of CO_2 in water is directly proportional with the pressure whereas it is inversely proportional with the temperature and water salinity. As the amount of dissolved CO_2 in water increases, the density of water will start to increase and begin to sink downwards. As a result of this phenomenon, CO_2 may become more dispersed in the water, and by time, amount of dissolved CO_2 in water may also increase.

Table 4.1 illustrates the summary of the trapping mechanisms and their characteristics such as; nature of trapping, effective time frame, areal size and occurrence in basins.

Table 4. 1 Characteristics of trapping mechanism (Adapted from Bradshaw *et al*., 2007)

Trapping Mechanism	Nature of trapping	Effective time frame	Areal size	Occurrence in basins
Structural & Stratigraphic	Buoyancy trapping within anticline, fold, fault block, pinch-out. CO_2 remains as a fluid below physical trap (seal)	Immediate	10 to 100 s km	Dependent on basins tectonic evolution. Hundreds of small traps to single large traps per basin
Residual gas	CO_2 fills interstices between pores of the grains of the rocks	Immediate to thousands of years	Basin scale, e.g. 1000 s km	Along migration pathway of CO_2
Dissolution	CO_2 migrates through reservoir beneath seal and eventually dissolves into formation fluid	100 to 1000 s of years if migrating more than 1000 s of years if gas cap in structural trap and longer if reservoir is thin and has low permeability	Basin scale, e.g. 10,000 s km	Along migration pathway of CO_2 both up dip and down dip
Mineral precipitation	CO_2 reacts with existing rock to form new stable minerals	10 to 1000 s of years	Basin scale, e.g. 10,000 s km	Along migration pathway of CO_2
Coal adsorption	CO_2 preferentially adsorbs onto coal surface	Immediate	10 to 100 s km	Limited to extent of thick coal seams in basins that are relatively shallow

4.2 Sequestration in Saline Aquifers

Saline aquifers are sedimentary rocks that are saturated with formation water or brine. Efficiency of this technique is based on storage capacity and permanence of injected CO_2. Storage capacity is directly related with the porosity and thickness of the aquifer. Main advantage of this technique is the wide distribution of salt water, because anthropogenic CO_2 is generally not close to potential storage sites in oil or gas reservoirs. Mineral trapping and hydrodynamic trapping are the two main mechanisms that control the sequestration in saline aquifers. In this technique, injected CO_2 generally flows through easy flow pathways and flow is not dominated by the pressure gradient between the injection and production wells. In addition, due to density difference between the injected CO_2 and brine, gravity segregation occurs and preferential flow takes place. Injection of CO_2 well below the top of the aquifer may mitigate the effect of gravity segregation; however, it is nearly impossible to prevent this effect entirely.

Large aquifers with considerable permeability and thickness are good candidates for the disposal of CO_2. Furthermore, aquifers that have good pressure communication over long distances are very attractive since large volumes could be injected without increasing aquifer pressure significantly (Ennis-King & Paterson, 2003).

As the injected CO_2 dissolves in brine, density of brine will increase and this denser brine will start to move downwards. Therefore, denser brine will replace with the fresh brine and fresh brine is brought in contact with the CO_2 phase. Brine plays a significant role during the trapping of CO_2 and helps the immobilization of CO_2 as a residual phase. Considering the time required for dissolution and resulting vertical convection, it is stated that hundreds to thousands of years will be required to dissolve all the CO_2; however, until this

time significant amount of CO_2 will have been trapped in residual phase. Meanwhile, chemical reactions may sequester some of the CO_2 as minerals and the amount of stored CO_2 depends on the chemical composition of the brine and the minerals present in the aquifer (Johnson *et al.*, 2004).

4.3 Sequestration in Depleted Oil & Gas Reservoirs

Depleted gas reservoirs are perhaps the safest places for sequestration of CO_2, since produced natural gas had been trapped in the reservoir for long geological times. However, it is less attractive when compared with the injection into the oil field since there is little or no enhanced hydrocarbon recovery to offset injection costs. In general, recovery ratio is about 90% or more for the conventional high permeability gas reservoirs. Therefore, due to this high recovery, it is very likely that large pore space will become available while little remaining mobile natural gas will remain to be recovered. CO_2 injection into the depleted gas reservoirs always includes the risk of contaminating remaining natural gas reserves with injected CO_2. Considering the advances in the recovery technology and rise in the natural gas prices, injection process may seem unattractive; however, proposals have been made to inject CO_2 into natural gas reservoirs to improve recovery, or as cushion gas in natural gas storage fields.

Furthermore, active oil reservoirs can also be used for the CO_2 injection and oil production may be enhanced in this way. When the reservoir conditions are favorable (oil gravity > 22 ^{o}API and depth > 1200 m) injected CO_2 is miscible with residual oil within the reservoir (Taber *et al.*, 1997). As the CO_2 dissolves in oil, oil begins to swell and its viscosity will decrease; therefore, its mobility will increase. Consequently, an additional 5 to 20% of the original oil in place (OOIP) may become recoverable, when the reservoir conditions are not favorable (low reservoir pressure and heavy oil).

4.4 Sequestration in Coal Seams

Coal seams, which are at great depths and considered to be uneconomical for mining, could be a good candidate for the safe sequestration of anthropogenic CO_2. Coal seams are geological formations that had entrapped gases such as CO_2, methane, nitrogen etc. However, among these gases, coal has greater affinity and adsorption capacity for CO_2. This phenomenon provides good ground for the concept of methane recovery in coal seam with the sequestration of CO_2, which is defined as Enhanced Coalbed Methane (ECBM) recovery. It offsets the cost of capture, compression, transportation, and storage of CO_2 by producing natural gas. It is stated that, by means of conventional techniques (Hydraulic fracturing), only 50% of methane in coalbed methane reservoirs can be produced. However, ECBM has the potential to increase this recovery to a value of 90% (Stevens *et al.,* 1996). Adsorption is the main mechanism of gas storage in coal (Gray, 1995).

Since coal has a large surface area, the quantity of adsorbed gas is extremely large. Through careful design of the layout of injection and production wells, most injected CO_2 will be adsorbed by coal and should stay in coal. Storage capacity of coal seam, injectivity and the potential leakage ways are the key parameters that should be considered before the implementation of CO_2 sequestration in coal seams. Also, interaction of CO_2 and coal should be well established to determine the feasibility of sequestration. It has been shown that, as the amount of adsorbed CO_2 increases coal begins swelling. For this reason, permeability will decrease and as a result some injectivity problems may occur.

Table 4.2 provides the summary of the storage sites and gives brief information about advantages, challenges, applicability and data availability about storage sites.

Table 4. 2 Characteristics of potential storage sites (Modified from Rhudy & Bock, 2002)

Storage Sites	Advantages	Challenges	Applicability	Data Availability
Depleted oil & gas reservoir	Global storage capacity of 140 Gt and 40 Gt for disused gas and oil fields respectively • Reservoir properties are well known • Infrastructure of wells and pipelines are already available • Proven containment over geologic time frames	• Concern over leaky wells or improperly abandoned wells- a safety threat • Today very few reservoirs depleted	• Limited to areas where there are disused oil and gas reservoirs	• Good
Saline aquifers	• Best potential CO_2 storage capacity (1000~104 Gt) • Stored CO_2 expected to be isolated from the near surface for thousands of years • Available everywhere • Offshore aquifers eliminate most safety concerns	• Lack of characterization experience • Absence of financial incentive	• Ubiquitous and large, so widespread availability	• Good- in progress
Coal bed storage	• CH_4 by-product makes option economically attractive • Coal deposit present worldwide	• Unminable coal seams are likely to be hundreds of meter deep, hence less permeable and limiting the capacity of CO_2 stored	• Unclear as to how many types of coal formations will be practical to use for coal bed CH_4 production	• Limited

4.5 Sequestration in Basalt Formations

Basalt is a dark-colored, silica-rich, volcanic rock that can be found in many areas of the world. Basalt contains cations like calcium, magnesium, iron and by combining these cations with CO_2; it may promote the formation of carbonate minerals. Although these formations have not received much attention, they have the potential to sequester CO_2 by creating stable carbonates. Unlike sedimentary rock formations, basalt formations have some distinct characteristics that serve to chemically trap the anthropogenic CO_2. As the number of studies that focus on sequestration in basalt formations is very limited, some fundamental information on injectivity, storage capacity, and rate of conversion of gaseous CO_2 to solid carbonates is not available. Experiments conducted at Pacific Northwest National Laboratory (PNNL) have proven that carbonate mineral formation occurs when basalts from the Columbia River Basalt Group (CRBG), Central Atlantic Mafic Province, and Newark Basin are exposed to supercritical CO_2. However, data obtained from these experiments are not enough to make reliable projections of CO_2 conversion rates under large-scale sequestration conditions. Furthermore, data gathered from these experiments are only representative for specific site and further experiments and investigations are required to determine on the ability of basalts from other parts of the world to support in situ mineralization reactions (Plasynski *et al.*, 2008).

4.6 Sequestration in Salt Caverns

After reaching the success on hydrocarbon storage in salt, proposals began to sequester the anthropogenic CO_2 on salt caverns. Salt caverns may be a suitable permanent (>1000 yr) storage sites for the CO_2 (Dusseault *et al.*, 2004). This technique is perhaps the least attractive one among the geological carbon sequestration schemes due to cost of cavern mining and other potential environmental issues. However, high capacity, high filling rate and the potential economic value of leached brine can make this technique viable for the CO_2 sequestration. Also, besides the impermeable structure of the pure salt (<10-19 m^2) bounding strata generally have pores plugged by crystalline salt for some distance beyond the massive salt bed, which decreases the risk of CO_2 escape through porous media (Dusseault *et al*., 2001).

4.7 Sequestration in Shales

Another option for the sequestration of CO_2 is the utilization of organic-rich shales. Shale is a fine-grained, clastic sedimentary rock composed of silicate minerals that is a mix of flakes of clay minerals and tiny fragments of other minerals, especially quartz and calcite. Shale is characterized by the plate-like structure of these clay particles. Accumulation of these clay particles in a flat manner provides the extremely low permeability in the vertical direction. For this reason, shales are generally used in a petroleum system as a seal or caprock. There are number of issues (CO_2 trapping mechanisms & their kinetics and monitoring & modeling tools etc.) that should be considered before the safe implementation of CO_2 sequestration in organic-rich shale basins. Also, it is stated that interaction of the acidic CO_2-rich fluids with shale tend to be a two edged sword; though they can provide the metals essential to trapping CO_2 in carbonate minerals, the leaching of these metals may create easy flow pathways leading to the escape of CO_2 to the atmosphere, such as suggested by the field study reported by Moore *et al.* (2005).

4.8 Other Alternatives

In addition to above mentioned sequestration techniques, recent researches consider the feasibility of CO_2 sequestration as gas hydrates. CO_2 hydrate is a novel option for the permanent CO_2 disposal over long time periods. Moreover, by means of hydrates more CO_2 can be sequestrated when compared with the other techniques. Furthermore, injection of CO_2 into methane hydrate may disassociate the methane hydrate and form CO_2 hydrate; therefore, produced methane may offset the cost of CO_2 transportation and disposal.

There are several options for storing CO_2 as a hydrate phase. First of all, researchers have considered the feasibility of releasing liquid CO_2 into the deep oceans (Brewer *et al.*, 1999). The idea behind this disposal option is that, interaction of the CO_2 with seawater under the suitable conditions may form CO_2 hydrate. In this technique, CO_2 hydrate would eventually dissipate through equilibration with the seawater. However, when the slow rate of dissipation and slow turnover of the deep oceans is considered it can be concluded that, CO_2 hydrates can be stable at least hundreds of years (Herzog, 1996). On the other hand, this technique has two important drawbacks. The first one is that, large amounts of CO_2 may damage the flora and fauna in the deep oceans. The second one is that, disposal of large amounts of CO_2 into the deep oceans is prohibited under the terms of international agreements, such as the 'London Dumping Convention' (IMO, 1997) and 'OSPAR Convention' (OSPAR, 1992).

Other researches have focused on sequestrating CO_2 hydrate directly to shallow sediments on the deep sea floor (IEA GHG, 2004). According to this technique, CO_2 hydrate which is formed in the laboratory conditions may be transported as large blocks on board ships, and then may be released to the deep sea floor. However, this technique is also prohibited under the above international conventions.

Both of these approaches involve direct disposal of CO_2 hydrate on the ocean floor. These approaches are not allowed since possible disassociation of CO_2 hydrate will diminish the seawater pH and damage the marine ecosystem. One possible approach, which involves CO_2 hydrate formation in the deep ocean and minimum risk of CO_2 release to the ocean floor, is formation of CO_2 hydrate in deep sea sediments. In addition, presence of large quantities of CH_4 hydrate in deep sea sediments proves that CO_2 can be stored in deep sea sediments as hydrate form. Also, studies on natural CH_4 hydrate accumulations in deep sea sediments may give a valuable insight for CO_2 hydrate formation in deep sea sediments.

CHAPTER 5

CO_2 SEQUESTRATION AS HYDRATES INTO DEEP SEA SEDIMENTS

Recently, secure sequestration of anthropogenic carbon dioxide in geological formations has become one of the most important global scientific problems. Injection into deep sea sediments offers some unique and significant advantages such as, huge storage capacities and significant risk reduction for possible CO_2 leakage when compared with the other potential geological storage techniques. Disposal of CO_2 into deep sea sediments is safer than disposal into land since the water pressure and dilution by oceanic water prevent direct emission of CO_2 into the air.

Basic idea behind the CO_2 storage into deep sea sediments is that, storing CO_2 in a geological structures in such a way that it cannot escape in the short-term into the atmosphere. For the storage of huge amounts of CO_2, geological structure must contain an impermeable barrier. In general such a barrier may consist of clay or salt. In this study long term fate of the CO_2 disposal under the methane hydrate zone will be investigated.

Until recently, hydrate studies have mainly focused on methane hydrate (CH_4) which is considered to be one of the most important possible future energy sources. However, over the past few years studies have concentrated on disposal of anthropogenic CO_2 as hydrates. CO_2 hydrates enable storage of the large amount of CO_2 and CO_2 stored in this solid phase will not be released to the atmosphere over relatively short timescales.

Formation and dissociation of both methane and carbon dioxide hydrate are influenced by several factors such as, pressure, temperature, mole fraction of carbon dioxide and methane in the mixture and porous medium characteristics. At a given temperature, equilibrium pressure for methane hydrate dissociation is higher than that required for carbon dioxide. In addition, equilibrium conditions for hydrate formation and dissociation depends on the mole fraction of carbon dioxide gas in the CO_2–CH_4 mixture. The equilibrium conditions in porous media require higher pressures and lower temperatures when compared with those in bulk medium. Sloan (2003) stated that, in bulk medium solid hydrate film forms at the interface of water and hydrate former. This layer acts as a barrier to prevent further contact of the water and hydrate former; therefore, water surface renewal is required for continued clathrate formation.

As it was stated before, equilibrium conditions are also function of pore diameter. They require higher pressure and lower temperatures as the pore diameter reduces. Furthermore, if the pressure is high enough carbon dioxide may pass to the liquid phase; therefore, considerably lower temperature and higher pressure values are required for the hydrate formation. As a result, interactions between the liquid carbon dioxide and methane hydrate and carbon dioxide gas and methane hydrate are quite different.

Both disposal of carbon dioxide below the methane hydrate and sequestering carbon dioxide while producing methane hydrate requires complete understanding of several properties such as: viscosity and density differences between the injected carbon dioxide and the dissociated methane gas; interfacial mass transfer between the two; interfacial tension between different phases: gas, liquid, water, and hydrate; wettability of the porous media; pore size distribution; pore throat diameter; saturation of different phases in the sediment; amount of the dissociated water; pore water salinity; thickness of the unfrozen water on the grain surface; and interfacial mass transfer.

5.1 Storage of CO_2 as hydrate phase within sediments

First of all, the deep storage of CO_2 requires injection into warm rocks that are at least 800 m deep. During deep storage of CO_2, there is always great possibility that some CO_2 may migrate upwards at some time. CO_2 leakage may occur through small faults/fractures, or poorly sealed boreholes. At this time, CO_2 hydrate stability zone becomes a crucial phenomena. Because, if the CO_2 is stored below a deep enough and cold enough body of water, then leaked CO_2 may enter into CO_2 hydrate stability region. Therefore, formation of CO_2 hydrate may decrease the permeability of cap rock by partially or even completely plugging flow pathways (As in the case of methane hydrate plugs pipelines).

In addition, CO_2 hydrate may also form at relatively warm temperatures. Pruess (2003) modeled fate of the liquid CO_2 rising along easy flow pathways. Pruess (2003) suggested that, liquid CO_2 starts to boil off when it is depressurized. Liquid CO_2 takes the heat required for the vaporization from the surrounding rocks. Therefore, boiling process cools the surrounding rocks to the point, at which CO_2 hydrate, or even ice, may form. Consequently, easy flow pathways could be blocked partially or even completely. Pruess (2003) also stated that, depending on the geological characteristics, cool zone may reach up to several hundreds of meters, which may mitigate the vertical flow of the CO_2 and cause it to spread out laterally. However, Pruess (2003) indicated that his model was idealized and models including more realistic geological structures should be developed.

Another scenario involves the usage of CO_2 hydrate as a primary sealing mechanism for the injected CO_2 (Koide *et al*., 1997) (Sasaki & Akibavashi 2000). According to this approach, CO_2 is injected into deep sea sediments or sub-permafrost region just below the hydrate stability zone. As the injected CO_2 rises within the sediments, it enters into the cooler sections and finally reaches hydrate stability zone. Therefore, by time, significant amount of CO_2 hydrate

formation may impede the further upward migration of CO_2. As a result, injected CO_2 spread out below the impermeable layer of CO_2 hydrate (Figure 5.1).

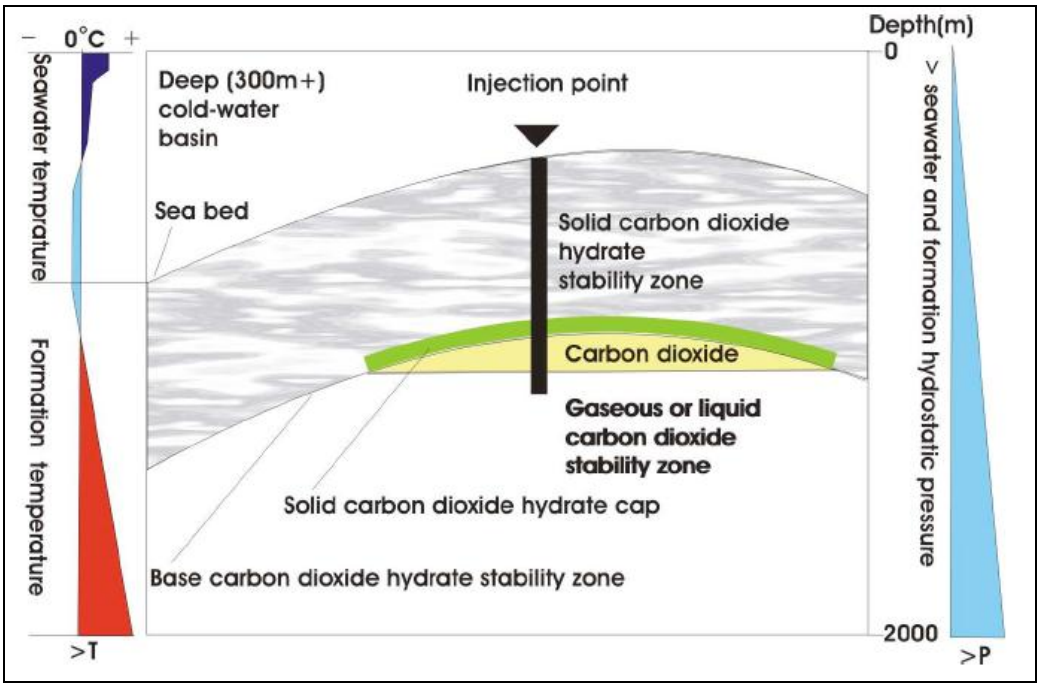

Figure 5. 1 Schematic diagram showing the relative position of the injected CO_2 and associated 'cap' of CO_2 hydrate (Rochelle *et al.*, 2009)

Any injected CO_2, which is able to find pathways through the impermeable CO_2 hydrate layer, may also form CO_2 hydrate as long as it encountered water-rich sediment. Therefore, if the CO_2 hydrate stability zone thick enough, then impermeable hydrate barrier may have a capacity to self-seal, increasing the feasibility of the storage scheme. This self-sealing process is very important for the disposal of CO_2 when the ease of CO_2 hydrate formation is considered. In the literature it is indicated that CO_2 hydrate forms relatively rapidly (probably faster than for methane hydrate) under appropriate conditions (Brewer *et al.*, 1999).

5.2 CO_2 and CH_4 hydrate stability within sediments

Gas hydrates form as long as the proper physical conditions exist with the presence of hydrate formers. Therefore, ocean floors, with high pressure and low temperatures are possible candidates for the hydrate formation. However, as the density of methane hydrate (0.913 g/cm^3) is always lower than the water column, hydrate will rise because of the buoyancy effect and it will finally dissociate as soon as enters the region, where the hydrate is unstable. However, methane hydrate that formed in the pore space of the unconsolidated sediments will remain stable. If water temperatures are colder, then the upper limit for methane hydrate is shallower. In closed ocean basins, where bottom water temperature values are high, hydrate occurrence depth is also high.

It is crucial to understand conditions of CO_2 hydrate stability zone and the steps for CO_2 hydrate formation within sediments thoroughly for the selection of suitable sites and safe disposal of large quantity of CO_2. Both storage of CO_2 under the impermeable barriers that consists of clay, salt or CH_4 hydrate and self-sealing of CO_2 include CO_2 hydrate formation within sediments. Moreover, understanding the interaction between injected CO_2 and CH_4 hydrate and identification of CH_4 hydrate stability zone is very important. Furthermore, by means of these type of studies, besides the disposal of CO_2, even liberation of methane from CH_4 hydrate during CO_2 hydrate formation may become possible.

Evgeny *et al*. (2002) studied the influence of sediment properties on methane hydrate formation. They concluded that depending on the sediment type, percentage of pore water that transformed to hydrate changes drastically. The portion of water transformed to hydrate was found to be maximum (about 80%) in sandy sediments whereas, it takes its minimum value (about 15%) in montmorillonite clay. Therefore, as the bonding energy of pore water and mineral surface increases, hydration ratio decreases. Furthermore, fraction of water transformed to hydrate also inversely related with the increase of salinity.

Moreover, field experiments indicated that, type and the amount of hydrate formation is dependent on the characteristics of host material. For instance, in the Mackenzie Delta, NWT Canada (Mallik 2L-38 well), hydrate occurs in coarser-grained units. However, in the Gulf of Mexico, where near-surface sediments are generally fine grained, hydrates recovered in giant piston cores did not appear to be lithologically controlled.

Also, several studies indicated that, under prevailing conditions methane hydrate is stronger than water ice. Experiments conducted by Zhang *et al.* (1999) showed the interesting strength contrast between water ice and methane hydrate. Additionally, Winters *et al.* (2001) observed that, Ottawa sand with methane hydrates as pore filling is drastically stronger than Ottawa sand with ice as pore filling during the initial stage of deformation experiment. Furthermore, Helgerud (2001) concluded that, at -20 ^{o}C, stress necessary for full compaction of granular methane hydrate more than ten times greater than that required for granulated ice. In 2003, Durham *et al*. (2003) observed that methane hydrate is more than 20 times stronger than ice. These compression and deformation experiments were carried out between the temperature values of -13 ^{o}C (260 K) and 0 ^{o}C (273 K). Therefore, when identical conditions exist, ice deforms significantly faster than pure methane hydrate. Additionally, it was suggested that deformation of ice occurs by the coordinated motion of crystalline defects, which are generally diffusion limited (Poirier, 1985). As a result, Durham *et al.* (2003) concluded that, higher mechanical strength of methane hydrate relative to ice may be related to the rate of diffusion of water in methane hydrate being two orders of magnitude slower than ice.

Winters *et al.* (2000) indicated that compressive strength of a core containing methane hydrate in the pore space is greater than without hydrate in the pore space. Also, Ebinuma *et al*. (2005) conducted series of compression tests on samples consisting of different saturations (48–52%) of methane hydrate filling

the pores of silica sand. Throughout their studies, methane hydrate saturation represents the ratio of the hydrate volume to pore volume. The mechanical strength of hydrate samples which were prepared by combining sand, ice and gas was shown to remain constant until the methane hydrate saturation reached up to 25%. After that point, mechanical strength was found to increase proportionally with the methane hydrate saturation. On the other hand, the mechanical strength of hydrate samples prepared from water-wet sand/gas was found to increase monotonically with methane hydrate saturation.

Winters *et al.* (2004-c) suggested that the sediment strength is much lower in the pore filling model when compared with the cementing model. They used laboratory hydrates made from Ottawa sand, which shows strong cementing behavior and a natural gas hydrate sample from the Mallik 2L-38 well, which exhibits pore filling behavior in their experiments. Furthermore, acoustic measurements carried out on Mallik sediment in the field and the laboratory are more consistent with natural hydrate occurrence filling pores, rather than by grain cementation.

5.3 CO_2 and CH_4 hydrate within pore spaces

With the assumption of the suitable pore space exists within the hydrate stability region, it is necessary to know the effects of hydrate formation on the sediments and which sediments may trigger hydrate formation. Some questions which are required to be addressed are, whether hydrate will form in the center of pores or on grain surfaces, whether it will cement grains together and make the sediment stronger, whether presence of CO_2 will increase the stability zone of CH_4 hydrate and whether CO_2 hydrate formation will mitigate upward movement of injected CO_2. Experimental studies are necessary to obtain some useful insights for the behavior of CO_2 and CH_4 hydrate within pore spaces. However, it is almost impossible to bring together the effects of sediments, water salinity, and other parameters to the hydrate formation and CO_2 disposal.

Studies showed that the CO_2 hydrate replaced the water film completely and cemented the grains together to a certain extent. Some parts of the pores filled with hydrate crystals, other parts of the pores remained open. It was suggested that the factor that limits the hydrate formation is the availability of water (Gorman *et al.,* 2002). Cementation of sediment grains by CO_2 hydrate is beneficial for CO_2 disposal in several aspects. First of all, some of the CO_2 is trapped as a solid phase. Secondly, sediments become stronger, which is especially important if the sediments are poorly consolidated (which is the common situation in the deep sea sediments). Finally, vertical migration of CO_2 is mitigated or even prevented with sufficient hydrate formation. Last point is particularly important since it mentions about the thickness of the hydrate section. Laboratory experiments showed that, relatively thin layer of rapidly-formed CO_2 hydrate is capable of withstanding a significant differential pressure across it (Someya *et al*., 2006).

Zatsepina & Buffett (2001) carried out some experiments to determine the stability of CO_2 hydrate in porous media. According to their studies, when the vapor phase of CO_2 is absent, the volume of hydrate is limited by the transfer of CO_2 from solution. This phenomenon was also proved by mass balance and mass balance showed that less than 1% of the pore volume was filled with hydrate. On the other hand, when the vapor phase of CO_2 is present, CO_2 hydrate appeals CO_2 from both phases. In addition, they also developed a mathematical model to estimate the surface tension between hydrate and water. By using their experimental data and mathematical model they found that surface tension between hydrate and water is 18 times smaller than the surface tension between ice and water.

5.4 Properties of CO_2 and CH_4 mixtures

When carbon dioxide is injected into the methane hydrate, there will be occurrence of both methane and carbon dioxide gas. Oldenburg *et al.* (2001)

stated that, mixing of these gases would take place either by molecular diffusion, advection and/or dispersion. Therefore, equilibrium conditions for hydrate formation and dissociation would automatically change. Adisasmito *et al.* (1991) tried to determine equilibrium pressure and temperature for hydrate formation from mixtures of carbon dioxide and methane gases and offered the following equation;

$$\ln(P_{cal}) = 175.3 - \frac{89009}{T} + 0.07392 * y + \frac{1.1307 * 10^{7}}{T^{2}} - \frac{23.392 * y}{T} + 3.9566 * 10^{-5} * y^{2} \quad (5.1)$$

where y is mole percent of carbon dioxide in the vapor phase (water-free basis). The above equation was fitted to the experimental data gathered in between 0 ^{o}C (273 K) and 15 ^{o}C (288 K) and pressure from 1.2 to 11 MPa. Plots that were prepared by using the above equation were presented in Figure 5.2.

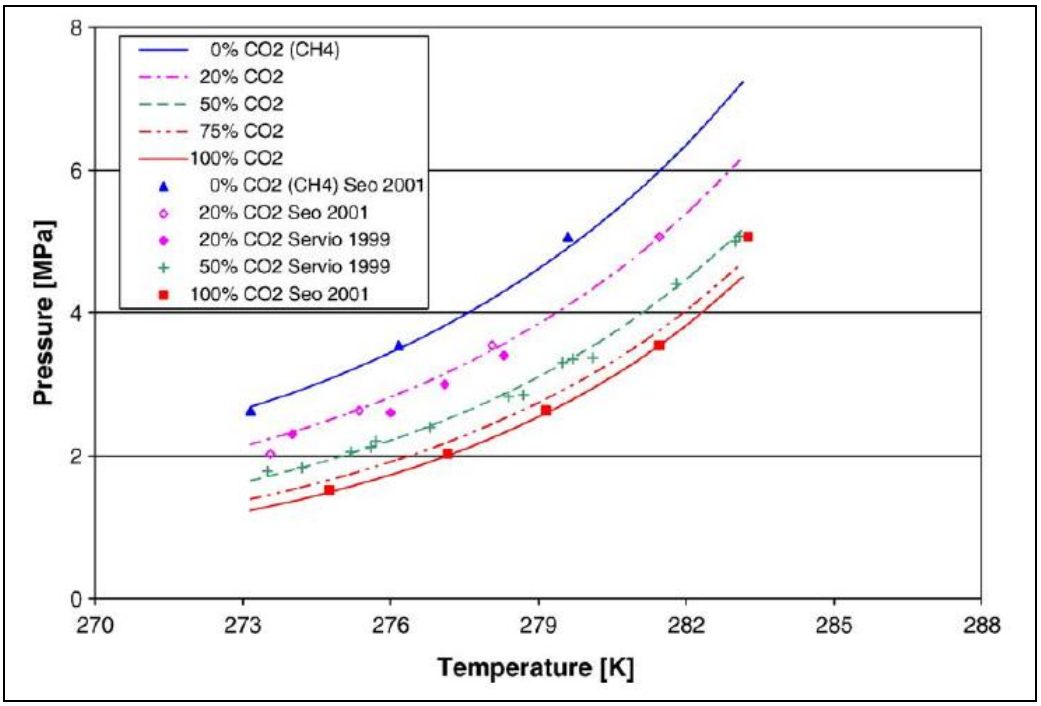

Figure 5. 2 Phase equilibrium of mixtures of carbon dioxide and methane gases (Lines were prepared by using Equation (5.1) and dots represent the experimental data (Adapted from Goel, 2006)

As expected, equilibrium conditions for hydrate formation from mixtures of carbon dioxide and methane gases lie between the conditions for individual methane and carbon dioxide hydrates. As can be seen from the Figure 5.2, as the mole percent of carbon dioxide gas in the mixture increases, the equilibrium conditions move to lower pressure or higher temperature.

Figure 5.2 also includes experimental data for mixtures of methane and carbon dioxide gases (Servio *et al.*, 1999) (Seo *et al.*, 2001). As can be seen from the figure, values calculated by above equation and the experimental data shows good match.

Lee *et al.* (2003) stated that both methane and carbon dioxide form Structure I hydrates; therefore, their mixture also forms the same hydrate structure.

However, methane molecules fill both small and large cavities while the carbon dioxide molecules preferentially fill the large cavities. For this reason, during the formation of hydrates from the carbon dioxide and methane mixture, the methane occupies the small cavities and is out-numbered by the carbon dioxide in the large cavities and the relative occupancy of carbon dioxide in small cage is very small. According to Nakano & Ohgaki (2000), this phenomenon is related with the size of each molecule. The van der Waals diameter of carbon dioxide is 0.47 nm and that of methane is 0.43 nm. The lattice constant of Structure I hydrate is 1.2 nm (Sloan, 2008).

As the carbon dioxide favorably fills the larger cavities, methane will remain as guest in the small cavities and will not be fully removed from the hydrate phase even the carbon dioxide saturation reaches 100%. As a result, when carbon dioxide injected into the methane hydrate, substitution of carbon dioxide in the methane hydrates would be limited even when the equilibrium conditions are achieved. It was predicted that about 64% of the methane gas could be recovered from a regular methane hydrate composition (Lee *et al*., 2003). In addition, reverse reaction of carbon dioxide hydrate with methane gas was slow. Therefore, once the carbon dioxide hydrate formed, then it is very difficult to decompose and form the methane hydrate. In the light of above discussion, it can be concluded that, carbon dioxide is a much better guest molecule than methane, and would be preferably sequestered as hydrate.

5.5 Equilibrium conditions in porous media

Figure 5.3 shows the comparison of equilibrium conditions for methane and carbon dioxide hydrates in porous media with those in the bulk medium. According to Clennell *et al*. (1999), bulk medium can be defined as where the local changes in material properties are negligible and the surface energy effects are small.

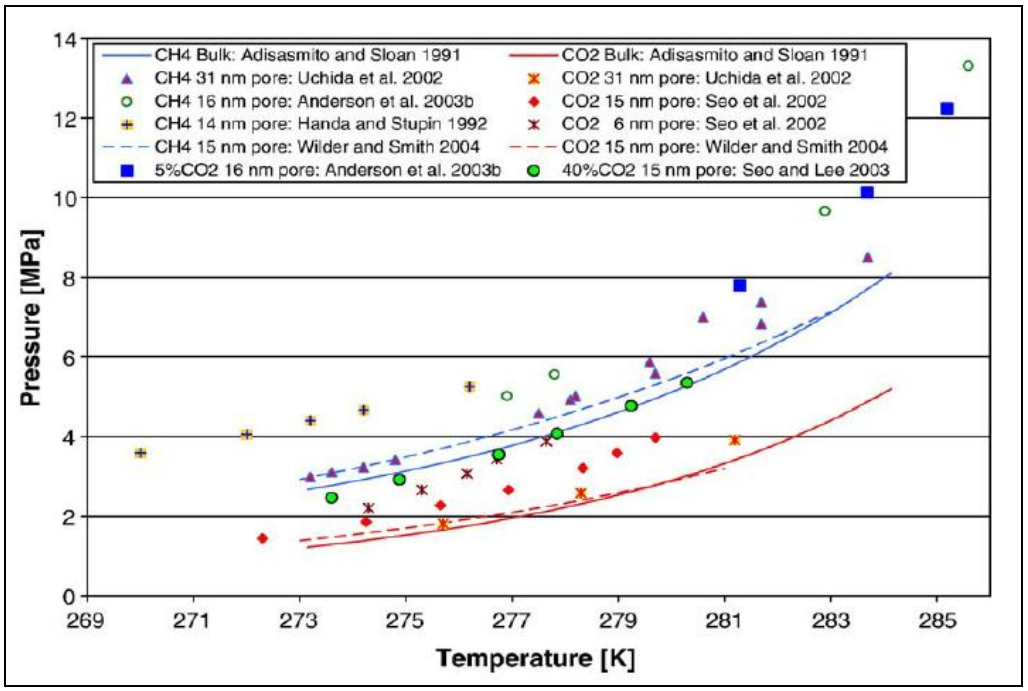

Figure 5. 3 Equilibrium conditions for methane and carbon dioxide hydrates in porous media (Adapted from Goel, 2006)

In Figure 5.3, experimental data are illustrated by various symbols, whereas the lines correspond the data obtained by the several published correlations. Also, blue squares and green circles indicate the data for the hydrates of methane carbon dioxide gas mixture, which includes 5 and 40 mol% of CO_2 respectively. In these experiments, porous medium is described with mean pore diameter. The experiments were carried out by using two different porous media: porous silica gels (Handa & Stupin, 1992) (Seo *et al*., 2002) (Seo & Lee, 2003), and porous glass (Uchida *et al*., 2002) (Anderson *et al*., 2003-a-b).

In a porous media, hydrate formation initiates in the larger pore sizes and then continues in the smaller pore sizes as the temperature decreases. On the other hand, Wilder *et al.* (2001) stated that, dissociation of hydrates begins in the smallest pores and then continues in larger size pores as the temperature is increased. Therefore, since the formation and dissociation of hydrate process

are not exactly same, some hysteresis effect might be expected between the dissociation and formation curves in porous media.

5.6 Modeling the effect of porous media

For the equilibrium conditions for hydrates, comprehensive statistical based model that was proposed by van der Waals & Platteeuw (1959) is widely used. However, this model does not take into account the influence of porous media on hydrates in sediments. The improvements can be done by modeling the experimental observations of the hydrate formation/dissociation in porous media and including in the equation.

The porous media decreases the activity of water, which means higher pressures at a given temperature or lower temperatures at a given pressure are required for hydrate formation. In other words, geometrical constraint imposed by the pore walls is similar to the chemical constraint imposed by inhibitors. Also, salinity of water in pores contributes to the equilibrium condition for hydrate formation in a negative manner. As a result, all the above mentioned parameters will decrease the stability region of hydrates.

Yousif & Sloan (1991) proposed a simple model for the additional pressure required to form hydrates in porous media:

$$\Delta P = 3.26399 * \sigma * \left(\frac{\phi}{k} \right)^{1/2} \tag{5.2}$$

where ΔP is in psia, σ in dynes/cm, k in md and ϕ is a fraction.

Uchida *et al.* (1999) proposed the following equation for the reduction in equilibrium temperature in a porous media:

$$\left(\frac{\Delta T}{T_d}\right) = 0.0016 - \frac{2.3}{d_a} \tag{5.3}$$

where T_d denotes final dissociation temperature in K and d_a denotes the pore diameters in Å.

Wilder & Smith (2004) developed an explicit empirical equation for predicting the equilibrium conditions in porous media:

$$\ln f \approx a + \frac{b}{T} + c\ln\left(\frac{T_0}{T}\right) + \frac{e}{T_r} + d' \frac{\exp\left(a + \frac{b}{T} + c\ln\left(\frac{T_o}{T}\right) + \frac{e}{T_r}\right)}{(T_0 + T)} \tag{5.4}$$

where f is the fugacity of the hydrate guest, and the parameters a, b, c, d' and e are: for methane hydrate: -3.679, 1242.7, -27.903, 8.694, 696, respectively; for carbon dioxide hydrate: 7.639, -2079.1, -16.949, 60.387, 748.87, respectively.

5.7 Effect of pore size

Gas hydrates in sediments are generally associated with the presence of organic matter rich fine grained silts, muds and clays, with lesser coarser sandy layers. Pore size, porous material and texture are the most important parameters that directly influence the hydrate growth pattern. In fine grained sediments, hydrates are generally found in the form of segregated nodules, lenses, pellets or sheets. However, in coarser layers, clathrates form an interstitial pore fill between sediment grains. To sum up, hydrate morphology and hydrate distribution within the sediments are function of host sediment properties. (Clennell *et al*., 1999).

As can be seen from the Figure 5.3 the effect of porous medium on equilibrium conditions increases when pore diameter decreases. In a porous media, lower temperature values are required for hydrate formation in smaller pores than that required for larger pores at a given pressure. Therefore, at a given temperature value, it is expected that, some pores may contain hydrates while others contain water and free gas.

In addition, there should be a maximum pore size above which the porous media shows the similar characteristics with the bulk medium. Likewise, there should be a minimum pore size below which the hydrate could not form in a porous media. Furthermore, capillary pressure in the small size pores may also prevent the free gas entrance into these pores. In the light of above discussion, for the hydrate formation minimum pore diameter must exceed the unit cell size of the hydrate structure that is 1.2 nm for Structure I (Sloan, 2008).

Pores are coated with a layer of water, which does not participate in the hydrate formation. Tohidi *et al.* (2001-b) carried out several experiments to determine the effect of porous media. According to their observations, thin layer of water remains even after the hydrate formation. By means of thermoporometric analysis, Handa *et al*. (1992) found that thickness of this water layer is between 0.45 to 0.55 nm. Uchida *et al.* (2002) stated that, when the lattice parameters of Structure I type hydrate and the thickness of the bound water are considered, for the methane or carbon dioxide hydrate formation, minimum pore diameter of 3 nm is required.

As expected, hydrate formation in large size pores, reduces the volume available for hydrate crystal to grow. A pore that has a diameter of 100 μm may not show the porous media effect. However, as the hydrate crystal grows, available pore space automatically diminishes to the value less than 100 μm. Goel *et al.* (2004) experimentally determined that, ice formation in an

unconsolidated sand pack, which has a pore size ranging between few nanometers and 100 μm, causes a 4.5 ^{o}C decrease in temperature value. Also, they argued that the presence of ice diminishes the pore size significantly when compared with the pore size that includes only unfrozen water. After the reduction in pore size, temperature will decrease significantly and the water saturated sand pack will freeze at much lower temperature than the freezing point.

5.8 Effect of type of porous material

Hydrate formation in porous media is also affected by the type of porous media. Both physical and chemical characteristics of porous media have an influence on distribution and growth pattern of hydrates in porous media. Hydrates in porous media either present as segregated particles or fill the pore spaces in the sediments. In fine grained sediments such as clays and silts, hydrates will be present as segregated particles, which might form lenses, nodules or sheets (Clennell *et al.*, 1999). Also, in unconsolidated sands, hydrates will not fill the pore space or coat the grains, but would form segregated nodules and lenses (Kleinberg *et al.*, 2003-a-b). In consolidated sands hydrates may uniformly disseminate in the pore spaces. In coarse grained formations, hydrates tend to form in the pore interstices (Henry *et al.*, 1999).

Different interfacial energy values were found by using different porous material such as porous glass and natural quartz sand. However, it is difficult to ascribe the difference to the porous media because there is no systematic study to understand the impact of the type of porous material on the interfacial tension of hydrate–water system.

Uchida et al. (2004) tried to determine the effects of surface texture, pore size distribution and water content of the sediments on hydrate formation/dissociation conditions in both natural and artificial porous samples.

According to their conclusion, pore size has a significant effect on hydrate dissociation, whereas surface texture and mineral composition have little effect. Moreover, Smith *et al*. (2002) experimentally investigated that, the equilibrium conditions for hydrate formation in the porous glass were in between the values for those in the porous silica gel and in the bulk medium.

5.9 Flow characteristics of hydrate containing porous media

In order to determine the mechanism of hydrate formation characteristics in the porous media, a good understanding of the flow characteristics of hydrate containing porous media is required. Also, by considering the hydrate growth pattern in the pore spaces, porosity and permeability of the reservoirs should be predicted. Kleinberg *et al*. (2003-b) proposed a simple model for relative permeability in a hydrate reservoir based on pore filling or surface coating properties. For a hydrate occupying pore center, the relative permeability is given by:

$$k_{hw} = \frac{(1-S_h)^{m+2}}{(1+S_h^{0.5})^2} \tag{5.5}$$

where saturation exponent m increases from 0.4 at $S_h = 0.1$ $(S_w = 0.9)$ to unity at $S_h = 1$ $(S_w = 0)$.

For a hydrate coating the grain surface, the relative permeability is given by:

$$k_{hw} = (1-S_h)^{m+1} \tag{5.6}$$

the exponent is 1.5 for $0 < S_h < 0.8$,but diverges for $S_h > 0.8$ (Kleinberg *et al*., 2003-b).

Masuda *et al.* (1997) assumed hydrate to line the walls of the pores and proposed the following equation:

$$k_{hw} = (1 - S_h)^m \tag{5.7}$$

where m changes between 10 and 15.

Moridis *et al.* (1998) proposed the following simple model for relative permeability in their gas hydrate study:

$$k_{hw} = (\bar{S})^{1/2}(1-(1-(\bar{S})^{1/m})^m)^2 \tag{5.8}$$

where

$$\bar{S} = \frac{S_w - S_{w,irreducible}}{1 - S_{w,irreducible}} \tag{5.9}$$

where m is 0.457 (Pruess *et al*., 2001).

5.10 Replacement of CH_4 in the hydrate by use of CO_2

CH_4 hydrates are expected to be a future energy resource, when the amount of CH_4 hydrate within deep sea sediments is considered. Therefore, recovering CH_4 from its hydrate has become a favorite subject and some possible production mechanisms have been proposed such as; thermal treatment, depressurizing and introducing inhibitors into the hydrates. However, production of hydrate is a tough process, since it always includes the risk of triggering the catastrophic slope failures since destabilization and decomposition processes may weaken the stability of ocean floor. Moreover, uncontrolled or rapid release of CH_4 in ocean or air could be a problem in terms of greenhouse effect.

One possible mechanism for CH_4 production from hydrate is the replacement of CH_4 in the hydrate with the injection of CO_2. This process can be carried out as long as the ocean floor remains stabilized after the replacement process. Possibility for CO_2–CH_4 replacement has been investigated both theoretically and experimentally. Studies on three phase equilibria (vapor–liquid–hydrate) indicated that the CO_2 hydrate is thermodynamically more stable than the CH_4 hydrate under low temperatures, below 10 ^oC (283 K), since the hydrate formation pressure of the CO_2 hydrate is lower than that of the CH_4 hydrate at low temperature values (Kang *et al.*, 1998) (Anderson *et al.*, 2003-b). Ohgaki *et al.* (1996) studied on distribution coefficients of CH_4 between the gas and the hydrate phase at 7 ^oC (280 K) and showed that the mole fraction of CH_4 in the gas phase was larger than that in the hydrate phase. Also, molecular simulation studies conducted by Yezdimer *et al.* (2002) indicated that, Gibbs free energy for the replacement has a negative value. In the light of these evidences it can be said that, replacement is thermodynamically possible option when the conditions are appropriate.

Recovery of CH_4 from hydrate by replacing CO_2 was demonstrated and succeeded in laboratory scale. Hirohama *et al.* (1996) performed the replacement reaction with saturated liquid CO_2 at 1 ^oC (274 K) and stated that the driving force for the replacement is probably the fugacity difference between the fluid and the hydrate phases, assuming a direct replacement mechanism. On the other hand, Ohgaki *et al.* (1996) noted that, replacement may result from CH_4 hydrate decomposition due to the heat that is liberated from the formation of CO_2 hydrate. Ota *et al.* (2005) studied the replacement mechanism in the two kinds of cages (M and S-cage). They concluded that, decomposition of the medium cage (M-cage) in the CH_4 hydrate proceeded faster than that of the small cage (S-cage). They also stated that, S-cage in the CH_4 hydrate is more stable than M-cage or after decomposition of hydrate re-formation of S-cage is easier than M-cage. However, guest molecule exchange

of CH_4 with CO_2 could occur in the M-cage. Zhou *et al.* (2008) showed in their study that the use of CO_2 emulsions is advantageous compared to the use of liquid CO_2 in replacing CH_4 from its hydrate. Komai *et al*. (2002) suggested that in bulk conditions methane in methane hydrate could be measurably replaced by CO_2 within 12 hours.

The CH_4-CO_2 swap process is influenced by several factors and coexisting processes, such as pressure and temperature dependent relative viscosity, permeability, density and solubilities among water, CH_4 and CO_2 (Jung *et al.*, 2010). Studies conducted by Stevens *et al.* (2008) indicated that there is no apparent hydrate dissociation during the swap process. Also, another study showed that CH_4-CO_2 swap occurs locally and gradually so that the overall hydrate mass remains solid and no stiffness loss should be expected at the sediment scale (Jung & Santamarina, 2010).

McGrail *et al*. (2007), who studied the CH_4-CO_2 replacement ratios and rates, indicated that swap rate increases as the CO_2 gas pressure increases and it will reach a constant value when the CO_2 liquefies. Park *et al*. (2006) concluded that swap ratio increases when the CO_2 is mixed with N_2 since the smaller N_2 molecules facilitate the replacement of CH_4 from the small cage in structure I hydrate.

Several researches have been conducted to increase the replacement reaction rate; one of them, McGrail *et al*. (2004) introduced the method of enhanced gas hydrate recovery (EGHR). His method includes the preparation of the emulsion in which water is the continuous phase and CO_2 is the dispersed phase and use of this emulsion to replace CH_4 gas from hydrate. According to McGrail, use of emulsion has several benefits such as, controlled multiphase flow, heat, and mass transport processes in hydrate-bearing porous media, makes full use of the physical and thermodynamic properties of mixtures in the H_2O-CO_2 system,

thus it can increase the contact area between CO_2 molecules and CH_4 hydrate and enhance the replacement reaction. Also, White *et al.* (2009) performed numerical simulations to investigate the CO_2-CH_4 swap within hydrates with the use of gaseous CO_2, liquid CO_2 and CO_2 emulsion and they concluded that the replacement rate with CO_2 emulsion is the highest among the three alternative techniques.

Geng *et al.* (2009) investigated the stability of the CH_4 hydrate, CO_2 hydrate and CH_4–CO_2 mixed hydrate by using molecular dynamics (MD) simulations for a temperature range of -13 ^oC (260 K) to 7 ^oC (280 K) and at a pressure of 5 MPa. The study showed that, CH_4–CO_2 mixed hydrate is the most stable hydrate structure.

5.11 CO_2 Sequestration in the Black Sea

The Black Sea is one of the world's largest inland marine environments, which is located between the latitudes of 41° to 46° N and longitudes of 28° to 41.5° E with an area of 423,000 km^2, a volume of 534,000 km^3 and a maximum depth of 2200 m. Turkish Straits (Bosporus) at Istanbul, connects the Black Sea to the rest of the world's oceans. Besides Turkey, the Black Sea is bordered by Romania, Bulgaria, Ukraine the Russian Federation and Georgia.

The Black Sea was a fresh water basin until the rise in the world sea level nearly 9000 years ago. Due to increase in the sea level, an influx of the warm and saline waters coming from the Mediterranean Sea took place. Therefore, fresh water of the Black Sea and saline water of the Mediterranean Sea were stratified according to their density difference. As a result of this activity, anoxic condition that is crucial for the deposition of organic matter, started to evolve in the deep sections of the basin. Although, 90% of its water is anoxic, shallow parts (a depth of 50 meters) are fed by rivers that are rich in nutrient

content. Therefore, conditions of the Black Sea region meet the required criteria for the formation and deposition of the organic matter (Oguz *et al*., 2005).

Vassilev & Dimitrov (2002) stated that pressure, temperature and salinity conditions of the Black Sea basin are suitable for hydrate occurrence. According to their estimations, extent of reservoir is 100250 km^3, which corresponds to the $77350*10^9$ m^3 of actual gas hydrates. Figure 5.4 indicates the sea floor water temperatures that were prepared by means of dataset composed of 2320 points monitored over the last 100 years. As it is shown in the figure, bottom water temperatures in the Black Sea slightly oscillates around 8.9 ^oC with an amplitude of 0.3 ^oC.

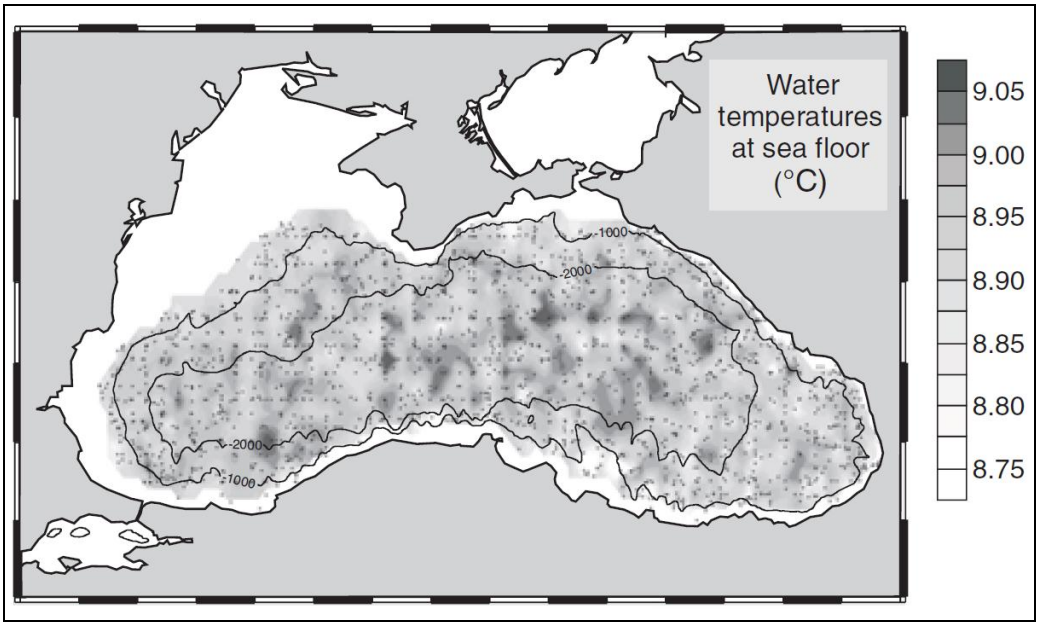

Figure 5. 4 Map of the sea floor water temperature distribution in the Black Sea at water depths greater than 300 m. Measurement sites are represented by dots (Poort *et al.*, 2005).

Vassilev & Dimitrov (2002) also made an estimation about gas hydrate stability zone (GHSZ) in the Black Sea basin. Their work suggests that, methane hydrate occurrence begins at a water depth of 670-700 m.

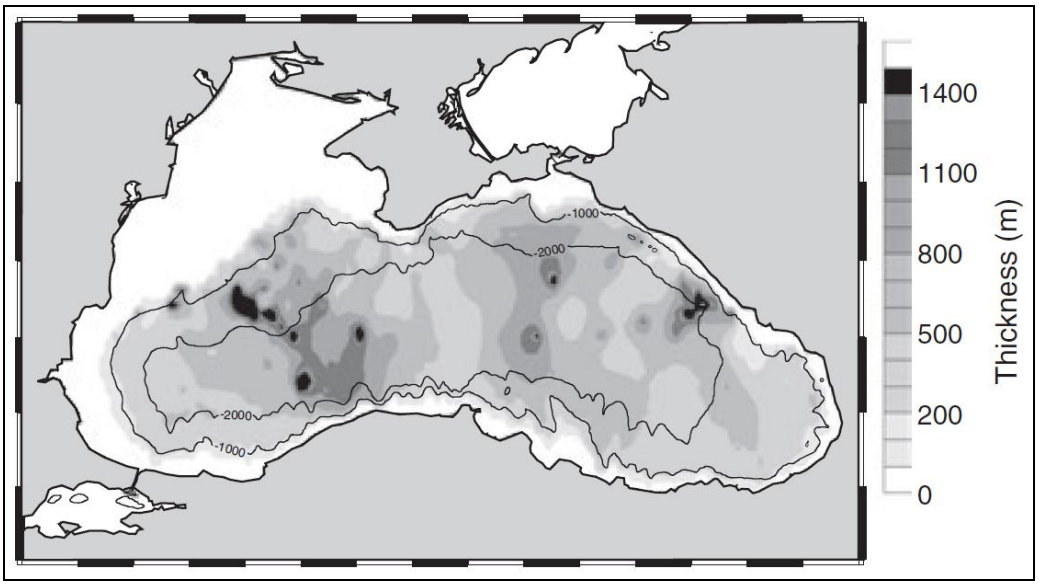

Figure 5. 5 The calculated thickness of the GHSZ in meters (Poort *et al.*, 2005).

Furthermore, Parlaktuna & Erdogmus (2001) estimated the hydrate stability zone (ZHF) in the sedimentary section of the Black Sea region. They calculated hydrate stability zone with geothermal gradients of 3, 3.5, and 4 °C/100 m for different sea bottom depths. Table 5.1 lists the thickness of methane hydrate ZHF in the Black Sea as functions of depth and geothermal gradient. An example of the methane hydrate stability curve taken from their study is also presented in Figure 5.6.

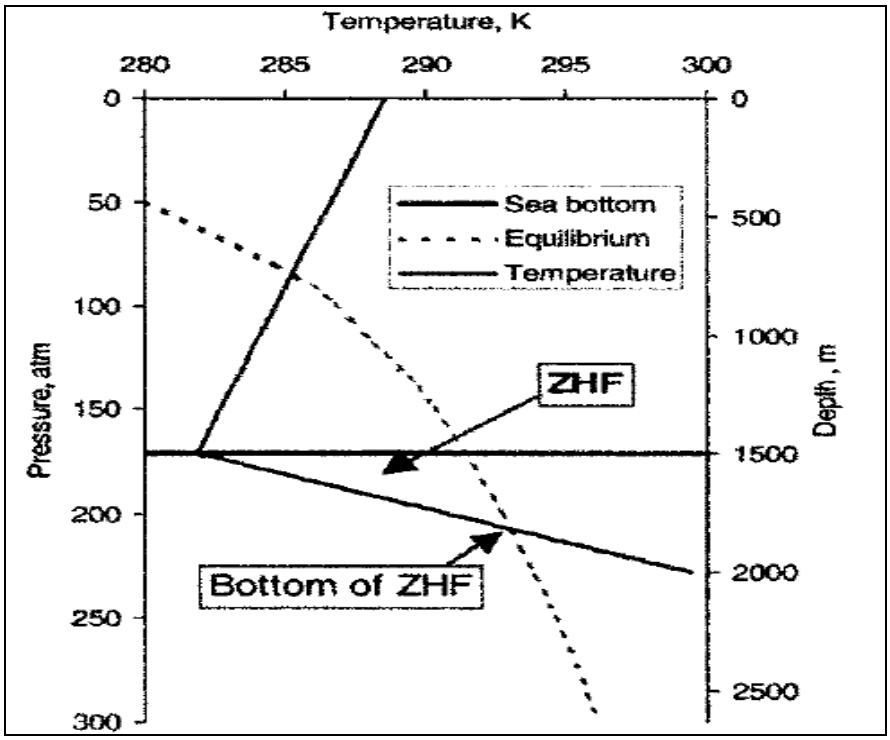

Figure 5. 6 Methane hydrate stability zone at 1500 m sea bottom depth and 3.5° C/100m geothermal gradient (Parlaktuna & Erdogmus, 2001).

Table 5. 1 Thickness of methane hydrate in the Black Sea (Parlaktuna & Erdogmus, 2001).

	Thickness (m)		
Depth (m)	3°C/100m	3.5°C/100m	4°C/100m
600	80	60	50
700	160	130	100
800	200	160	140
900	240	200	160
1000	270	220	190
1100	300	250	210
1200	320	270	230
1300	340	290	240
1400	370	310	260
1500	380	320	270
1600	400	340	290
1700	420	350	300
1800	430	360	310
1900	440	370	320

CHAPTER 6

STATEMENT OF PROBLEM

Recently, climate change has become one of the most important global challenges of the world; therefore, limiting the emission of greenhouse gases is the serious problem of this century that should be addressed immediately. Among all the greenhouse gases, CO_2 deserves particular attention as the increase in global temperature level commonly correlated with the increase in the CO_2 concentration in the atmosphere. As a result, many studies and researches have focused on CO_2 sequestration techniques. Some proposed options for geologic storage of CO_2 are; CO_2 injection into depleted oil and gas reservoirs, deep saline aquifers, and unmineable coalbeds. However, all the above mentioned techniques include some shortcomings; therefore, globally acknowledged sequestration option is required.

This study, considers the injection of CO_2 into the sediments of the Black Sea, especially in the regions where significant methane hydrate accumulation exists. Therefore, existing methane hydrate layer may act as a seal for the injected CO_2. Any injected CO_2, which is able to find flow pathways through the impermeable methane hydrate layer, will form CO_2 hydrate as long as it encountered water-rich sediment. Furthermore, CO_2 hydrate may be more stable than the methane hydrate under the prevailing conditions. Moreover, as the presence of CO_2 increases the stability zone of the methane hydrate, injected CO_2 may increase the sealing capacity of the methane hydrate. Therefore, main objective of this study is to observe the interaction between CO_2 and methane hydrate.

CHAPTER 7

EXPERIMENTAL SETUP & PROCEDURE

7.1 Experimental Setup

Throughout this study, various tests were performed to determine the feasibility of CO_2 sequestration in the Black Sea sediments. These include the CH_4 hydrate formation in both bulk conditions and within sand particles, determination of the permeability of unconsolidated sand particles that includes 30% and 50% methane hydrate saturations and injection of CO_2 into the CH_4 hydrate for the observation of the interaction between CO_2 and CH_4 hydrate. The experimental setup that was used to perform the experiments is indicated in Figure 7.1.

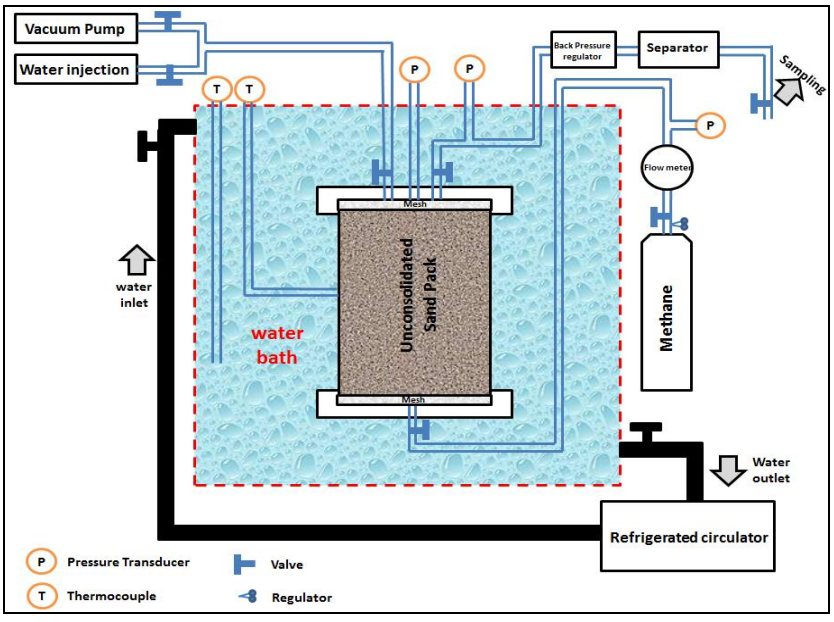

Figure 7. 1 The schematic diagram of the experimental setup

The system contains a cylindrical high-pressure cell that has a volume of 670 cm^3 when all the connections are considered. Photo of the cell can be seen in the Figure 7.2. The cell is packed with medium grained sandstone. ASTM Numbers of the metal screens that are used to screen sand particles are 35 (0.5 mm) and 60 (0.25 mm). The high-pressure cell is placed into a constant temperature water bath, which also includes certain amount of antifreeze to prevent the freezing of water. Photo of the water bath can be seen in the Figure 7.3.

Figure 7. 2 The high pressure cell of hydrate formation and dissociation

A refrigerated bath circulator is used for the cooling process and then to keep the temperature of the water bath constant.

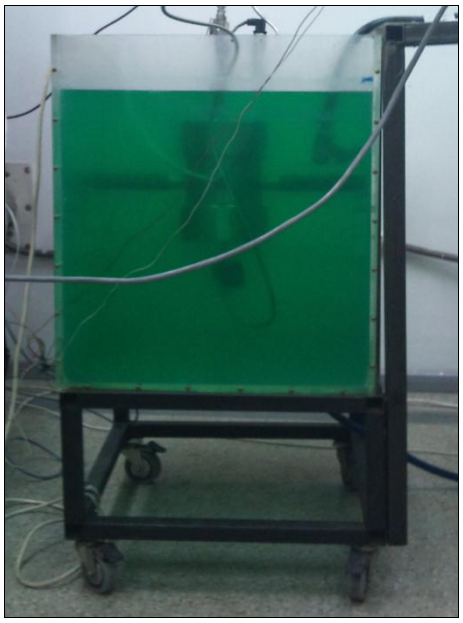

Figure 7. 3 Constant temperature water bath

In order to record the pressure and temperature of the cell, a thermocouple and two pressure transducers (in case one of them may become plugged) are connected to the cell. Also, another thermocouple is added to see the temperature of the water bath. The thermocouples are calibrated according to the refrigerated water circulator which is company calibrated. The pressure transducers are also calibrated using Beamex MC5 Multifunction Calibrator. During the permeability measurements, third pressure transducer is connected to the system after the flow meter to indicate the inlet pressure. Furthermore, a back pressure regulator is added to the end of the system to keep the pressure above the hydrate stability pressure at a given temperature value. The data logger and a personal computer are used for recording temperature and pressure data in every 5 seconds.

Figure 7. 4 Back and front covers are sealed with metal screens

As can be seen from the Figure 7.4 back and front covers of the cell are sealed with metal screens to prevent the leakage of sand particles out of the cell. Also, these metal screens suggest that there are not any sand particles within the connections. In static and bulk conditions it is difficult to form hydrate and hydrate formation, which may occur at the interface between the water and gas cap is not enough to plug the connections. For this reason we are not expecting any plugging within the connections at bulk medium.

An high pressure syringe pump is used for injection of both water and gas and occasionally to pressurize the system. A vacuum pump is also added to the system to vacuum the cell and remove the air before the injection of water and methane. A mass flow meter is used for controlling or measuring the flow rate during the permeability measurements. This mass flow meter is company calibrated for CO_2 gas. For this reason, measured and recorded flow rates in the data acquisition system is converted to the CH_4 by means of a K-factor. The K-factor for CO_2 and CH_4 that are taken from the user's manual of the mass flow meter and they are 0.7382 and 0.7175 respectively. Equation 7.1 is used for conversion.

$$Q_{CH_4} = \left(\frac{K_{CH_4}}{K_{CO_2}} \right) * Q_{CO_2} \tag{7.1}$$

Moreover, a small separator is installed after the back pressure regulator in order to separate produced water if any. A high pressure syringe is used to take samples from the system for the gas chromatography analysis. A methane pressure bottle with 99.99 percent purity and a carbon dioxide pressure bottle with 99.99 percent purity are used during the experiments. Also air pressure bottle is used for leakage test, drying the sand packs and displacing the unwanted water.

Figure 7.5 shows the complete system of the experimental set-up.

Figure 7. 5 The system of the experimental set-up

Table 7.1 shows the properties of the equipment that are used during the experimental studies.

Table 7. 1 Specifications of the equipment used in the experimental set-up

Pressure Transducers	
Trademark	GEMS Sensors
Pressure Range	0 - 100 and 0 - 60 bar G
Output	4 - 20 mA
Supply	12 to 35 V
Precision	± 1 psig
Thermocouples	
Trademark	Elimko
Model	PT - 100 (RT06 - 1P06 - 4)
Temperature Range °C	-30 to +40
Precision	± 0.2 °C
Data Logger and Controller	
Trademark	Elimko
Model	E-680-08-2-0-16-1-0
Voltage	220 V
Data Transfer	RS485 Mod Bus
Data Analysis	A package program of Elimko, Turkey
Vacuum Pump	
Trademark	Javac
Model	DS40
Voltage	220 V/ 50 Hz
Type	Single stage high vacuum
High Pressure Syringe Pump	
Trademark	Teledyne Isco
Model	500D Pump Module
Capacity	507 ml
Flow Range ml/min	0. 001 - 204
Flow Accuracy	0.5% of setpoint

Table 7. 1 Specifications of the equipment used in the experimental set-up (continued)

Refrigerated circulator	
Trademark	WiseCircu WCL Ultra Low Temperature Refrigerated Circulator
Model	WCL - P12
Capacity	12 lt
Refrigerator	368 W
Temperature range	-40 ^{o}C to 100 ^{o}C
Temperature accuracy	± 0.1 °C
Temperature uniformity	± 0.2 °C at -20 ^{o}C
Temperature sensor	PT 100
Pump	15 Lt. / min
Flow meter	
Trademark	Aalborg Mass Flow controller
Model	AFC 26
Gas	CO_2
Flow range	50 ml/min
Accuracy	± 1% of full scale
Repeatability	± 0.2% of full scale
Temperature Coefficient	0.1% of full scale/^{o}C
Pressure Coefficient	0.01% of full scale/psi (0.07 bar)

7.2 Experimental procedure for the hydrate formation in bulk conditions

The experimental procedure includes the following steps:

1. The cell is placed into the water bath and leakage test is carried out by injecting air at a pressure greater than 1000 psi.
2. After making sure that there is no leakage in the system, the high-pressure cell is evacuated by creating vacuum in the cell (less than -1 bar) by means of a vacuum pump.
3. A known volume of water is injected into the cell.
4. Then, hydrate former gas (in this experiment both CO_2 and CH_4 was used) is injected into the cell at a pressure greater than the hydrate stability pressure at the desired temperature. After hydrate former is introduced to the system, cooling process is initiated.

Rocking or stirring the cell during the cooling process enables continued clathrate formation; however, in our experiments experimental procedure was performed at static conditions. As a result, in bulk and static conditions, hydrate formation at the interface of water and free gas was observed.

7.3 Experimental procedure for the hydrate formation within sediments

The experimental procedure includes the following steps:

1. First of all sandstone is screened in order to obtain medium grained sand particles. For this process, ASTM Numbers of the metal screens are selected as 35 (0.5 mm) and 60 (0.25 mm).
2. Back and front covers of the cell are sealed with metal screens and then the cell is packed with sand grains.
3. The cell is placed into the water bath and leakage test is carried out by injecting air at a pressure greater than 1000 psi.
4. After making sure that there is no leakage in the system, the high-pressure cell is evacuated by creating vacuum in the cell (less than -1 bar) by means of a vacuum pump.

5. A known volume of water is injected into the cell in order to determine the pore volume of the media. When the amount of injected water makes the sufficient pressure in the cell (approximately 10 bar), injection is stopped and the injected volume is recorded as a pore volume.
6. The system is left for few hours in order to let water to distribute itself in the porous medium by the capillary forces. By means of high pressure syringe pump a known volume of water (depending on the required water saturation in the cell) is drained from the cell. Then the system was left to equilibrate for couple of hours for the uniform distribution of water.
7. Then, methane is injected into the cell at a pressure greater than the hydrate stability pressure at the desired temperature. After methane is introduced to the system, cooling process is initiated.
8. The system is left at the hydrate formation conditions until the pressure in the cell becomes stabilized at the pressure of hydrate stability region. Then the pressure increased to a value greater than the pressure of hydrate stability region. This process is repeated for several times and after some time, the pressure of the system is stabilized at a pressure greater than the pressure of hydrate stability region. This means that, all the water in the system is consumed and hydrate formation has completely occurred.

7.4 Experimental procedure for the permeability tests

The experimental procedure includes the following steps:

1. After making sure that all the remaining water in the cell is converted to hydrate, permeability measurements can be initiated.
2. Before the measurement, the pressure in the cell is gradually reduced by means of back pressure regulator. During this process there should not be any hydrate dissociation and this can be tracked from the temperature data.
3. After decreasing the pressure to the desired level, which must be greater than the pressure of the hydrate stability region, the back pressure regulator is also set to the same value. This pressure is the outlet pressure of the system.
4. After setting the back pressure regulator and setting the outlet pressure to a constant value, there are two options for the gas permeability measurement. First one is adjusting the gas supply source to maintain constant pressure. Second one is adjusting the flow meter to maintain a constant flow rate. During the former way, data coming from the flow meter and during the latter way, data coming from pressure transmitter at the inlet line is recorded.
5. Finally pressure difference across the cell is measured and the corresponding flow rate is recorded. For each hydrate saturation, this process can be repeated for different flow rates and different pressure differences.
6. Since all the parameters in the Darcy equation are known, permeability of the system can be determined easily. During permeability measurements, temperature of the system was constant; therefore, Peng-Robinson EOS was used for constant temperature and as a function of pressure.

CHAPTER 8

RESULTS & DISCUSSION

Throughout this study, various tests were performed to determine the feasibility of CO_2 sequestration in the Black Sea sediments. These include the CH_4 hydrate formation in both bulk conditions and within sand particles, determination of the permeability of unconsolidated sand particles that includes 30% and 50% methane hydrate saturations and injection of CO_2 into the CH_4 hydrate for the observation of the interaction between CO_2 and CH_4 hydrate. Table 8.1 summarizes the tests that were performed.

Table 8. 1 Tests performed throughout study

Run #	Explanation
1	Hydrate formation test with continuous CH_4 injection
2	Hydrate formation test at the interface of water and CH_4
3	Hydrate formation test within the sediments (particle size < 0.840 mm)
4	Hydrate formation test at different sediment size (particle size ranges between 0.5 mm and 0.25 mm)
5	Hydrate permeability test at 50% hydrate saturation (particle size ranges between 0.5 mm and 0.25 mm)
6	Hydrate permeability test at 30% hydrate saturation and CO_2 injection into CH_4 hydrate (particle size ranges between 0.5 mm and 0.25 mm)
7	Hydrate formation test with liquid CO_2 and water in porous media (particle size ranges between 0.5 mm and 0.25 mm)
8	Interaction of liquid CO_2 & CH_4 hydrate in presence of excess water in porous media (particle size ranges between 0.5 mm and 0.25 mm)

8.1 Hydrate formation test with continuous CH_4 injection (Run #1)

In the literature it is stated that, in bulk conditions and without shaking or stirring the cell it is nearly impossible to form methane hydrate or the amount of hydrate that is formed in these conditions will be limited. As it was stated before, sediments smooth the way for hydrate formation either by altering the thermodynamic conditions for stability or by providing nucleation sites. Without the help of sediments, shaking, stirring and considering the low solubility of methane in water, hydrate formation will be a tough process. In this experiment, high pressure cell, which has the volume of 670 ml with the connections, was filled with 550 ml water and remaining 120 ml space was reserved for free methane. Then the cell was placed to the water bath temperature of which is 5.8 ^{o}C. High pressure syringe pump that was fully filled with methane is connected to the cell (from the bottom) and the valve between the cell and high pressure syringe pump was opened. After that, methane was expanded into the cell from the bottom and it exerts a 640 psi pressure. This pressure is actually very close to the hydrate formation pressure at 5.8 ^{o}C, which is 663.905 psi. Then, the system was pressurized by means of piston of the high pressure syringe pump and methane was injected into the cell. Pressure is increased gradually until it reached a value of around 1200 psi. During this experiment volume of the high pressure syringe pump was reduced at a rate of 0.05 ml/min and methane was injected into the cell. During this experiment no hydrate formation and pressure decline due to hydrate formation was observed. Figure 8.1 shows the whole story of the experiment.

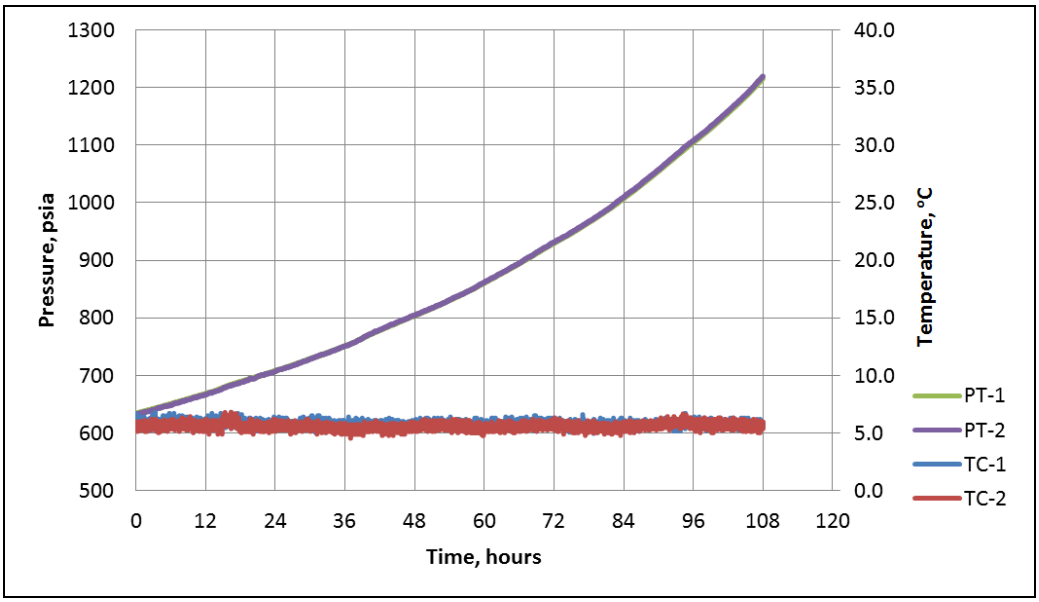

Figure 8. 1 A plot of pressure-temperature-time from the run #1 (Hydrate formation test with continuous CH_4 injection)

8.2 Hydrate formation test at the interface of water and free CH_4 (Run #2)

In this experiment, high pressure cell, which has the volume of 670 ml with the connections, was again filled with 550 ml water and 120 ml free space was reserved for free methane. Then the cell was placed to the water bath temperature of which is approximately 1.9 ^{o}C. The cell was filled with methane that exerts a pressure of 1310 psi. During this experiment, as can be seen from the Figure 8.2, it is difficult to observe decline in pressure or increase in temperature that proves the formation of hydrate. In this experiment, hydrate formation may occur at the interface of water and free gas; therefore, volume of hydrate and consumed methane would be limited, so it is difficult to understand the hydrate formation from the pressure data as the decline in pressure value may result from dissolution of CH_4 in water.

After 72 hours, cell was opened to check the formation of hydrate and as can be seen from the Figure 8.3 hydrate formation at the interface of water and free gas is observed.

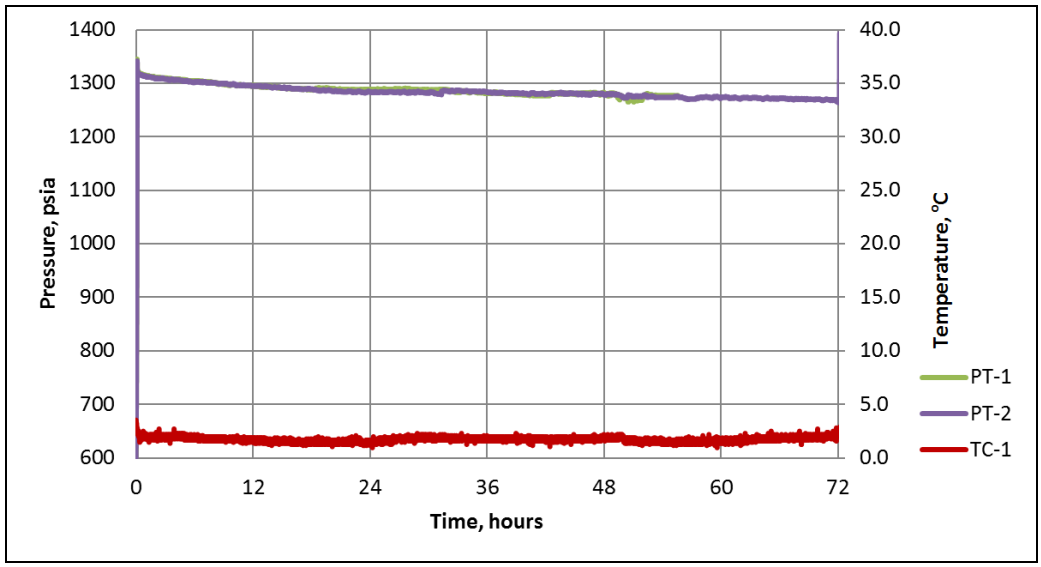

Figure 8. 2 A plot of pressure-temperature-time from run #2 (Hydrate formation test at the interface of water and CH_4)

Figure 8. 3 Hydrate formation at the interface of water and free methane gas from run #2 (Hydrate formation test at the interface of water and CH_4)

8.3 Hydrate formation test within the sediments (Run #3)

In this experiment, high pressure cell, which has the volume of 670 ml with the connections, was packed with sand grains. These sand grains were screened with a metal screens whose ASTM No. is 20 (0.840 mm) and this suggests that the sands are coarsely grained. After packing the cell, the cell was evacuated and water injection was initiated in order to measure the pore volume. Amount of injected water was determined as 330 ml and the corresponding porosity value was calculated as %49. After that, 140 ml water was drained from the cell and the remaining water filled the 57.6% of the pore volume. Remaining volume was filled with methane injection from the bottom until pressure value reaches to 1000 psi at 14 ^{o}C. Then the cooling process was initiated and temperature was reduced up to 3.8 ^{o}C. The aim of this experiment is to see the hydrate formation rate within the sediments and observing the hydrate growth pattern by opening the cell after the experiment. As can be seen from the Figure 8.4, one of the pressure transducers was plugged during the experiment. At first, we believed that the plugging results from the hydrate formation, but after opening the cell, it was observed that the material that was used to glue the metal screens to the front cover of the cell was plugging the lines.

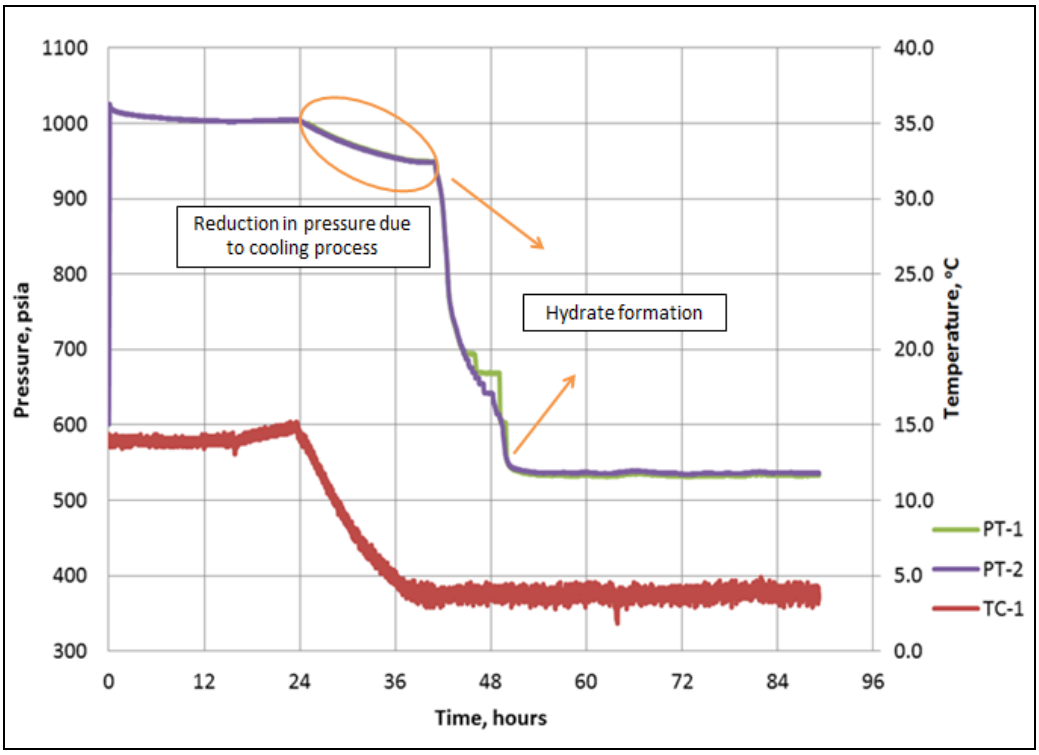

Figure 8. 4 A plot of pressure-temperature-time from run #3 (Hydrate formation test within the sediments particle size of which are lower than 0.840 mm)

After the experiment, cell was opened and hydrate formation at the top of the cell was observed (Figure 8.5).

Figure 8. 5 Hydrate formation at the top of the cell from run #3
(Hydrate formation test within the sediments particle size of which are lower than 0.840 mm)

8.4 Hydrate formation test at different sediment size (Run #4)

In this experiment, high pressure cell, which has the volume of 670 ml with the connections, was packed with sand grains. These sand grains were screened with metal screens whose ASTM No. are 35 (0.5 mm) and 60 (0.25 mm), therefore sands are medium grained. After packing the cell, the cell was evacuated and water injection was initiated in order to measure the pore volume. Amount of injected water was determined as 240 ml and the corresponding porosity value was calculated as %36. After that, 140 ml water was drained from the cell and the remaining water filled the 58.3% of the pore volume. Remaining volume was filled with methane that exerts a pressure of 1280 psi at 20 ^{o}C. Then the cooling process is initiated and temperature was reduced up to 6 ^{o}C. The aim of this experiment is to see the hydrate formation rate within medium grained sands and compare the results with the formation rate within coarse grained sands.

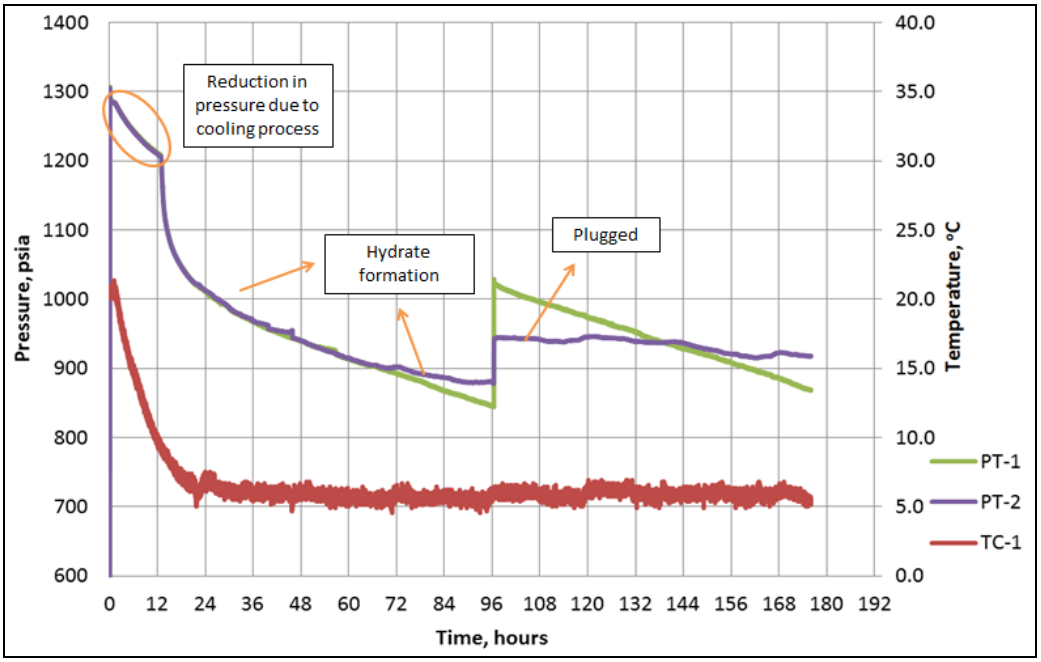

Figure 8. 6 A plot of pressure-temperature-time from run #4 (Hydrate formation test at different sediment size)

As can be seen from the Figure 8.6, one of the pressure transducers (PT-2) was plugged during the experiment. In this experiment, hydrate formation rate was considerably low when compared with the Run #3 that may stem from the higher temperature value. After 4 days, the system was pressurized again with methane to observe the hydrate formation rate at different pressure values. However, no change in the hydrate formation rate was observed and the decline rate of the pressure before and after the methane injection was nearly constant.

8.5 Hydrate permeability test at %50 hydrate saturation (Run #5)

In this experiment, high pressure cell, which has the volume of 670 ml with the connections, was packed with sand grains. These sand grains were screened with metal screens whose ASTM No. are 35 (0.5 mm) and 60 (0.25 mm), therefore sands are medium grained. After packing the cell, the cell was evacuated and water injection was initiated in order to measure the pore volume. Amount of injected water was determined as 240 ml and the corresponding porosity value was calculated as %36. After that, 120 ml water was drained from the cell and the remaining water filled the 50% of the pore volume. Remaining volume was filled with methane that exerts a pressure of 1050 psi at 16 ^{o}C. Then the cooling process was initiated and temperature was reduced up to 3 ^{o}C. The aim of this experiment is to see the sealing capacity of unconsolidated sediments which contain hydrate saturation of 50%. Figure 8.7 shows the whole process of the experiment. Whole experiment took approximately 20 days. During the first 10 days, hydrate formation rate was very low. As the methane was consumed in the system, pressure decline was observed and methane was injected into the system. It can be observed from the Figure 8.7 that after the injection of methane, hydrate formation rate was following almost the same trend.

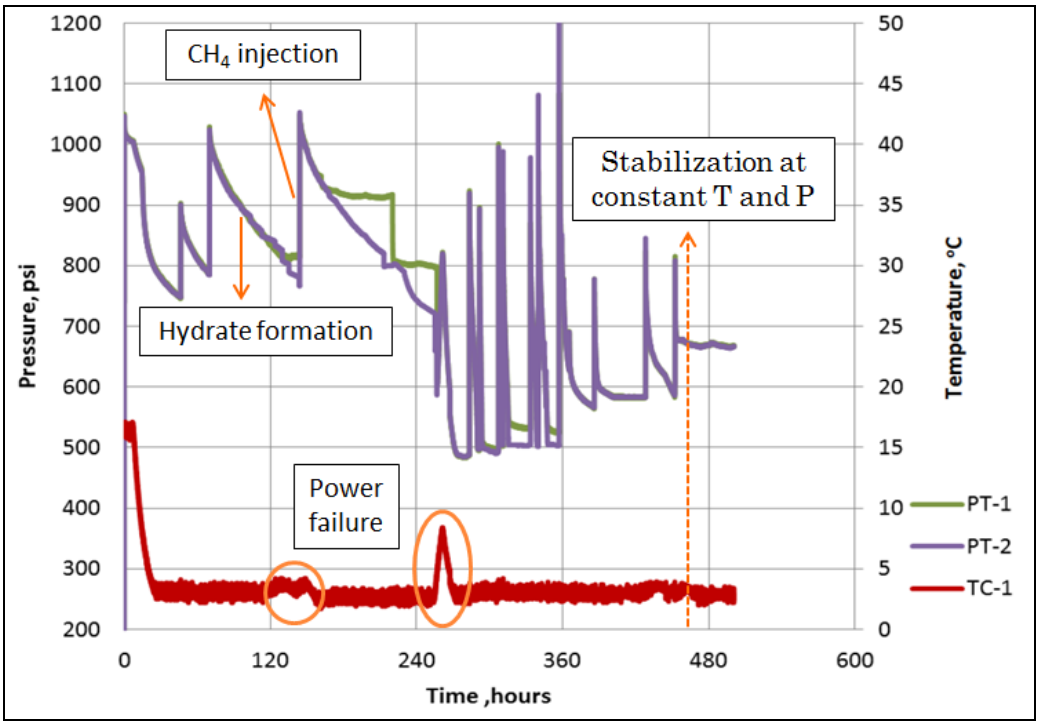

Figure 8. 7 A plot of pressure-temperature-time from run #5 (Hydrate permeability test at 50% hydrate saturation in unconsolidated sediments particle size of which range between 0.5 mm and 0.25 mm)

Also, during this experiment plugging was observed at the first pressure transducer and sharp increase in temperature results from the power failure. As can be seen from the Figure 8.8, hydrate is plugging the pathway; pressure builds up and then unplugs the hydrate and also the corresponding pressure responses are indicated with circles.

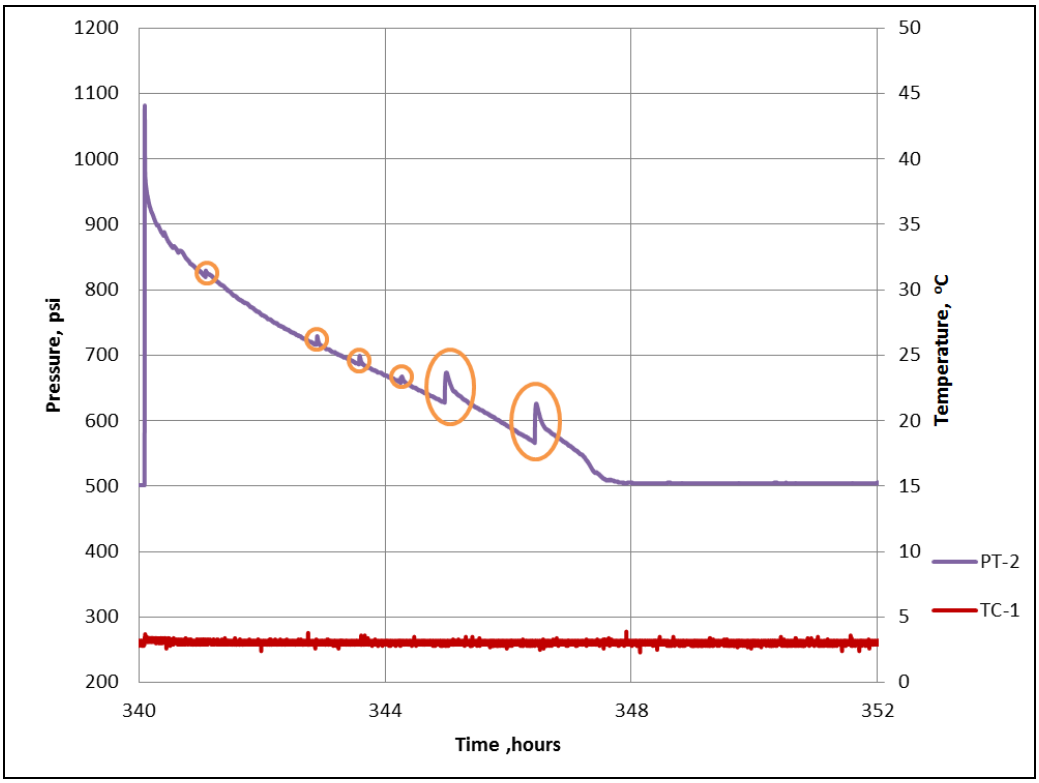

Figure 8. 8 A plot indicating the plugging of hydrate from run #5 (Hydrate permeability test at 50% hydrate saturation in unconsolidated sediments particle size of which range between 0.5 mm and 0.25 mm)

At the beginning of this experiment, initial idea was to convert all the water to the methane hydrate by keeping the excess methane concentration in the cell. After 404 hours, it was observed that pressure of the system was stable at a pressure value greater than the hydrate formation pressure at the corresponding temperature value, which suggests that all the water was converted to methane hydrate. In order to make sure about that pressure is again increased to 840 psi. However, as it is shown in the Figure 8.9, decline in the pressure is observed, also this decline trend suggests that there should be a leakage in the system.

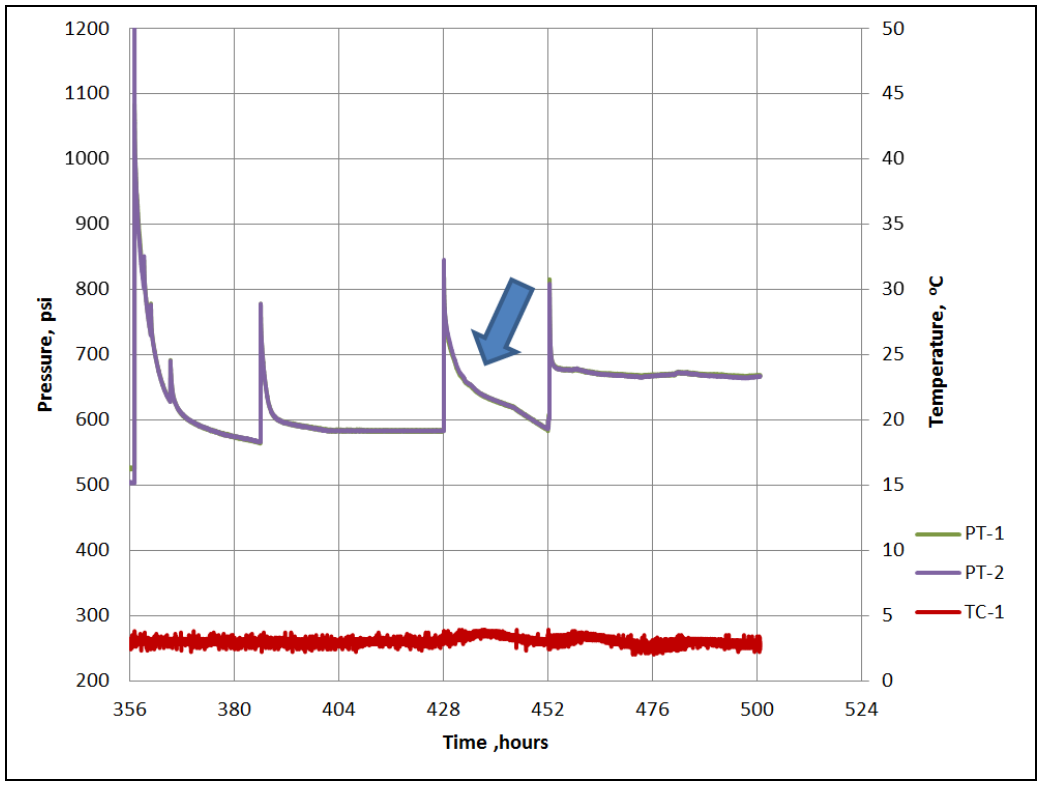

Figure 8. 9 A plot indicating that there is a leakage in the system from run #5 (Hydrate permeability test at 50% hydrate saturation in unconsolidated sediments particle size of which range between 0.5 mm and 0.25 mm)

When the connection between the valve below the cell and valve is checked, small gas bubbles are observed. As it is pointed in Figure 8.10, leakage problem is fixed by taking the cell out of the water bath for a while. For this reason, some fluctuations are observed in the pressure and temperature data. Finally, after another injection process, stable cell pressure is observed for a day (Figure 8.11).

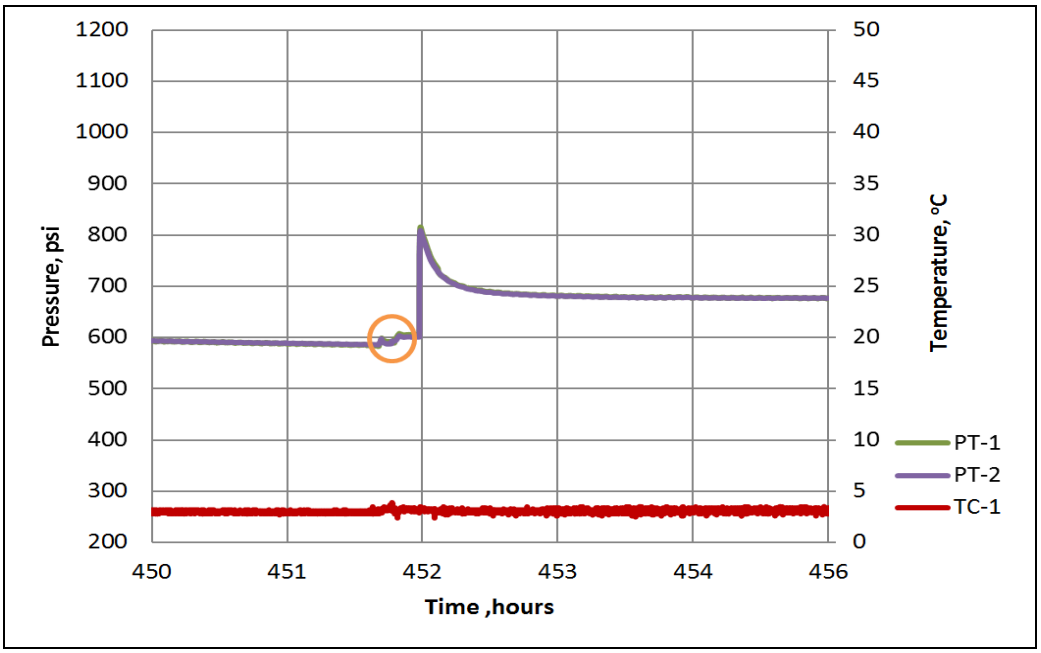

Figure 8. 10 A plot showing the leakage fixing process (Hydrate permeability test at 50% hydrate saturation in unconsolidated sediments particle size of which range between 0.5 mm and 0.25 mm)

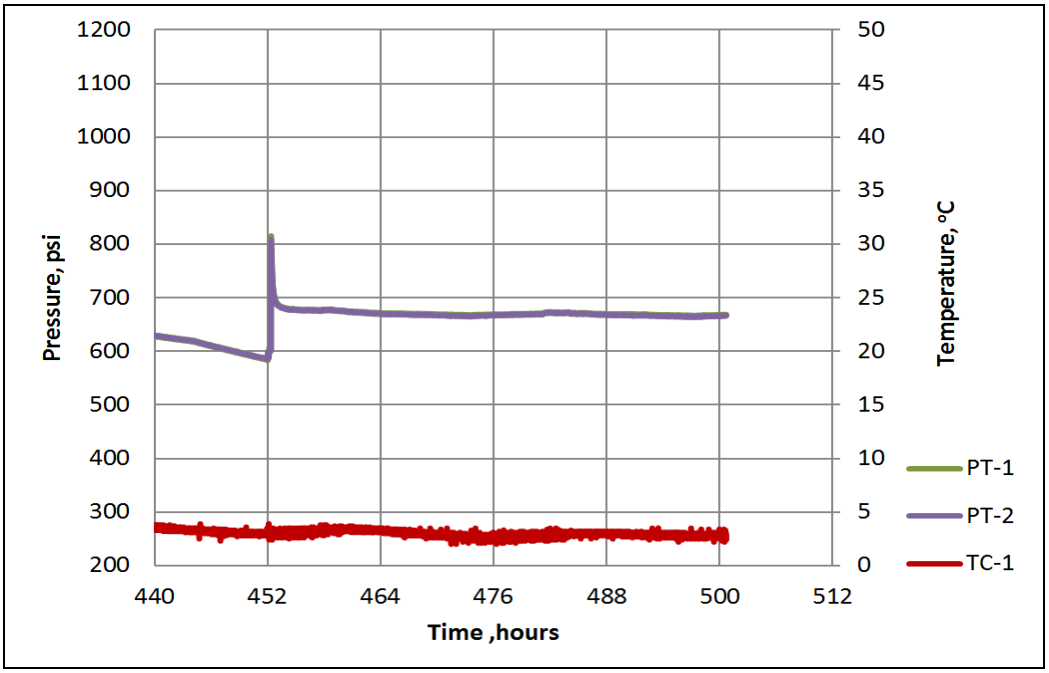

Figure 8. 11 A plot indicating the system pressure stabilized above the stability pressure which is 500.2 psi at 3 ^{o}C (Hydrate permeability test at 50% hydrate saturation in unconsolidated sediments particle size of which range between 0.5 mm and 0.25 mm)

Furthermore, during this experiment water consumption in the cell was estimated incrementally (Figure 8.12). During the hydrate formation experiment, it is important to have an idea about the water consumption, because it gives some clues about the future prediction of the experiment, possible leakage from the cell and cage occupancy. Determination of water consumption can be explained in following steps. Calculation process should be carried out in step-wise manner. First of all, initial number of moles of free gas should be calculated. To do this, real gas law can be used. In this equation, pressure is known; volume is the initial pore volume; temperature is known, z can be calculated through one of the EOS's (In this study Lee-Kesler Correlation was used). Then, step size in terms of pressure should be determined (In this study it was chosen as 10 psi). After that, number of moles of free gas should be determined at this decreased pressure value. The difference between initial and final number of moles of free gas gives the consumed number of moles of methane. It is known that, 1 mole of gas in hydrate structure requires 5.75 moles of water (46/8) for a completely filled hydrate. Therefore, water consumption at this increment can be calculated by multiplying the methane consumption with cage occupancy value 5.75, the molecular weight of water 18 g/g-mole and density of water 1 g/cm^3. Furthermore, it is known that during the methane hydrate formation volume increases by 26%. Makogon (1997) stated that, a water molecule occupies $3.3\times10^{-29}\ m^3$ in liquid state, while in hydrate it occupies $4.158\times10^{-29}\ m^3$. In this way increase in volume at this increment can be estimated and taken into account during the next increment.

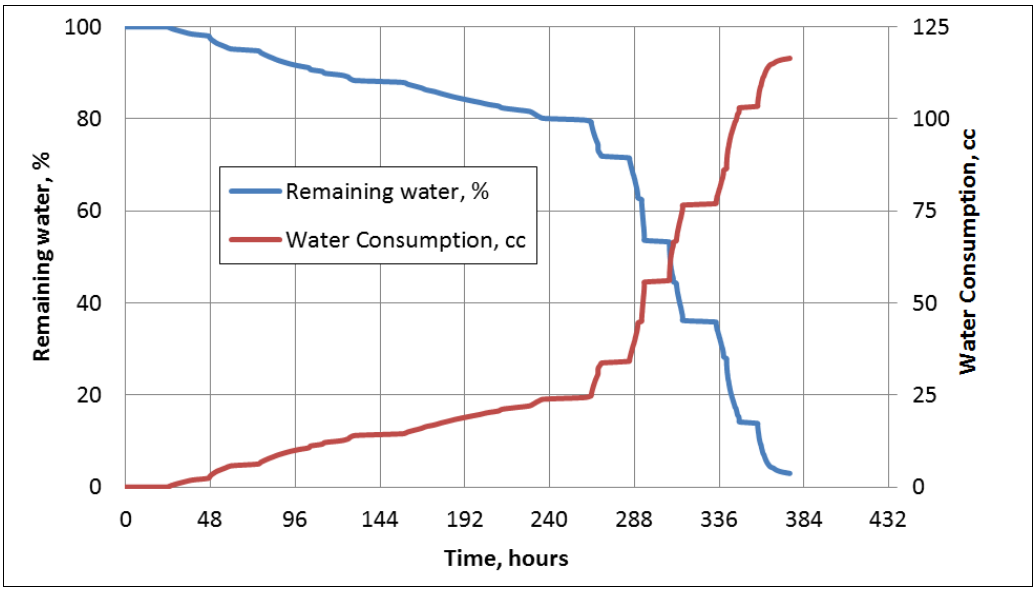

Figure 8. 12 A plot that shows the water consumption in the cell from run #5 (Hydrate permeability test at 50% hydrate saturation in unconsolidated sediments particle size of which range between 0.5 mm and 0.25 mm)

In this experiment, permeability of unconsolidated sediments which contains hydrate saturation of 50% was also determined. During the permeability determination tests, the system was kept above the hydrate stability pressure by means of back pressure regulator and the temperature was stable which suggests that there is no hydrate formation or decomposition. 5 different permeability tests were carried out at various differential pressures or flow rates and the following results were obtained.

Table 8. 2 Results of permeability measurements at 50% hydrate saturation

Permeability test #	1	2	3	4	5
Permeability, md	4.395	4.618	3.706	3.698	3.696

After permeability tests cell was opened and hydrate accumulation and dissociation within unconsolidated sand pack system was observed. Figure 8.13 shows the hydrate formation within unconsolidated sand pack system.

Figure 8. 13 Pictures indicating the hydrate formation within unconsolidated sand pack system (Hydrate permeability test at 50% hydrate saturation and CO_2 injection into CH_4 hydrate in unconsolidated sediments particle size of which range between 0.5 mm and 0.25 mm)

Figure 8. 14 Pictures indicating the hydrate formation within unconsolidated sand pack system. Photo on the left shows the top of the cell and photo on the right shows the bottom of the cell (Hydrate permeability test at 50% hydrate saturation and CO_2 injection into CH_4 hydrate in unconsolidated sediments particle size of which range between 0.5 mm and 0.25 mm)

After opening the front cover of the cell, dissociation process was initiated as the temperature of the system was increased to the room temperature (approximately 18 ^{o}C) and pressure of the system was reduced to the atmospheric pressure. During the dissociation process, as can be seen from the Figure 8.14 (Photo on the left), gas bubbles mostly occurred through the walls of the cell. Therefore, we can conclude that interaction between hydrate and steel is weak when compared with the interaction of hydrate and sand particles. Actually, during the permeability measurements, it is expected that injected CH_4 may bypass through the walls of the core holder. In such a system, hydrate saturation is crucial, as the hydrate formation may partially plug these easy flow pathways; however, it should be noted that, it may not be enough to fully prevent the bypass of injected methane through the walls of the core holder.

In addition, hydrate accumulation and dissociation process was recorded and corresponding video can be found in a cd attached to the thesis.

7.6 Hydrate permeability test at %30 hydrate saturation (Run #6)

In this experiment, high pressure cell, which has the volume of 670 ml with the connections, was packed with sand grains. These sand grains were screened with metal screens whose ASTM No. are 35 (0.5 mm) and 60 (0.25 mm), therefore sands are medium grained. After packing the cell, the cell was evacuated and water injection was initiated in order to measure the pore volume. Amount of injected water was determined as 310 ml and the corresponding porosity value was calculated as 46%. Then, approximately 217 ml of water was drained from the cell and the remaining water filled the 30% of the pore volume. Remaining volume was filled with methane that exerts a pressure of 1235 psi at 20 ^{o}C. Aim of this experiment is to determine the permeability of unconsolidated sediments which contain hydrate saturation of 30%. The other aim of the experiment is to observe the interaction between the carbon dioxide and methane hydrate at excess methane conditions. Figure 8.15

shows the complete hydrate formation and pressure stabilization above the hydrate stability pressure. Figure 8.16 indicates the water consumption data during the hydrate formation. However, it should be noted that, it was not an exact demonstration of the water consumption, because when the methane is injected into the cell, it directly goes to the pressure transducers and exerts the peak pressure value, whereas in order to obtain the correct pressure value some time is required. But there is not enough time to see the stabilization of the pressure in the cell as the hydrate formation initiates as soon as the methane is injected into the system. After the complete formation of methane hydrate, permeability tests were conducted to observe the permeability of unconsolidated sediments that contain 30% of hydrate. 5 different tests at various flow rates and differential pressures were conducted and following results were obtained.

Table 8. 3 Results of permeability measurements at 30% hydrate saturation

Permeability test #	1	2	3	4	5
Permeability, md	618.030	667.947	660.047	638.720	604.838

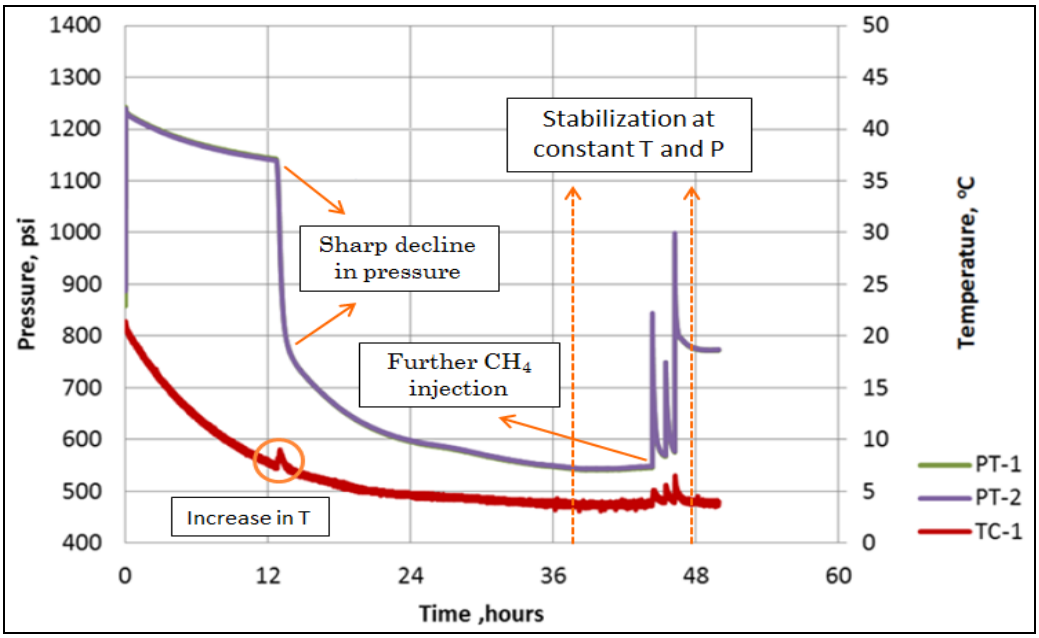

Figure 8. 15 A plot indicating the system pressure stabilized above the stability pressure of CH_4 which is 550.2 psi at 4 ^{o}C (Hydrate permeability test at 30% hydrate saturation and CO_2 injection into CH_4 hydrate in unconsolidated sediments particle size of which range between 0.5 mm and 0.25 mm)

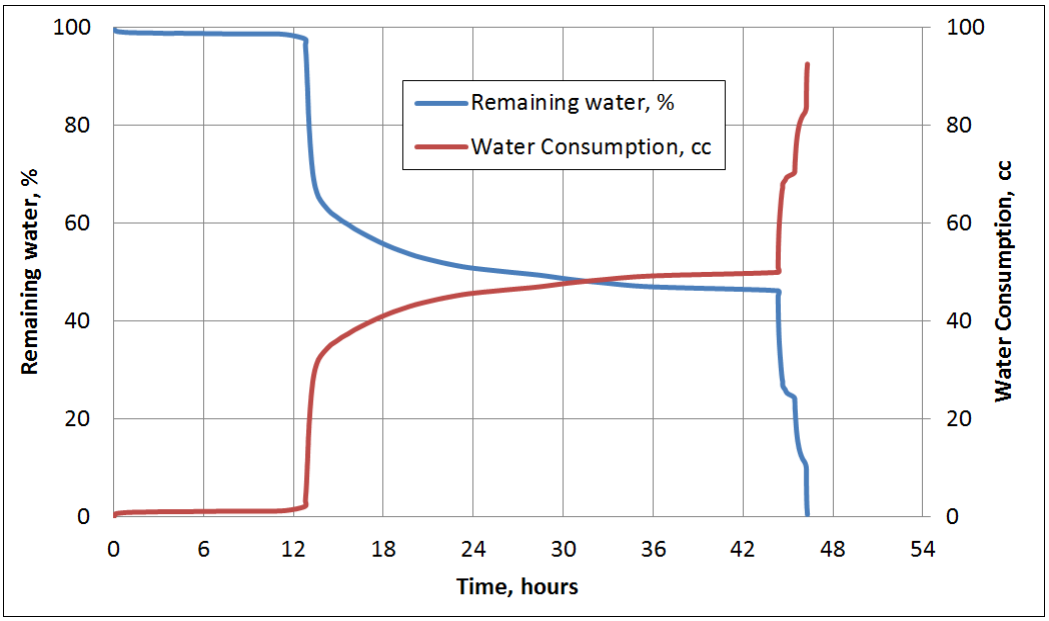

Figure 8. 16 A plot that shows the water consumption in the cell from run #6 (Hydrate permeability test at 30% hydrate saturation and CO_2 injection into CH_4 hydrate in unconsolidated sediments particle size of which range between 0.5 mm and 0.25 mm)

After measuring the permeability, a known amount of CO_2 was injected into the system to observe the interaction between the CO_2 and the methane hydrate. However, it should be noted that, CO_2 can pass to the liquid phase at comparatively low pressures (566.344 psi at 4 ^oC). At this point, amount of free methane in the system becomes an important parameter since it requires very high pressures to pass the liquid phase (3644.046 psi at 4 ^oC). Therefore, as long as the concentration of free methane in the system is enough to keep the boiling point of the mixture above the pressure of the system there will not be any liquid appearance. According to the calculations, 0.8981 gr mole of CH_4 is converted to hydrate and remaining pore volume of the cell is filled with 0.4799 gr mole of free CH_4. Then, 0.4883 gr mole of CO_2 is suddenly injected and corresponding peak in pressure is observed.

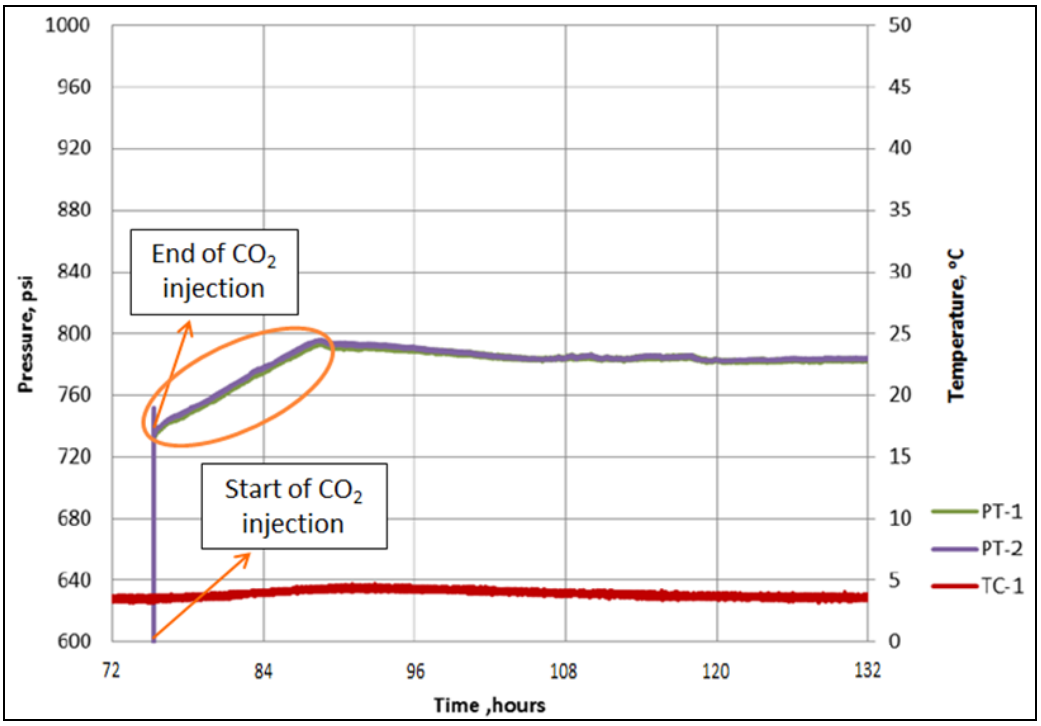

Figure 8. 17 A plot that indicates the CO_2 injection from run #6 (Hydrate permeability test at 30% hydrate saturation and CO_2 injection into CH_4 hydrate in unconsolidated sediments particle size of which range between 0.5 mm and 0.25 mm)

After CO_2 injection cyclic behaviors at the pressure gauges are observed, this behavior may result due to the CO_2-CH_4 swap within the hydrate cages. Therefore, gas chromatography analyses were done to confirm the swap process. Figure 8.18 and Figure 8.19 illustrate the cyclic behaviors at the pressure gauges after the CO_2 injection.

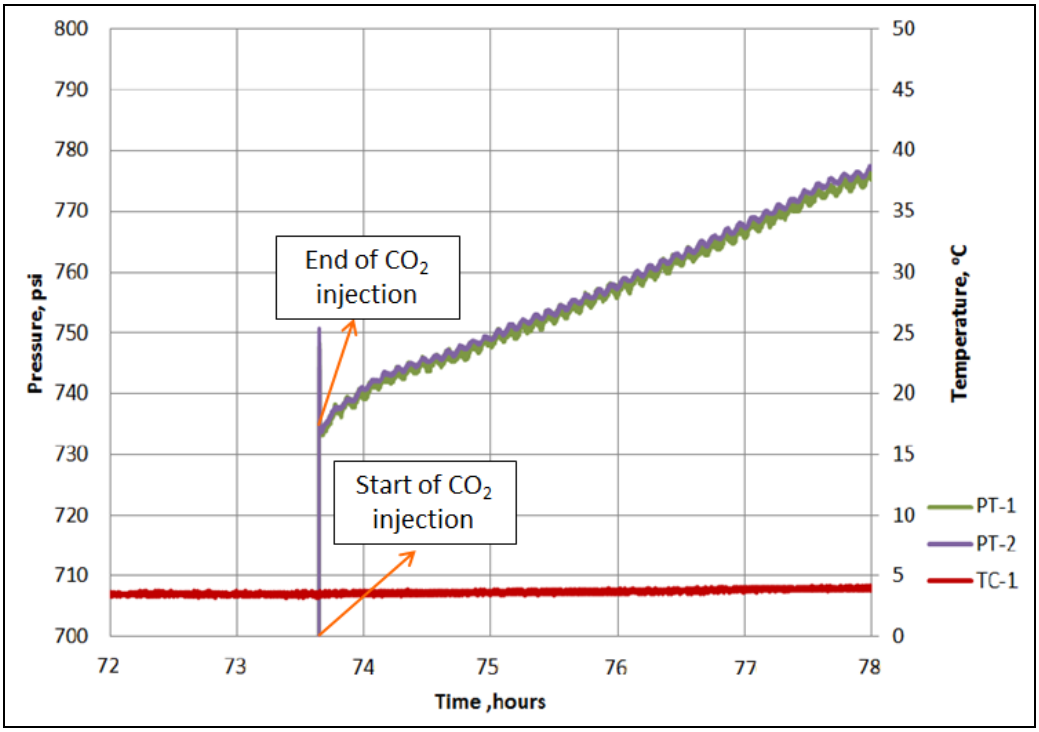

Figure 8. 18 Cyclic behaviors at the pressure gauges after the CO_2 injection from run #6 (Hydrate permeability test at 30% hydrate saturation and CO_2 injection into CH_4 hydrate in unconsolidated sediments particle size of which range between 0.5 mm and 0.25 mm)

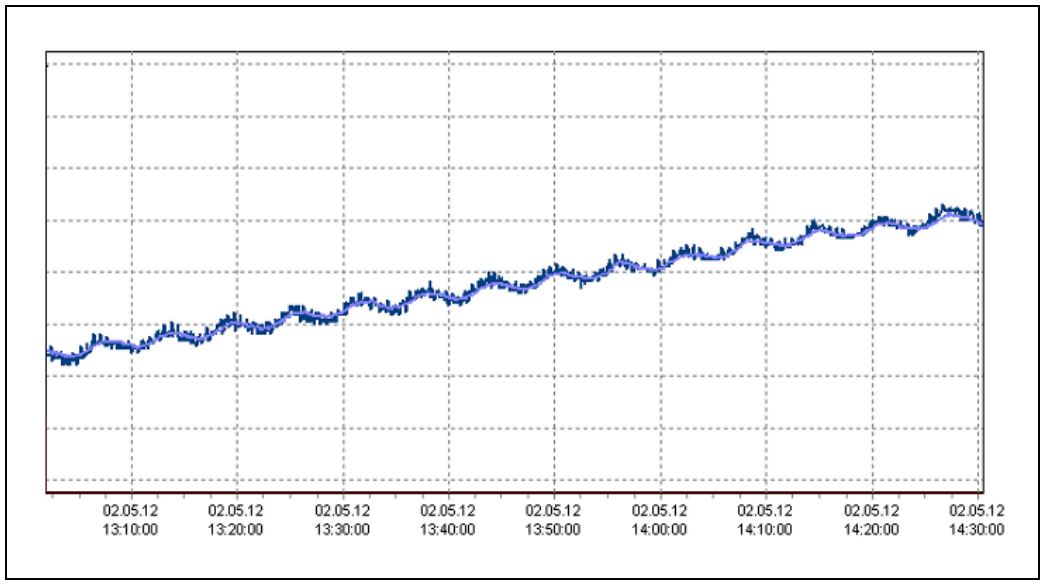

Figure 8. 19 Cyclic behaviors at the pressure gauges after the CO_2 injection from the interface of data logger from run #6 (Hydrate permeability test at 30% hydrate saturation and CO_2 injection into CH_4 hydrate in unconsolidated sediments particle size of which range between 0.5 mm and 0.25 mm)

As it was stated before, 0.8981 gr mole of CH_4 is converted to hydrate and remaining pore volume of the cell is filled with 0.4799 gr mole of free CH_4. Then, 0.4883 gr mole of CO_2 is suddenly injected and corresponding peak in pressure was observed. At the instant of CO_2 injection mole fraction of CO_2 was 0.504 and that of CH_4 was 0.496. At this moment; pressure and temperature in the cell and the mole fractions of CH_4 and CO_2 suggests that injected CO_2 and free CH_4 in the system should be in gaseous phase. CO_2-CH_4 swap within the hydrate cages and the corresponding increase in pressure took 6 hours and at the end of the process sample was taken from the top of the cell in order to analyze the gas composition. Gas chromatography analysis indicated that mole fractions of CH_4 and CO_2 were %92.310 and %7.690 respectively. Figure 8.20 illustrates the mole fractions in the cell at the instant of CO_2 injection and after the swap between CH_4-CO_2 molecules within the hydrate structures.

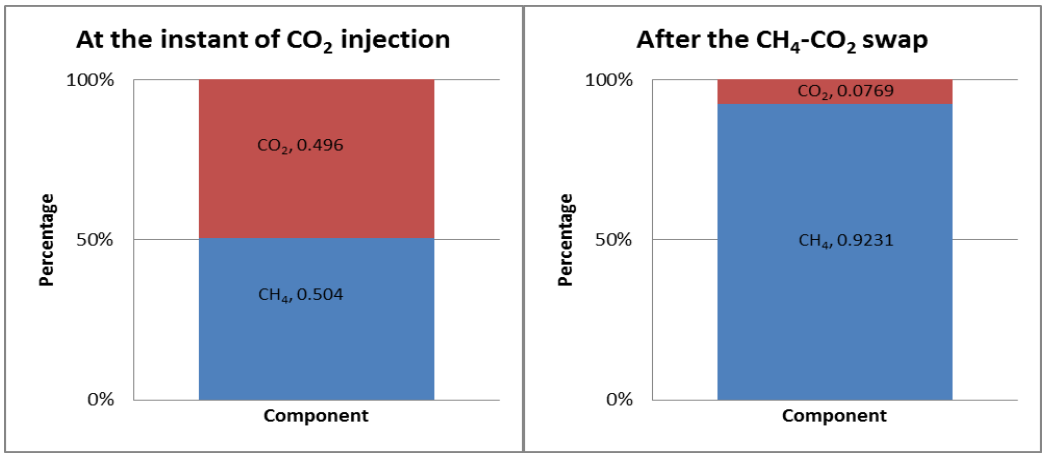

Figure 8. 20 Mole fractions in the cell at the instant of CO_2 injection and after the swap between CH_4-CO_2 molecules within the hydrate structures from run #6 (Hydrate permeability test at 30% hydrate saturation and CO_2 injection into CH_4 hydrate in unconsolidated sediments particle size of which range between 0.5 mm and 0.25 mm)

According to the calculations, finally, 0.80518 gr mole of free CH_4 and 0.06708 gr mole of free CO_2 were present in the cell which suggest that 86.26% of the injected CO_2 was went into the hydrate phase. Also, calculations indicated that, 0.32528 gr mole of additional CH_4 comes from hydrate phase whereas, 0.42122 gr mole of CO_2 went into hydrate phase. Then, dissociation was started by producing the free gas from the cell and several samples were taken for the gas chromatography analysis. Figure 8.21 and 8.22 shows the time and pressure intervals during the GC analysis.

Table 8. 4 Results of gas chromatography analysis

Analysis #	**1**	**2**	**3**	**4**
Comp. name	**Mole, %**	**Mole, %**	**Mole, %**	**Mole, %**
Methane	92.31	87.281	83.358	49.871
CO_2	7.69	12.719	16.642	50.129
Analysis #	**5**	**6**	**7**	**8**
Comp. name	**Mole, %**	**Mole, %**	**Mole, %**	**Mole, %**
Methane	91.191	97.842	96.012	95.471
CO_2	8.809	2.158	3.988	4.529

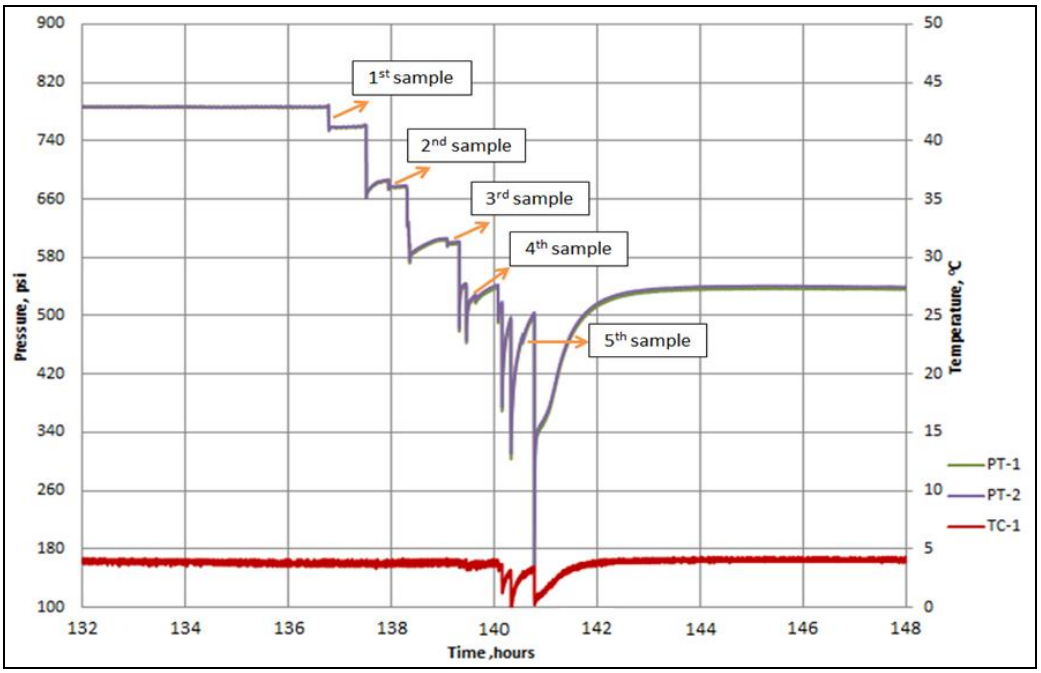

Figure 8. 21 Figure that indicates the time and pressure intervals during the GC analysis from run #6 (Hydrate permeability test at 30% hydrate saturation and CO_2 injection into CH_4 hydrate in unconsolidated sediments particle size of which range between 0.5 mm and 0.25 mm)

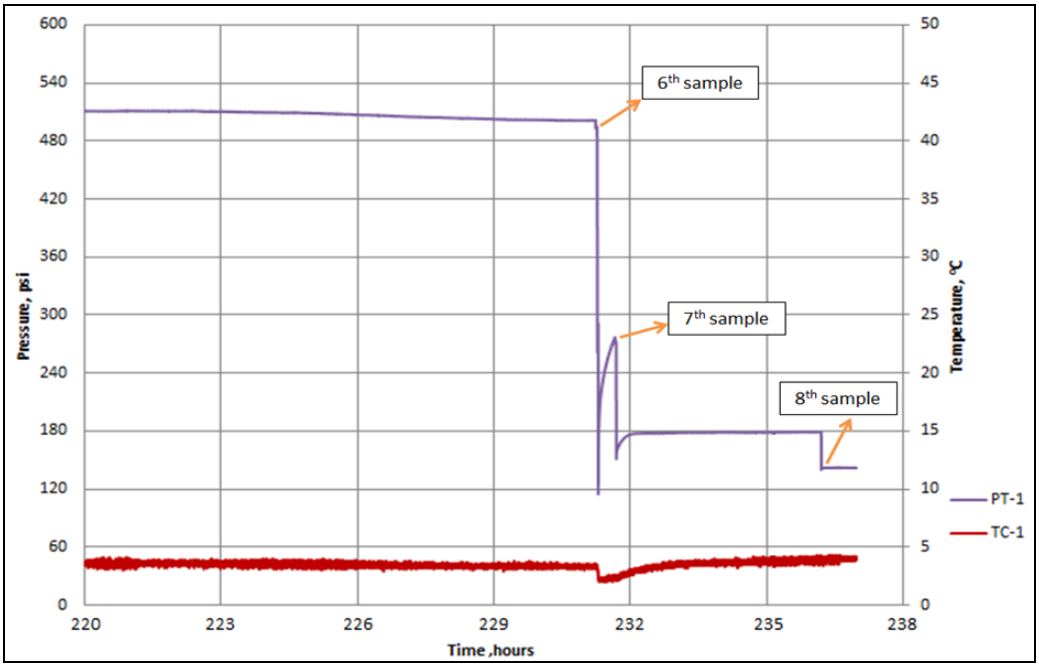

Figure 8. 22 Figure that indicates the time and pressure intervals during the GC analysis from run #6 (Hydrate permeability test at 30% hydrate saturation and CO_2 injection into CH_4 hydrate in unconsolidated sediments particle size of which range between 0.5 mm and 0.25 mm)

When the swap process was over, some of the hydrate was dissociated and GC Analysis showed that, amount of free CO_2 in the cell was increasing gradually (Figure 8.23). It should be noted that, produced gas mainly contains of methane up to fourth analysis. Up to fourth analysis produced amount of CO_2 that was dissociated from hydrate was increasing but at this point it reaches its peak value and then decreases gradually. Although the CO_2 hydrate is more stable than the methane hydrate at this temperature and pressure value, CO_2 has tendency to leave the cages.

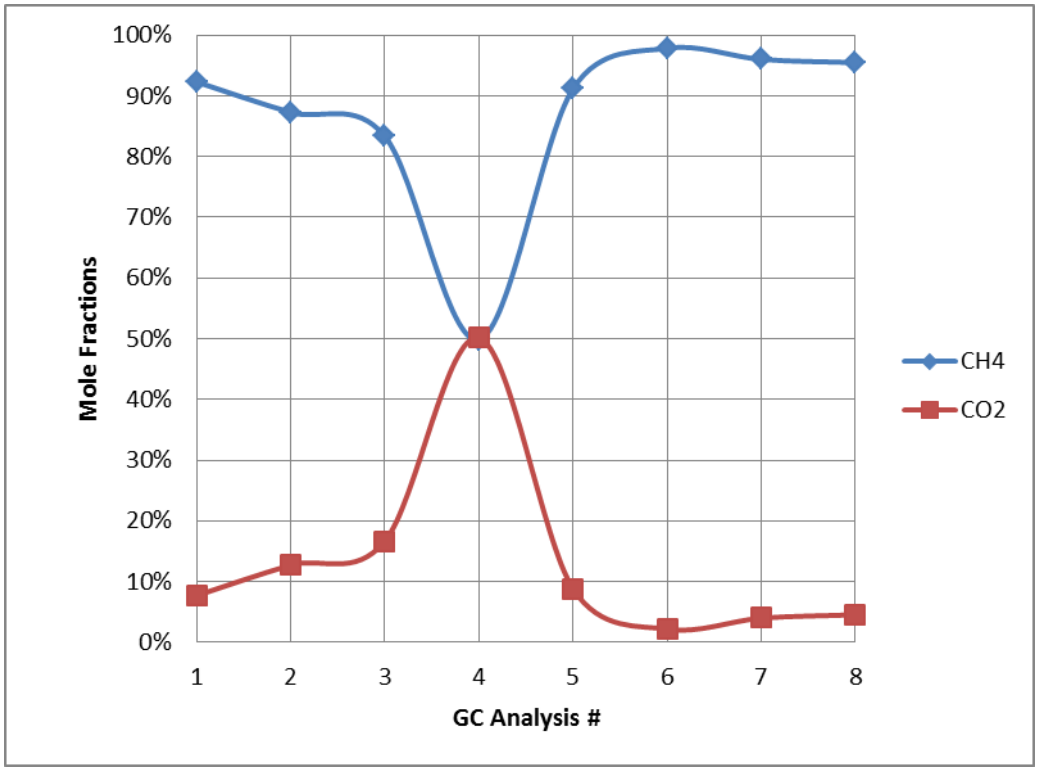

Figure 8. 23 Results of gas chromatography analysis from run #6 (Hydrate permeability test at 30% hydrate saturation and CO_2 injection into CH_4 hydrate in unconsolidated sediments particle size of which range between 0.5 mm and 0.25 mm)

As it was stated before, interaction between the steel and hydrate is expected to be weaker than the interaction of hydrate and unconsolidated sand pack system. This behavior was also observed during the dissociation of hydrate in unconsolidated sand pack system which is open to the atmosphere. Once the CO_2 is injected into the system from the bottom of the cell, it can be expected that injected CO_2 preferentially fills the volume between the unconsolidated sand pack system and walls of the core holder. Figure 8.24 schematically indicates the probable distribution of injected CO_2 inside the core holder.

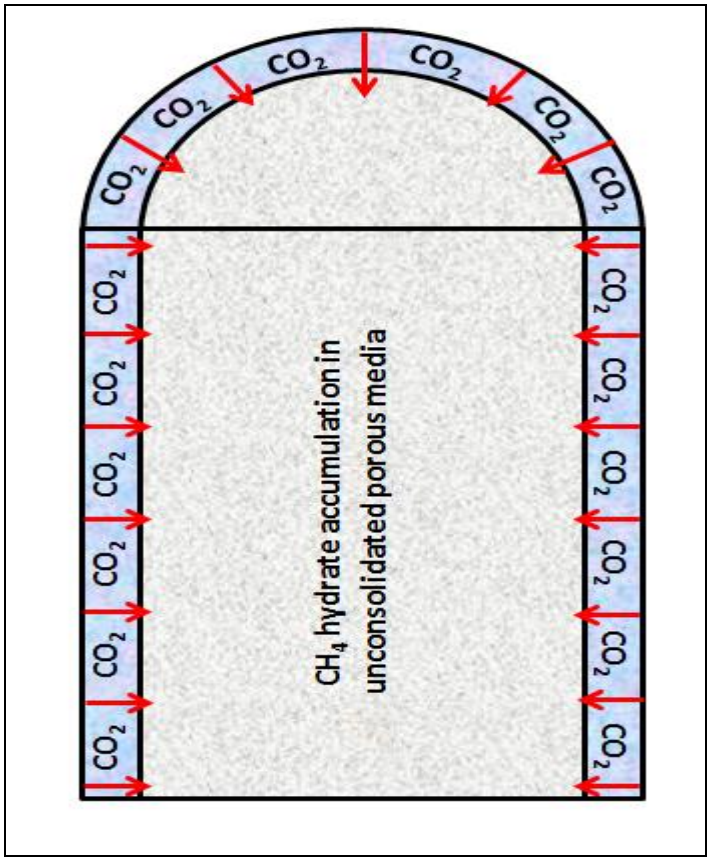

Figure 8. 24 Probable distribution of injected CO_2 inside the core holder (Hydrate permeability test at 30% hydrate saturation and CO_2 injection into CH_4 hydrate in unconsolidated sediments particle size of which range between 0.5 mm and 0.25 mm)

Interaction of CO_2 and CH_4 hydrate mostly occurs at the exterior part of the unconsolidated sand pack system. Therefore, at the end of the CO_2-CH_4 swap within hydrate cages, system is expected to take the following form (Figure 8.25). In this figure, it is expected that, exterior part of the unconsolidated sand pack system includes hydrate that is rich in CO_2 and interior part of the system includes hydrate that is rich in CH_4. Therefore, during the production period from the cell, increase in free CO_2 concentration implies that we are producing from exterior part of the system and increase in free CH_4 concentration implies that we are producing from interior part of the system.

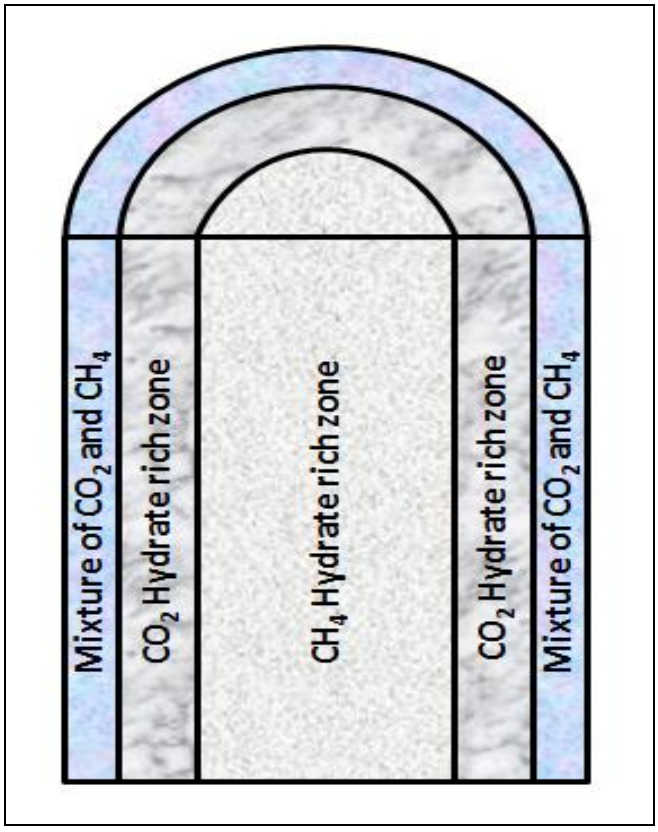

Figure 8. 25 Expected form of the unconsolidated sand pack system at the end of the swap reaction (Hydrate permeability test at 30% hydrate saturation and CO_2 injection into CH_4 hydrate in unconsolidated sediments particle size of which range between 0.5 mm and 0.25 mm)

8.7 Hydrate formation test with liquid CO_2 and water (Run #7)

In this experiment, high pressure cell, which has the volume of 670 ml with the connections, was packed with sand grains. These sand grains were screened with metal screens whose ASTM No. are 35 (0.5 mm) and 60 (0.25 mm), therefore sands are medium grained. After packing the cell, the cell was evacuated and water injection was initiated in order to measure the pore volume. Aim of this experiment is the observation of the interaction between liquid CO_2 and the water. Initially, temperature in the water bath was reduced up to 3.5 ^{o}C then the pressure in the cell was increased up to 700 psi by injection of CO_2. Phase diagram suggests that most of the CO_2 is in liquid state at this pressure and temperature. After that, system was left for the stabilization at these conditions. During first 17.5 hours, we did not observe any sharp decrease in the pressure that may indicate hydrate formation. Then, pressure in the cell was decreased to 445 psi to let the gaseous CO_2 to evolve in the cell. Pressure in the cell was diminished by retracting the piston and increasing the volume. During this process free gas evolved in the cell that also increased the temperature in the cell. Finally hydrate formation in the cell was observed and pressure was stabilized at the hydrate stability pressure. Figure 8.26 shows the whole story of the experiment, whereas decrease in pressure, corresponding increase in temperature, hydrate formation process can be more easily seen from Figure 8.27. At the end of this process, again CO_2 was injected into the system in liquid state and system was again left for stabilization for approximately 3 days. However, again we did not observe any sharp pressure decline.

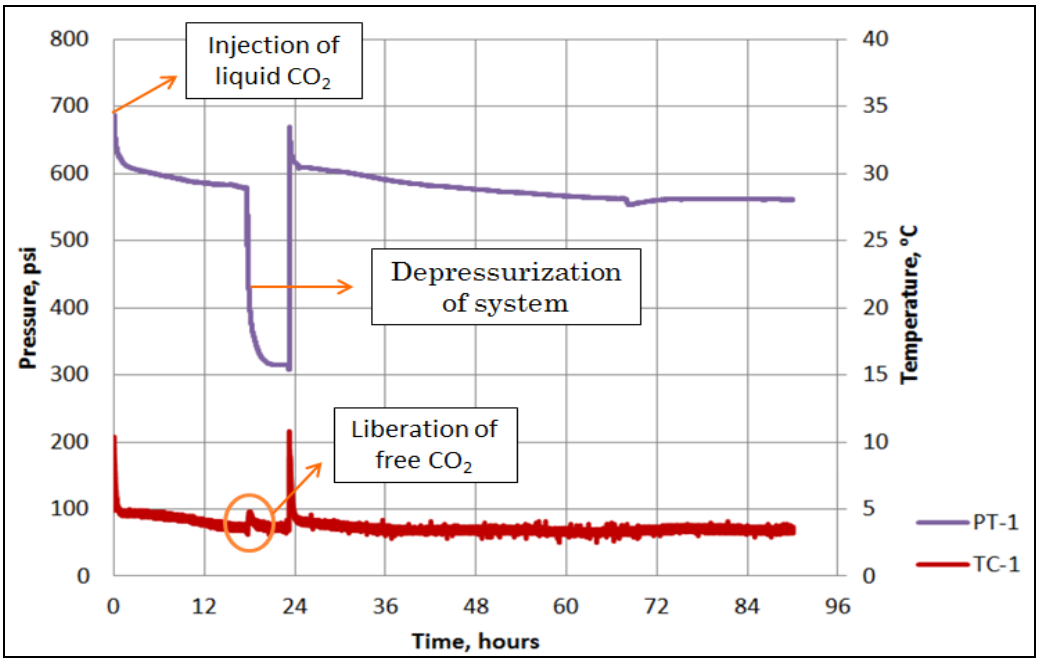

Figure 8. 26 A plot of pressure-temperature-time from run #7 (Hydrate formation test with liquid CO_2 and water in unconsolidated sediments particle size of which range between 0.5 mm and 0.25 mm)

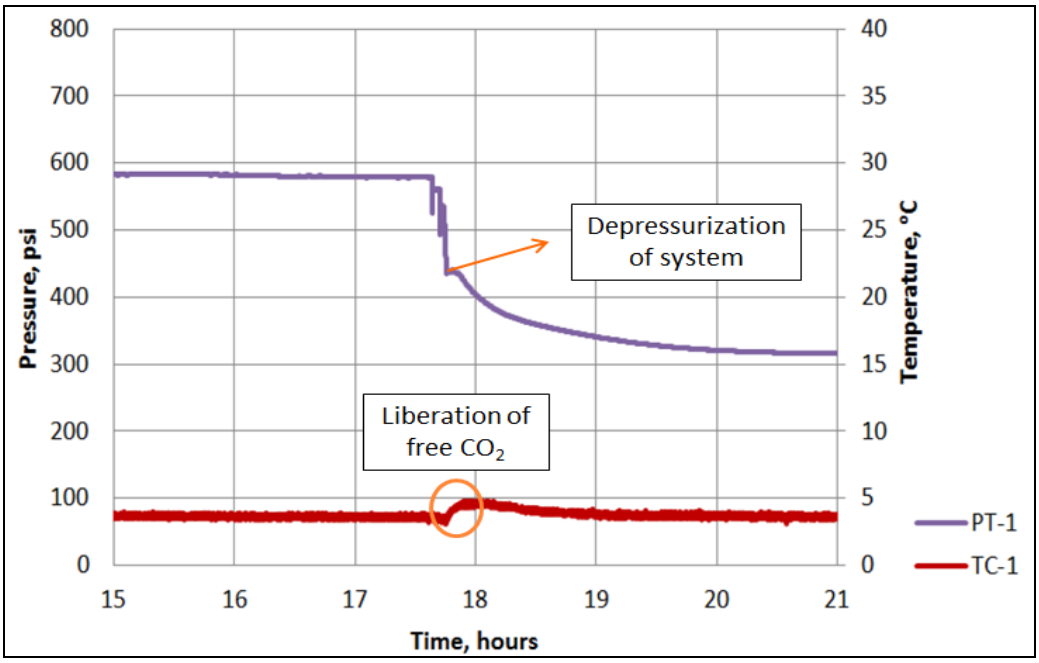

Figure 8. 27 A plot that indicates hydrate formation after decreasing the pressure and letting the gaseous CO_2 to evolve in the cell from run #7 (Hydrate formation test with liquid CO_2 and water in unconsolidated sediments particle size of which range between 0.5 mm and 0.25 mm)

8.8 Interaction of liquid CO_2 & CH_4 hydrate in presence of water (Run #8)

In this experiment, high pressure cell, which has the volume of 670 ml with the connections, was packed with sand grains. These sand grains were screened with metal screens whose ASTM No. are 35 (0.5 mm) and 60 (0.25 mm), therefore sands are medium grained. After packing the cell, the cell was evacuated and water injection was initiated in order to measure the pore volume. Aim of this experiment was the observation of the interaction between liquid CO_2 and methane hydrate in presence of excess water. Initially, 0.68546 gr mole of methane was injected into the cell and then the system was pressurized by water injection up to 1250 psi. Theoretically, this amount of methane converts 70.8975 cc volume of water to hydrate. After that, cooling process was initiated and temperature was reduced to about 5 ^oC. As the pressure declines in the cell due to hydrate formation and methane consumption, system was pressurized by further water injection. Finally, after about 72 hours, pressure in the system stabilized above the hydrate stability pressure of methane hydrate at the corresponding temperature and this suggests that all the methane in the cell was consumed since excess water was present in the system. By means of CO_2 injection, pressure in the cell was increased up to 1275 psi and at this pressure and temperature value, phase diagram of CO_2 suggests that it is in liquid phase. Amount of CO_2, which is injected into the cell, was determined as 1.066 gr mole. After CO_2 injection cyclic behaviors at the pressure gauges were observed, this behavior may result due to the CO_2-CH_4 swap within the hydrate cages. Therefore, gas chromatography analyses were done to confirm the swap process. Figure 8.30 and Figure 8.31 illustrate the cyclic behaviors at the pressure gauges after the CO_2 injection.

As it was stated before, amount of methane that is converted to hydrate was 0.68546 gr mole. Then, 1.066 gr mole of CO_2 was injected into the system. At the instant of CO_2 injection, mole fraction of CO_2 in the system was 1 since all the CH_4 was assumed to be converted to hydrate phase. After the injection of

CO_2, liquid CO_2 begun to attack CH_4 hydrate and methane molecules in the hydrate cages were displaced with CO_2 molecules. However, since water is available in the system, CH_4 that is coming from hydrate was again converted to CH_4 hydrate. At the beginning of the process, sharp decline in pressure was observed that may result from the fact that, interaction area between hydrate and CO_2 was very high so that, more CH_4 came from the hydrate phase and more CH_4 was again converted to the hydrate phase. CO_2-CH_4 swap within the hydrate cages, hydrate formation from the methane coming from the hydrate phase and corresponding decrease in pressure took approximately 3 days and finally pressure of the system was stabilized (Figure 8.29).

After that, temperature of the system was let to increase up to certain point, so that hydrate stability pressure of the system can be observed at various temperature values. Figure 8.32 shows both stability regions of CH_4 and CO_2 hydrate mixtures obtained by CSMHyd program and experimental data obtained from Run #8. Data obtained from the experiment indicates a stability region which is below the stability region of pure methane. At this point, it is worth to mention that, during all the experiments, observed methane hydrate stability region was narrower than the theoretical one that may results from the use of tap water instead of pure water. Actually, data obtained from this experiment was very close to the data obtained for pure methane hydrate at previous runs. In the light of this information one can claim that, at the end of the Run #8, hydrate was only composed of methane; however, it was observed several times during the experiments that, CO_2 that is entering into the cages of the methane hydrate does not make a noticeable effect on the stability region of CH_4 hydrate. At the end of the experiment, it was expected that, hydrate was mainly composed of CH_4, since all the methane that was coming from methane hydrate as a result of the swap process, was again converted to hydrate. Then, sample was taken from the cell and analyzed by gas chromatography. After that, dissociation was started by producing the free gas from the cell and several

samples were again taken for the gas chromatography analysis. Results of gas chromatography analysis can be seen from the Table 8.5. Also, Figure 8.31 shows the time and pressure intervals during the GC analysis. By combining these data with the previous knowledge from the experiment and pressure & temperature plot of this experiment, we can deduce that, swap process and hydrate formation process were more rapid at the instant of CO_2 injection. Also, as a result of this process great amount of CO_2 was stored into the hydrate phase. However, when the water is available in the system there would be a secondary hydrate formation from the methane coming from the hydrate phase, and as a result hydrate will mostly include methane. During this experiment, core of the hydrate may contain more CO_2 while hydrate at the surface may contain more CH_4. Also, it can be said that stability region of the hydrate formed from the CO_2 and CH_4 is different than the stability region of the hydrate that contains the same fraction from both components but formed as a result of the swap process.

Table 8. 5 Results of gas chromatography analysis

Analysis #	**1**	**2**	**3**
Comp. name	**Mole, %**	**Mole, %**	**Mole, %**
Methane	33.061	54.615	56.925
CO_2	66.939	45.385	43.075

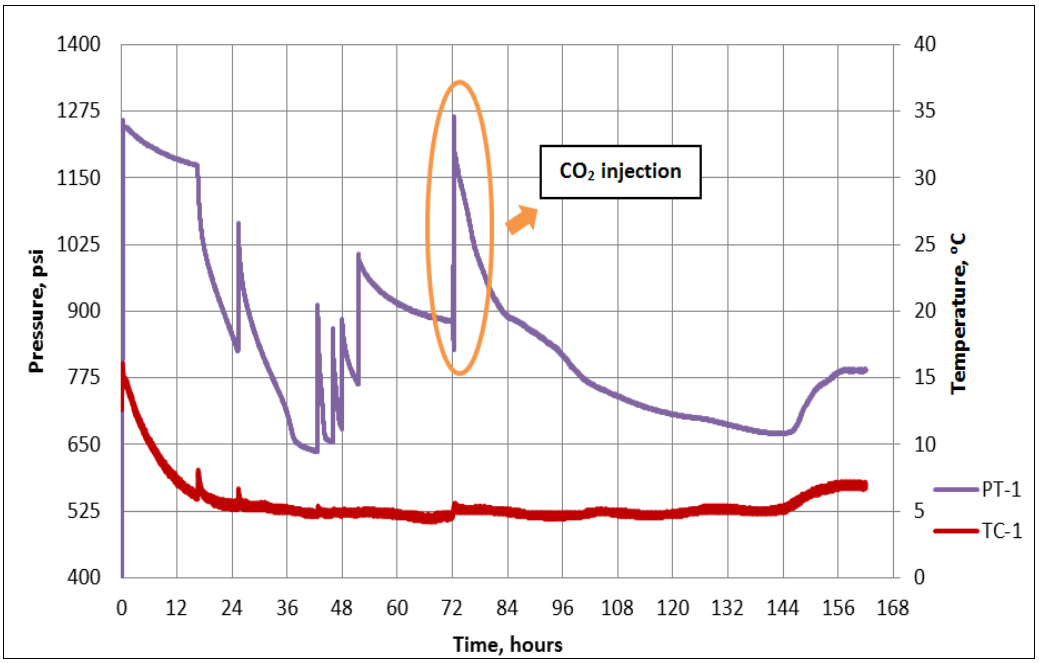

Figure 8. 28 A pressure and temperature plot from run #8 (Interaction of liquid CO_2 & CH_4 hydrate in presence of excess water in unconsolidated sediments particle size of which range between 0.5 mm and 0.25 mm)

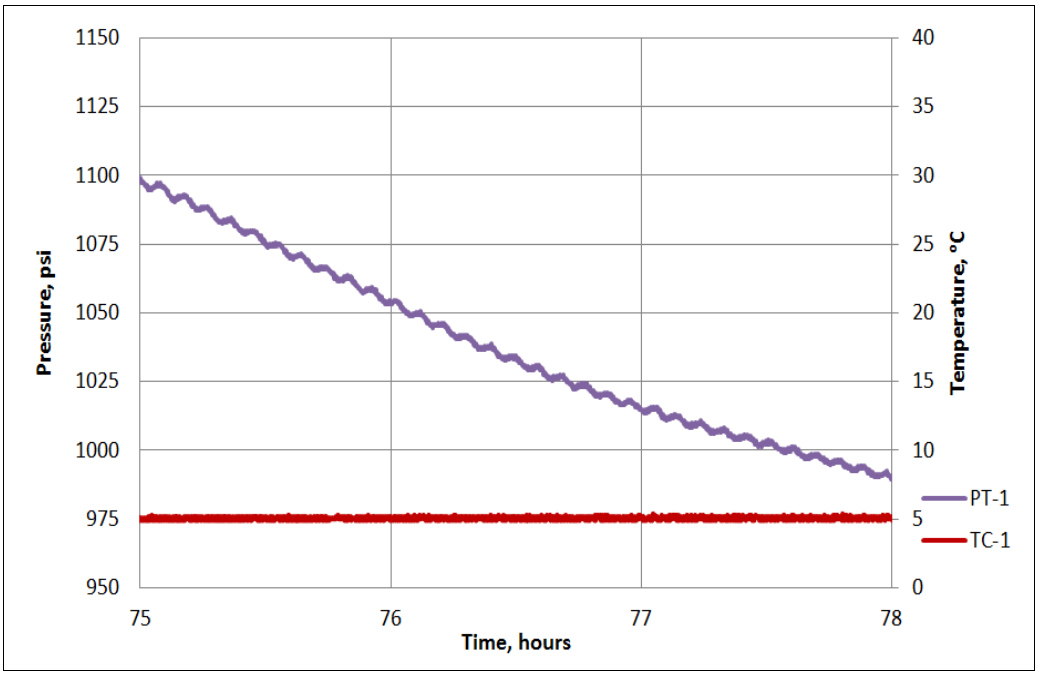

Figure 8. 29 Cyclic behaviors at the pressure gauge after the CO_2 injection from run #8 (Interaction of liquid CO_2 & CH_4 hydrate in presence of excess water in unconsolidated sediments particle size of which range between 0.5 mm and 0.25 mm)

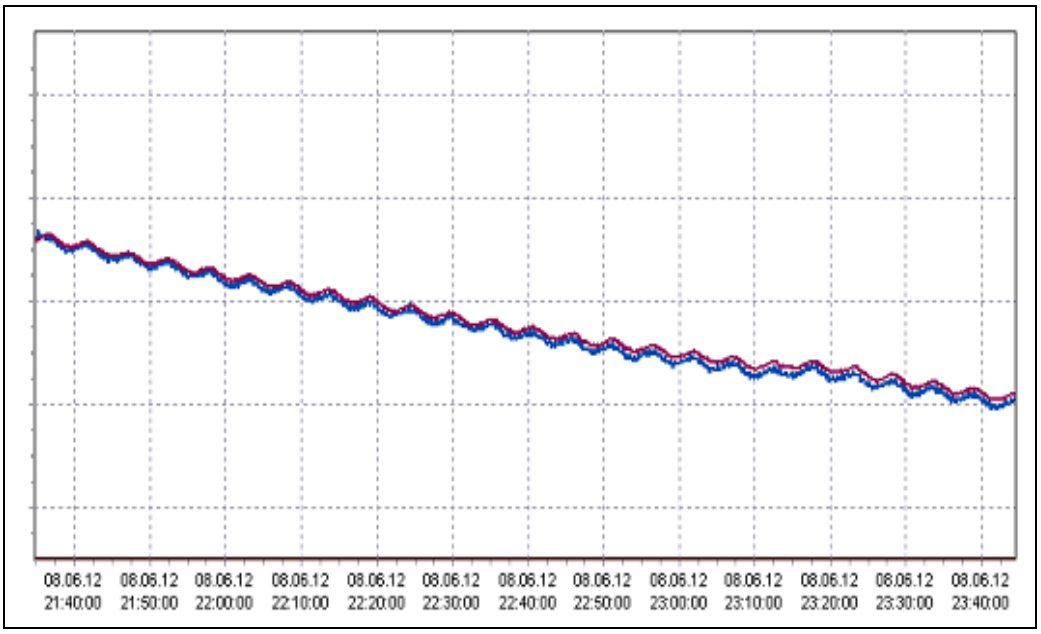

Figure 8. 30 Cyclic behaviors at the pressure gauges after the CO_2 injection from the interface of data logger from run #8 (Interaction of liquid CO_2 & CH_4 hydrate in presence of excess water in unconsolidated sediments particle size of which range between 0.5 mm and 0.25 mm)

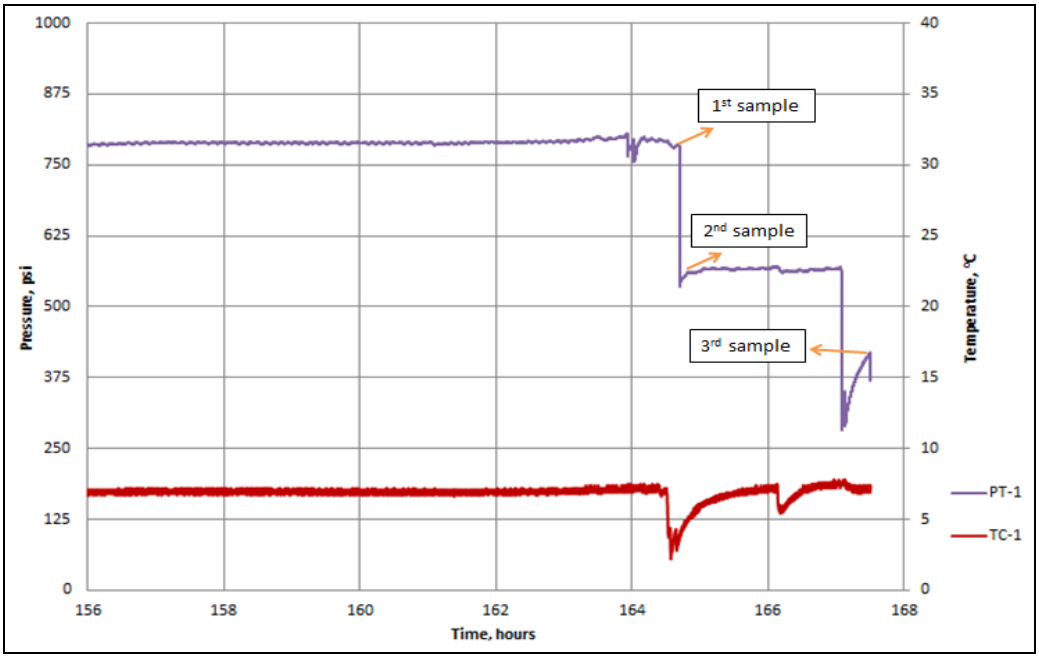

Figure 8. 31 Figure that indicates the time and pressure intervals during the GC analysis from run #8 (Interaction of liquid CO_2 & CH_4 hydrate in presence of excess water in unconsolidated sediments particle size of which range between 0.5 mm and 0.25 mm)

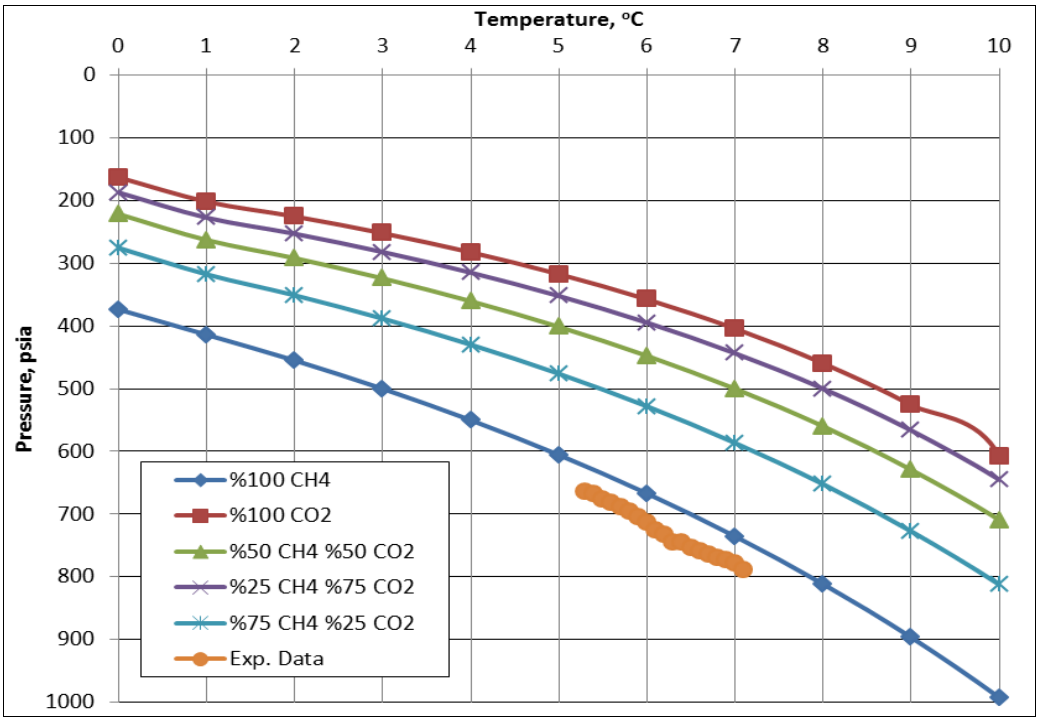

Figure 8. 32 Stability regions of CH_4 and CO_2 hydrate mixtures obtained by CSMHyd program (Experimental data obtained from run #8 was also indicated in this graph)

CHAPTER 9

CONCLUSION

In this study, an experimental work was performed in order to investigate the interaction between the CO_2 and CH_4 hydrate. The following concluding remarks are obtained:

- The permeability of the unconsolidated sand pack system in the presence of hydrate was determined by flowing CO_2 through the system. These measurements were performed with the assumption that all of the injected water in the cell was converted to hydrate. During the permeability tests it was observed that, presence of hydrate significantly lowers the permeability of the unconsolidated sand pack system. First of all, permeability of unconsolidated sand pack system was estimated as greater than 20 darcy. After that, permeability of unconsolidated sand pack systems whose hydrate saturations are 30% and 50% were estimated as about 600 md and 4 md. Therefore, it can be concluded that presence of hydrate in unconsolidated sand pack system may seal the injected CO_2, especially when the hydrate saturation in the system is high and easy flow pathways are plugged due to hydrate formation. Furthermore, in one of these tests, it was observed that gas was flowing through the walls of the core holder. Therefore, it can be concluded that, interaction between the hydrate and steel is weaker than that of hydrate and sand pack system. In our experiments, this interaction constituted primary flow path for the injected CO_2 and also it was mainly responsible for the permeability of the system.

- CO_2, in gaseous phase, was injected into the unconsolidated sand pack system whose hydrate saturation was %30 and contains excess CH_4. After CO_2 injection, cyclic behaviors at the pressure transducers were observed that suggests the CH_4-CO_2 swap within the hydrate cages. Furthermore, swap process was also confirmed via gas chromatography analysis and gas compositions at the instant of CO_2 injection and after the swap process were determined. Since, free gas volume in the cell before the CO_2 injection was known and we do not expect any hydrate formation or dissociation during the CO_2 injection (all the water was converted to hydrate and pressure of the system was well above the hydrate dissociation pressure) knowledge of the gas concentration in the system enables us to calculate the amount of free gas in the system.
- After swap process, system was let to dissociate and samples were taken and analyzed incrementally. Analysis indicated that, amount of free CO_2 in the cell were increasing gradually reached a peak value and then decreased. Actually, CO_2 hydrate is more stable than CH_4 hydrate at this pressure and temperature value, whereas CO_2 has tendency to leave the cages. This may result from the fact that, cages that are acting as a host for the methane molecules are more prone to dissociation process. Moreover, CH_4-CO_2 swap process may mostly take place at the surface of the system and center of the unconsolidated sand pack system may contain hydrate that is rich in CH_4, while, surface may contain hydrate that is rich in CO_2.
- CO_2 was injected into the unconsolidated sand pack system, which is saturated with water to observe the interaction between the liquid CO_2 and the water. Results indicated that, liquid CO_2 was not able to form CO_2 hydrate or only limited amount of CO_2 hydrate was formed which is not noticeable from the pressure response.
- CO_2 was injected into the unconsolidated sand pack system whose hydrate saturation is about %30 percent. This system was initially

pressurized with water. Therefore CH_4 that was liberated from hydrate reconverted to hydrate. At the beginning of the process, sharp decline in pressure was observed that may result from the fact that, interaction area between hydrate and CO_2 was very high so that, more CH_4 came from the hydrate phase and more CH_4 was again converted to the hydrate phase. For the CH_4-CO_2 swap process and dissociation of the hydrate system that is formed as a result of the CH_4-CO_2 swap process, determination of the interaction area between hydrate and CO_2 and rate of penetration of CO_2 into the methane hydrate are two crucial phenomenon that should be addressed.

- As a result of this study, it can be concluded that methane hydrate stability region in deep sea sediments would be a good alternative for the safe storage of CO_2 and that CH_4-CO_2 swap process may also contribute to the safe storage of CO_2 while the produced CH_4 may offset the storage costs.

CHAPTER 10

RECOMMENDATIONS

Based on the experience gained in the present study, the following suggestions are recommended for future research in this area:

In this thesis, interaction between the CO_2 and CH_4 hydrate was investigated on a relatively small scale. It was assumed that, CO_2 that is injected below the CH_4 hydrate containing layer, migrates upward and interacts with the CH_4 hydrate; therefore, this study mainly focuses on this interaction. However, when the CO_2 is injected below the stability region of CH_4 hydrate, there is a great possibility for CO_2 to form its own hydrate and self-seal the injected CO_2 plume. In order to simulate the fate of the injected CO_2 in the hydrate stability region and to acquire more representative data, it would be crucial to use core holder, length of which is equal to the distance that is expected to be travelled by the CO_2 in the reservoir. This kind of experimental setup may provide knowledge about hydrate saturations at different locations, resulting decrease in permeability, time required to seal CO_2 plume and amount of CO_2 which will interact with the CH_4 hydrate layer. Also, repeating the experiment with varying CO_2 injection rates and pressures, optimum injection rate and pressure may also be determined.

REFERENCES

Adisasmito, S., Frank, R. J., & Sloan, E. D., (1991). Hydrates of carbon dioxide and methane mixtures. *J. Chem. Eng. Data 36*, 68–71.

Anderson, R., Llamedo, M., Tohidi, B., & Burgass, R. W., (2003-a). Characteristics of clathrate hydrate equilibria in mesopores and interpretation of experimental data. *J. Phys. Chem., B 107*, 3500–3506.

Anderson, R., Llamedo, M., Tohidi, B., & Burgass, R. W., (2003-b). Experimental measurement of methane and carbon dioxide clathrate hydrate equilibria in mesoporous silica. *J. Phys. Chem., B 107*, 3507–3514.

Baillie, C., & Wichert, E. (1987). Chart gives hydrate formation temperature for natural gas. *Oil & Gas J., 85* (4), 37-39.

Berge, L. I., Jacobsen, K. A., & Solstad, A. (1999). Measured acoustic wave velocities of R11 (CCl_3F) hydrate samples with without sand and function of hydrate concentration. *J. Geophys. Res., 104* (15).

Birkedal, K. A., Ersland, G., Husebø, J., Kvamme, B., & Graue, A. (2010, 06). Geomechanical stability during CH_4 production from hydrates - Depressurization or CO_2 sequestration with CO_2-CH_4 exchange. *Paper presented at 44th U.S. Rock mechanics symposium and 5th U.S. Canada rock mechanics symposium*, Salt Lake City, Utah.

Bradley D. J. & Pitzer K. S. (1979). Thermodynamics of Electrolytes. 12. Dielectric Properties of Water and Debye-Huckel Parameters to 350 ^{o}C and 1 kbar. *The Journal of Physical Chemistry, 83* (12), 1599-1603.

Bradshaw, J., Bachu, S., Bonijoly, D., Burruss, R., Holloway, S., Christensen, N. P., & Mathiassen, O. M. (2007). CO_2 storage capacity estimation: issues and development of standards. *International Journal of Greenhouse Gas Control 1*, 62-68.

Brewer, P. G., Friederich, G., Peltzer, E. T. & Orr, F. M. Jr. (1999). Direct experiments on the ocean disposal of fossil fuel CO_2. *Science, 284*, 943-945.

Buffett, B. A., & Zatsepina, O. Y. (2000). Formation of gas hydrate from dissolved gas in natural porous media. *Marine Geology, 164*, 69–77.

Carroll, J. J. (2009). *Natural Gas Hydrates - A Guide for engineers*. (2nd ed.). Elsevier.

Carson, D. B., & Katz, D. L. (1942). Natural gas hydrates. *Trans. AIME, 146* (150), 8.

Cha S. B., Ouar, H., Wildeman, T. R., & Sloan, E. D. (1988). A third-surface effect on hydrate formation. *J. Phys. Chem., 92* , 6492–6494.

Clennell, M. B., Hovland, M., Booth, J. S., Henry, P., & Winters, W. J. (1999). Formation of natural gas hydrates in marine sediments. Part 1: Conceptual model of gas hydrate growth conditioned by host sediment properties. *J. Geophys. Res. 104*, 22985–23003.

CRC, (2004/2005). *Handbook of Chemistry and Physics*. (85th ed.) CRC Press, Cleveland, OH.

Dickens, G. R., & Quinby-Hunt, M. S. (1994). Methane hydrate stability in seawater. *Geophys. Res. Lett. 21*, 2115–2118.

Dullien, F. A. L., (1992). *Porous Media Fluid Transport and Pore Structure*. (2nd ed.) Academic Press, San Diego, 333–486.

Durham,W. B., Stern, L. A., & Kirby, S. H. (2003). *Can. J. Phys., 81*, 373.

Dusseault, M. B., Bachu, S., & Davidson, B. C. (2001, 10). Carbon Dioxide Sequestration Potential in Salt Solution Caverns in Alberta, Canada. *Solution Mining Research Institute*, Technical Meeting Albuquerque, New Mexico, USA.

Dusseault, M. B., Bachu, S., & Rothenburg, L. (2004). Sequestration of CO_2 in Salt Caverns. *JCPT, 43* (11).

Ebinuma, T., Kamata, Y., Minagawa, H., Ohmura, R., Nagao, J., & Narita, H. (2005). Mechanical properties of sandy sediment containing methane hydrate, in *Proceedings of 5th International Conference on Gas Hydrates*, 3037, 958–961, Tapir Acad., Trondheim, Norway.

Elgibaly A. A., Elkamel A. M. (1998). A new correlation for predicting hydrate formation conditions for various gas mixtures and inhibitors. *Fluid Phase Equil. 152* , 23–42.

Englezos, P. & Bishnoi, P. R. (1988). Prediction of gas hydrate formation conditions in aqueous electrolye. *American Institute of Chemical Engineers*, 34 (10), 1718-1721.

Ennis-King, J., & Paterson, L., (2003). Rate of dissolution due to convection mixing in the underground storage of carbon dioxide, in *Proceedings of the 6th International Conference on Greenhouse Gas Control Technologies*, 1, 507–510.

Enns, T., Scholander, P. F., & Bradstreet, E. D. (1965). Effect of hydrostatic pressure on gases dissolved in water. J. Phys. Chem., 69 , 389.

Evgeny, M. C., Kozlova, E. V., Makhonina, N. A., Yakushev, V. S., & Dubinyak, D. V. (2002, 03). Peculiarities of methane hydrate formation/dissociation P/T conditions in sediments of different composition. *4th International Conference on Gas Hydrates*, Yokohama, Japan.

Geng, C. Y., Wen, H., & Zhou, H. (2009). Molecular simulation of the potential of methane reoccupation during the replacement of methane hydrate by CO_2. *J. Phys. Chem. A 113*, 5463–5469.

Goel, N. (2006). In situ methane hydrate dissociation with carbon dioxide sequestration: Current knowledge and issues. *Journal of Petroleum Science and Engineering 51*, 169–184.

Goel, N., De Sousa, J. T. V., Flenniken, J., Shah, S., & Liddell, B. (2004). Fabrication and testing of an apparatus for laboratory simulation of Alaska frozen rock encountered during hydrate gas reservoir coring. *J. Cold Reg. Eng. 18* (2), 53–69.

Gorman, A. R., Holbrook, W. S., Hornbach, M. J., Hackwith, K. L., Lizarralde, D., & Pecher, I. (2002). Migration of methane gas through the hydrate stability zone in a low-flux hydrate province. *Geology, 30* (4), 327-330.

Gray, I. (1995). Stress, gas, water and permeability – their interdependence and relation to outbursting, International symposium, *workshop on Management and control of high gas emissions and outbursts in underground coal mines* , Wollongong, NSW, Australia, 331-334.

Gunter, W. D., & Perkins, E. H., (1993). Aquifer disposal of CO_2-rich gases: reaction design for added capacity, in *Proceedings of the international energy agency carbon dioxide disposal symposium*, Energy Conservation Management, 34 (9-11), Oxford, Pergamon Press, 941-948.

Handa, Y. P. (1990). Effect of hydrostatic pressure and salinity on the stability of gas hydrates. *J. Phys. Chem. 94* , 2652–2657.

Handa, Y. P., & Stupin, D. (1992). Thermodynamic properties and dissociation characteristics of methane and propane hydrates in 70 Å-radius silicagel pores. *J. Phys. Chem., 96* , 8599–8603.

Handa, Y. P., (1986). Compositions, enthalpies of dissociation, and heat capacities in the range 85 to 270 K for clathrate hydrates of methane, ethane, and propane, and enthalpy of dissociation of isobutene hydrate, as determined by a heat-flow calorimeter. *Journal of Chemical Thermodynamics 18*, 915–921.

Handa, Y. P., Zakrzewski, M., & Fairbridge, C. (1992). Effect of restricted geometries on the structure and thermodynamic properties of ice. *J. Phys. Chem*., 96, 8594-8599.

Hearst, J. R., Nelson, P. H., & Paillet, F. L. (2000). *Well logging for physical properties*. New York, McGraw-Hill.

Helgerud, M. B. (2001). *Wave speeds in gas hydrate and sediments*. (Doctoral dissertation, Stanford University).

Henry, P., Thomas, M., & Clennell, M. B. (1999). Formation of natural gas hydrates in marine sediments 2-Thermodynamic calculations of stability conditions in porous media. *J. Geophysical Research, 104*, B10, 23005-230022.

Herzog, H. J., Adams, E. E., Auerbach, D. & Caulfield, J. (1996). Environmental impacts of ocean disposal of CO_2. *Energy Conversion and Management, 37* (6-8), 999-1005.

Hirohama, S., Shimoyama, Y., Wakabayashi, A., Tatsuta, S., & Nishida, N. (1996). Conversion of CH_4 hydrate to CO_2 hydrate in liquid CO_2. *J Chem Eng Jpn 29* 1014–1020.

Holder, G. D. & Corbin G., Papadopoupoulos K.D. (1980). Thermodynamic and Molecular Properties of Gas Hydrates from Mixtures Containing Methane, Argon and Krypton. *Industrial and Engineering Chemistry Fundamental, 19*, 282-286.

Holder, G., Mokka, L., & Warzinski, R. (2001). Formation of hydrates from single-phase aqueous solutions and implications for ocean sequestration of CO_2, in *Preprints of Spring 2000 National Meeting in San Diego*, CA, ACS Division of Fuel Chemistry.

Holloway, S., Heederik, J. P., van der Meer, L. G. H., Czernichowski-Lauriol, I., Harrison, R., Lindeberg, E., Summerfield, I. R., Rochelle, C., Schwarzkopf, T., Kaarstad O., & Berger, B. (1996). The underground disposal of carbon dioxide. *Summary report for the Joule II Project CT 92-0031*.

House, K. Z., Schrag, D. P., Harvey, C. F. & Lackner, K. S. (2006). Permanent carbon dioxide storage in deep-sea sediments. *Proceedings of the National Academy of Science*, USA, 103 (33), 12291-12295.

Hwang, M. J., Wright, D. A., Kapur, A., & Holder, G. D. (1990). An experimental study of crystallization and crystal growth of methane hydrates from melting ice. *J. Inclusion Phenom., 8* , 103–116.

Hyndman, R. D., & Davis, E. E. (1992). A mechanism for the formation of methane hydrate and seafloor bottom-simulating reflectors by vertical fluid expulsion. *J. Geophys. Res., 97* , 07025-7041.

IEA GHG (2004). Gas hydrates for deep ocean storage of CO_2. *IEA Greenhouse Gas R&D Programme Report PH4/26*.

IMO (1997). Convention on the prevention of marine pollution by dumping of wastes and other matter (London Convention 1972). Compilation of the full texts of the London Convention 1972 and of the 1996 Protocol thereto. LCO2/Circ.380, 63, International Maritime Organisation, London.

Intergovernmental Panel on Climate Change (2007). Working Group 1, Climate Change, Chapter 2.10.2.

Jeffrey, G. A. (1984). Hydrate Inclusion Compounds. *J. Inclusion Phenom., 1* , 211-222.

Johnson, J. W., Nitao, J. J., & Knauss K. G. (2004). Reactive transport modeling of CO_2 storage in saline aquifers to elucidate fundamental processes, trapping mechanisms, and sequestration partitioning. *Geological Society of London Special Publication on Carbon Sequestration Technologies*.

Jung, J. W., & Santamarina, J. C. (2010). CH_4-CO_2 replacement in hydrate bearing sediments. *A pore scale study, AGU, 11*.

Jung, J. W., Espinoza, D. N., & Santamarina, J. C. (2010), Properties and phenomena relevant to CH_4-CO_2 replacement in hydrate bearing sediments, *J. Geophys. Res., 115*.

Kang, S. P., Chun, M. K., & Lee, H. (1998). Phase equilibria of methane and carbon dioxide hydrates in the aqueous $MgCl_2$ solutions. *Fluid Phase Equilibria 147*, 229–238.

Kashchiev, D., & Firoozabadi, A. (2002). Nucleation of Gas Hydrates. *Journal of Crystal Growth, 243* , 476-489.

Klauda, J. B., & Sandler, S. I. (2003). Predictions of Gas Hydrate Phase Equilibria and Amounts in *Natural Sediment Porous Media. Marine Petroleum Geology*, 20 , 459-470.

Kleinberg, R. L., Flaum, C., Griffin, D. D., Brewer, P. G., Malby, G. E., Peltzer, E. T., & Yesinowski, J. P., (2003-b). Deep sea NMR: methane hydrate growth habit in porous media and its relationship to hydraulic permeability, deposit accumulation, and submarine slope stability. *J. Geophys. Res. 108* (B10), 2508.

Kleinberg, R. L., Flaum, C., Straley, C., Brewer, P. G., Malby, G. E., Peltzer, E. T., Friederich, G.,Yesinowski, J. P., (2003-a). Seafloor nuclearmagnetic resonance assay of methane hydrate in sediment and rock. *J. Geophys. Res. 108* (B3), 2137.

Kobayashi, R., Song, K. Y., & Sloan, E. D. (1987). *Petroleum engineers handbook* . Richardson, TX: SPE.

Koide, H., Takahashi, M., Shindo, Y., Tazaki, Y., Ijiima, M., Ito, K., Kimura, N., & Omata, K. (1997). Hydrate formation in sediments in the sub-seabed disposal of CO_2. *Energy, 22* (273), 279-283.

Komai T., Kawamura T., Kang S., Nagashima K., & Yamamoto Y. (2002). In situ observation of has hydrate behavior under high pressure by Raman spectroscopy. *Journal of Physics: Condensed matters 14*, 11395-11400.

Korsakov, O. D., Byakov, Y. A., & Stupak, S. (1989). Gas hydrates in the black sea basin. *International Geology Review*, 1251-1257.

Kumar, A. (2005). *Formation and decomposition of gas hydrates in porous media*. (Master's thesis, University of Calgary).

Kvenvolden, K .A. (1998). A primer on the geological occurence of gas hydrate, in *Gas Hydrates: Relevance to World Margin Stability and Climate Change*, 137: Special Publications: London, Geological Society, 9-30.

Kvenvolden, K. A. (2003). *Natural Gas Hydrate: Background and History of Discovery in Natural Gas Hydrate in Ocenic and Permafrost Environments*. Kluwer Academic Publishers, Netherlands.

Kvenvolden, K. A., Gingsburg, G. D., & Soloviev, V. A. (1993). Worldwide distribution of subaquatic gas hydrates. *Geo-Marine Letters*, 13, 32-40.

Lamb, H. (1945). *Hydrodynamics.* (p. 331–332). New York: Dover, Mineola.

Lee, H., Seo, Y., Seo, Y. T., Moudrakovski, I. L., & Ripmeester, J. A., (2003). Recovering methane from solid methane hydrate with carbon dioxide. *Angew. Chem. 115*, 5202–5205.

Makogon Y. F. (1997). *Hydrates of hydrocarbons*. Tulsa, OK: PennWell Publishing Co.

Makogon, Y. F., Makogon, T. Y., & Holditch, S. A. (1999). Gas Hydrate Formation and Dissociation with Thermodynamic and Kinetic Inhibitors. *SPE 56568*.

Mann S. L., McClure L. M., Poettmann F. H., & Sloan E. D. (1989, 03). Vapor-solid equilibrium ratios for structure I and Structure II natural gas hydrates. *Proceedings of the 69th Annual Gas Proc. Assoc. Conv*. San Antonio, TX.

Masuda, Y., Naganawa, S., Ando, S. & Sato, K (1997, 10). Numerical calculation of gas production performance from reservoirs containing natural gas hydrates, paper presented at the *Annual Technical Conference, paper 38291, Soc. of Petrol. Eng*., San Antonio, Tex.

McGrail, B. P., Schaef, H. T., White, M. D., Zhu, T., Kulkarni, A. S., Hunter, R. B., Patil, S. L., Owen, A. T., & Martin, P. F. (2007). Using Carbon Dioxide to Enhance Recovery of Methane from Gas Hydrate Reservoirs. *Final Summary Report. PNNL-17035*, Pacific Northwest National Laboratory, Richland, WA.

McGrail, B. P., Zhu, T., Hunter, R. B., White, M. D., Patil, S. L., & Kulkarni, A. S. (2004, 09). A New Method for Enhanced Production of Gas Hydrate with CO_2. In *Proceedings of the AAPG Hedberg Conference on Gas Hydrates, Energy Resource Potential and Associated Geologic Hazards*, Vancouver, Canada.

Miller, S. L., (1974). The nature and occurrence of clathrate hydrates. In *Natural Gas in Marine Sediments*, Plenum Press, New York, 151–177.

Moore, J., Adams, M., Allis, R., Lutz, S., & Rauzi, S. (2005). Mineralogical and geochemical consequences of the long-term presence of CO_2 in natural reservoirs: an example from the Springerville–St. Johns Field, Arizona, and New Mexico, U.S.A. *Chem. Geol. 217*, 365–385.

Moridis, G., Apps, J., Pruess, K., & Myer, L. (1998). EOSHYDR: A TOUGH2 module for CH_4-hydrate release and flow in the subsurface, Rep. LBNL-42386, Lawrence Berkeley Natl. Lab., Berkeley, Calif.

Motiee M. (1991). Estimate possibility of hydrate. *Hydro. Proc. 70* (7), 98 – 99.

Nakano, S., Moritoki, M., & Ohgaki, K. (1998). High-pressure phase equilibrium and Raman microprobe spectroscopic studies on the CO_2 hydrate system. *J. Chem. Eng. Data 43*, 807–810.

Nasrifar K. & Mohfeghian M. (2001). A model for prediction of gas hydrate formation conditions in aqueous solutions containing electrolytes and/or alcohol. *J. Chem. Thermodynamics*, *33*, 999-1014.

Natarajan, V., Bishnoi, P. R., & Kalogerakis, N. (1994). *Chem. Eng. Sci. 49*, 2075.

Ng H. J., & Robinson D. B. (1977). The prediction of hydrate formation in condensed systems. *AIChE J., 23*, 477–482.

Oguz, T., Tugrul, S., Kideys, A. E., Ediger, V., & Kubilay, N. (2005). Physical and biogeochemical characteristics of the Black Sea. *The Sea, 14* (33), 1331-1369.

Ohgaki, K., Sangawa, H., Matsubara, T., & Nakano, S. (1996). Methane exploitation by carbon dioxide from gas hydrates phase equilibria for CO_2–CH_4 mixed hydrate system. *J Chem Eng Jpn 29*, 478–483.

Oldenburg, C. M., Pruess, K., & Benson, S. M., (2001). Process modeling of CO_2 injection into natural gas reservoirs for carbon sequestration and enhanced gas recovery. *Energy & Fuels 15*, 293–298.

OSPAR (1992). Convention for the protection of the marine environment of the north-east Atlantic, 32, OSPAR Commission, London.

Ota, M., Morohashi, K., Abe, Y., Watanabe, M., & Smith, R. L. Jr. (2005). Hiroshi Inomata Replacement of CH_4 in the hydrate by use of liquid CO_2. *Energy Conversion and Management 46*.

Otto, C., (1998). Aquifer disposal of carbon dioxide: An examination. Centre for Groundwater Studies, Technical Report.

Park, Y., Kim, D., Lee, J., Huh, D., Park. K., Lee, J., & Lee, H. (2006). Sequestering carbon dioxide into complex structures of naturally occurring gas hydrates. *Proc. Natl. Acad. Sci.103*, 12690–12694.

Parker, J. C., Lenhard, R. J., & Kuppusamy T. (1987). A parametric model for constitutive properties governing multiphase flow in porous media. *Water Resour. Res., 23*, 614– 618.

Parlaktuna, M., & Erdogmus, T. (2001). Natural Gas Hydrate Potential of the Black Sea. *Energy Sources, 23* (3), 203-212.

Parrish W. R., & Prausnitz J. M. (1972). Dissociation pressures of gas hydrates formed by gas mixtures. *Ind. Eng. Chem. Process Des Devel., 11* (1), 26–35.

Pedersen K. S., Fredenslund A., & Thomassen P. (1989). *Properties of Oils and Natural Gases* Chap. 15. Houston, TX: Gulf Publishing.

Peng D. Y., & Robinson D. B. (1976). A New Two-constant equation of state. *Ind. Eng. Chem. Fundam., 15* , 59–65.

Pitzer K. S. & Mayorga G. (1973). Thermodynamics of Electrolytes. II. Activity and Osmotic Coefficient for Strong Electrolytes with One or both Ions Univalent. *The Journal of Physical Chemistry, 77* (19), 2300-2308.

Plasynski, S., McNemar, A., & McGrail, P. (2008). CO_2 Sequestration in Basalt Formations. U.S. Department of Energy Office of Fossil Energy National Energy Technology Laboratory.

Poirier, J.P. (1985). *Creep of Crystals*. Cambridge University Press, New York.

Poort, J., Vassilev, A., & Dimitrov, L. (2005). Did postglacial catastrophic flooding trigger massive changes in the black sea gas hydrate reservoir?. *Terra Nova, 17*, 135-140.

Prieto-Ballesteros, O., Kargel, J. S., Fernandez-Sampedro, M., Selsis, F., Martinez, E. S. & Hogenboom, D. L. (2005). Evaluation of the possible presence of clathrate hydrates in Europa's icy shell or seafloor. *Icarus, 177* (2), 491-505.

Pruess, K. (2003, 03). Numerical simulation of leakage from a geologic disposal reservoir for CO_2, with transitions between super and sub-critical conditions. *Proceedings of the 'TOUGH Symposium 2003'*, Lawrence Berkeley National Laboratory, Berkeley, California.

Pruess, K., Xu, T., Apps, J., & Garcia, J. (2001, 02). Numerical modeling of aquifer disposal of CO_2. Paper SPE 66537 *Presented at the SPE/ EPA/DOE Exploration and Production Environmental Conference*, San Antonio, TX.

Reid, R. C., Prausnitz, J. M. & Poling B. E. (1987). *The Properties of Gases and Liquids*, McGraw-Hill, New York, 332-337.

Rhudy, R. G., & Bock, B. R. (2002). Economic evaluation of CO_2 storage and sink enhancement options.

Ripmeester J. A., Tse J. S., Ratcliffe C. I., & Powell B. M. (1987). A new clathrate hydrate structure. *Nature 325*, 135–136.

Rochelle, C. A., Camps, A. P., Long, D., Milodowski, A., Bateman, K., Gunn, D., Jackson, P., Lovell, M. A., & Rees, J. (2009). Can CO_2 hydrate assist in the underground storage of carbon dioxide? In: *Sediment-hosted gas hydrates : new insights on natural and synthetic systems*. London, UK, Geological Society of London, 171-183. (Special publications Geological Society, 319).

Sakai, H., Gamo, T., Kim, E-S, Tsutsumi, M., Tanaka, T., Ishibashi, J., Wakita, H., Yamano, M. & Oomori, T. (1990). Venting of Carbon Dioxide-Rich Fluid and Hydrate Formation in Mid-Okinawa Trough Backarc Basin. *Science, 248* , 1093-1095.

Sasaki, K., & Akibayashi, S. (2000). A calculation model for liquid CO_2 injection into shallow sub-seabed aquifer. In: *Gas Hydrates, challenges for the future*, Annals of the New York Academy of Sciences, 912, 211-225.

Sawyer, W. K., Boyer II, C. M., Frantz Jr., J. H. & Yost II, A. B. (2000). Comparative assessment of natural gas hydrate production models, paper presented at the *Annual Technical Conference, paper 62513*, Soc. of Petrol. Eng., Dallas, Tex., 1 – 4.

Scheidegger, A. E. (1960). *The Physics of Flow Through Porous Media*. New Jersey: Macmillan, Old Tappan.

Seo, Y., & Lee, H. (2001). Multiple-phase hydrate equilibria of the ternary carbon dioxide, methane, and water. *J. Phys. Chem., B 105*, 10084–10090.

Seo, Y., & Lee, H. (2003). Hydrate phase equilibria of the ternary CH_4+NaCl+water, CO_2+NaCl+water and CH_4+CO_2+water mixtures in silica gel pores. *J. Phys. Chem., B 107*, 889–894.

Seo, Y., Lee, H., & Uchida, T. (2002). Methane and carbon dioxide hydrate phase behavior in small porous silica gels: three phase equilibrium determination and thermodynamics modeling. *Langmuir 18*, 9164–9170

Servio, P., Lagers, F., Peters, C., & Englezos, P. (1999). Gas hydrate phase equilibrium in the system methane–carbon dioxide–neohexane and water. *Fluid Phase Equilb.* (158–160), 795–800.

Sloan, E. D. & Koh, C. A. (2008). *Clathrate Hydrates of Natural Gases*. (3rd ed.), Boca Raton, CRC Press.

Sloan, E. D. Jr., (1991). Natural Gas Hydrates. *JPT , SPE Technology Today Series*, SPE 23562.

Sloan, E. D. Jr., (1998-a). *Clathrate hydrates of natural gases*. (2nd ed.), Marcel Dekker, New York.

Sloan, E. D. Jr., (1998-b). Gas Hydrates: Review of Physical/Chemical Properties. *Energy and Fuels, 12* , 191-196.

Sloan, E. D. Jr., (1998-c). Physical/chemical properties of gas hydrates and application to world margin stability and climatic change. In: *Gas Hydrates: Relevance to World Margin Stability and Climate Change*, 137 , Special Publications: London, Geological Society, 31-50.

Sloan, E. D. Jr., (2003). Fundamental principles and applications of natural gas hydrates. *Nature*, 426.

Smith, D. H., Wilder, J. W., & Seshadri, K. (2002). Methane hydrate equilibria in silica gels with broad pore size distributions. *AIChEJ 48* (2), 393–400.

Soave, G. (1972). Equilibrium constants from a modified Redlich-Kwong equation of state. *Chem. Eng. Sci., 27* , 1197–203.

Someya, S., Saito, K., Nishio, M., & Tsutsui, K. (2006, 01). CO_2 sequestration under a sealed layer with clathrate hydrate in sediments. *Proceedings of 'Sediment-hosted gas hydrates: New insights on natural and synthetic systems'*, London, 34, Geological Society.

Spangenberg, E. (2001). Modeling of the influence of gas hydrate content on the electrical properties of porous sediments. *J. Geophys. Res., 106* , 6535 – 6548.

Stevens, C. J., Howard J. J., Baldwin B. A., Ersland, G., Husebø, J., & Graue, A. (2008). Experimental hydrate formation and gas production scenarios based on CO_2 sequestration, paper presented at the *6th International Conference on Gas Hydrates*, U.S. Dep. of Energy, Vancouver, B. C., Canada.

Stevens, S. H., Kuuskraa J. A., & Schraufnagel R. A. (1996). Technology spurs growth of U.S. coalbed methane. *Oil and Gas Journal, 94* (1), 56-63.

Suekane, T., Mizumoto, A., Nobuso, T., Yamazaki, M., Tsushima, S., & Hirai, S., (2006). Solubility and residual gas trappings of CO_2 in geological storage. In: *Proceedings of the 8th International Conference on Greenhouse Gas Control Technologies*, Elsevier.

Sychev, V. V., Vasserman, A. A., Zagoruchenko, V. A., Kozlov, A. D., Spiridonov, G. A., & Tsymarny, V. A. (1987). *Thermodynamic properties of methane*. Hemisphere Publishing Corp, Washington.

Taber, J. J., Martin, F. D., & Seright, R. S. (1997). EOR screening criteria revisited. *Society of Petroleum Engineers. Reservoir Engineering, 12*, 189–198.

Tohidi, B., Anderson R., Clennell, M.B., Burgass, R.W., & Biderkab, A.B. (2001-a). Synthetic porous media by means of glass micromodels. *Geology*, *29* (9), 867-870.

Tohidi, B., Anderson, R., Clennell, M. B., Burgass, R. W., & Biderkab, A. B. (2001-b). Visual observation of gas–hydrate formation and dissociation in synthetic porous media by means of glass micromodels. *Geology 29* (9), 867–870.

Towler, B. F., Mokhatab S. (2005). Quickly estimate hydrate formation conditions in natural gases. *Hydro. Proc. 84* (4), 61–62.

Uchida, T., Ebinuma, T., & Ishizaki, T. (1999). Dissociation condition measurements of methane hydrate in confined small pores of porous glass. *J. Phys. Chem., B 103*, 3659–3662.

Uchida, T., Ebinuma, T., Takeya, S., Nagao, J., & Narita, H., (2002). Effects of pore sizes on dissociation temperatures and pressures of methane, carbon dioxide and propane hydrates in porous media. *J. Phys. Chem., B 106*, 820–826.

Uchida, T., Takeya, S., Chuvilin, E. M., Ohmura, R., Nagao, J., Yakushev, V. S., Istomin, V. A., Minagawa, H., Ebinuma, T., & Narita, H., (2004). Decomposition of methane hydrates in sand, sandstone, clays, and glass beads. *J. Geophys. Res. 109*.

van der Waals, J. H., & Platteeuw, J. C. (1959). Clathrate solutions. *Adv. Chem. Phys. 2*, 1–57.

van Genuchten, M. T., (1980). A closed form equation for predicting the hydraulic conductivity of unsaturated soils. *Soil Sci. Soc. Am. J., 44*, 892– 898.

Vassilev, A., & Dimitrov, L. (2002). Spatial and quantity evaluation of the Black Sea gas hydrates. *Russian Geol. Geophys*., *43*, 637-649.

Vassilev, A., & Dimitrov, L. (2003). Model evaluation of the black sea gas hydrates. *Comptes Rendus de l'Academie Bulgare des Sciences, 56* (3), 15-20.

White, M., & McGrail, P. (2009). Designing a Pilot-Scale Experiment for the production of natural gas hydrates and sequestration of CO_2 in class I hydrate accumulations. *Energy Procedia, 1*, 3099–3106.

Wilder, J. W., & Smith, D. H. (2004). Simple predictive relations, fugacities, and enthalpies of dissociation for single guest clathrate hydrates in porous media. *Chem. Eng. Sci. 59*, 3945–3954.

Wilder, J. W., Seshadri, K., & Smith, D. H. (2001-a). Modeling hydrate formation in media with broad pore size distribution. *Langmuir 17*, 6729–6735.

Winters, W. J., Dallimore, S., Collett, J. K., & Katsube, J. (2000). in *Proc. Gas Hydrates: Challenges for the Future*, 912, 94.

Winters, W. J., Mason, D. H., & Waite, W. F. (2004-c). Methane hydrate formation in partially-water saturated Ottawa sand. *Am. Mineral., 89*, 1202.

Winters, W. J., Pecher, I. A., Waite, W. F., & Mason, D. H. (2004-a). Physical properties and rock physics models of sediments containing natural and laboratory formed methane gas hydrate. *American Mineralogist, 89*, 1221-1227.

Winters, W. J., Waite, W. F., Dillon, W. P., Mason, D. H., & Pecher, I. A. (2001). Relationships between frozen and gas hydrate-containing sediment, in *2nd Russian Conference on Geocryology*, Russia.

Winters, W. J., Waite, W. F., Pecher, I. A., Mason, D. H., Hutchinson, D. R., Gilbert, L. Y., Birchwood, R. A., Noeth, S., & Jones, E. (2004-b). Comparison of methane gas hydrate formation on physical properties of fine and coarse grained sediments. in *Gas Hydrates: Energy Resource Potential and Associated Geologic Hazards*. Vancouver, BC; Canada.

Yezdimer, E. M., Cummings, P. T., & Chialvo, A. A. (2002). Determination of the Gibbs free energy of gas replacement in SI clathrate hydrates by molecular simulation. *J Phys Chem A 106*, 7982–7987.

Yokozeki, A. (2004). Solid, liquid, vapor phases of water and water, carbon dioxide mixtures using a simple analytical equation of state. *Fluid Phase Equilibria*, (222–223), 55-56.

Yousif, M. H., & Sloan, E. D. (1991). Experimental investigation of hydrate formation and dissociation in consolidated porous media. *SPE Reserv. Eng*. 452–458.

Yousif, M. H., Abass, H. H., Selim, M. S., Sloan, E. D. (1991). Experimental and theoretical investigation of methane-gas-hydrate dissociation in porous media. *SPE Reservoir Engineering*. 69-76.

Zatsepina, O. Y., & Buffett, B. A. (1997). Phase equilibrium of gas hydrate: implication for the formation of hydrate in the deep sea floor. *J. Geophys. Res., 24*, 1567–1570.

Zatsepina, O. Y., & Buffett, B. A. (2001). Experimental study of the stability of CO_2 hydrate in a porous medium. *Fluid Phase Equilibrium, 192*, 85–102.

Zhang, W., Durham, W. B., Stern, L. A., & Kirby, S. H. (1999). Experimental deformation of methane hydrate: New results. *Eos Trans. AGU, 80* (17), Spring Meet.Suppl., S337.

Zhou, X., Fan, S., Liang, D., & Du, J. (2008). Replacement of Methane from Quartz Sand-Bearing Hydrate with Carbon Dioxide in Water Emulsion. *Energy & Fuels 2008, 22*, 1759–1764.